Investigating the influence of solute type and solute concentration on ice scale formation on Polypropylene Graphite (PP-GR) during Eutectic Freeze Crystallization

Master's Dissertation

Author: Madimetsa Matau

Supervisors: Senzo Mgabhi, Jemitias Chivavava, Prof. Alison Lewis

This dissertation is submitted in fulfilment of the requirements for the degree of Master of Science in Chemical Engineering

Department of Chemical Engineering,

University of Cape Town

2025

Declaration

I know the meaning of plagiarism and declare that all the work in the document, save for that which is properly acknowledged, is my own. This thesis/dissertation has been submitted to the Turnitin module (or equivalent similarity and originality checking software) and I confirm that my supervisor has seen my report and any concerns revealed by such have been resolved with my supervisor.

Signed by:

Samuel Madimetsa Matau

10 February 2025

Acknowledgements

I would like to express my gratitude to my sponsors: Coaltech, UCT Financial Aid, and the Anglo-American De Beers Chairman's Fund Award, for their generous support throughout my journey. A special thank you to Technoform for supplying the PP-GR tubes and to Coaltech for providing the industrial brines. Thank you to my supervisors, Senzo Mgabhi, Jemitias Chivavava, and Alison Lewis, for the technical support and guidance. Thank you so much again, Ntate Senzo and Mr. Jemitias, for everything you have done for me. You were not only supervisors but also big brothers to me. You always ensured that I was okay, and even when things were not going well in the lab, you motivated me to keep going, believe in myself, and reminded me that I would get there one day. Ausi Lerato, you were like a big sister to me. Beyond the lab work, you were always there when I needed to talk. I will forever be grateful for your support and guidance.

A big shout-out to my friend Sive, who ensured I took care of myself and my mental health. Though we've been friends for only a year, it feels like we've known each other forever. Magata Mangatane, my brother since 2017, inspired me to work hard throughout this master's journey. Thabo Sibanda, we've faced many challenges together, and your energy always pushed me to do better. Your technical assistance and selflessness mean the world to me. I am forever grateful.

Hilton treated me like a son. He helped me pick myself up after I failed one of my final year Chem Eng courses and instilled hope in me. Thank you. A big thank you to my twin brother, Ephraim Matau. He has been there for me since day one, and I could list a million things he has done for me. One thing that stood out for me during this journey was I didn't even have to tell him that I was not feeling well; he would just know and cheer me up. Gerald, also another brother from another mother. He taught me a lot about surviving and thriving during this master's journey. Thank you, abuti. To my best friend, Kensane, thank you for always being there for me, encouraging me, and checking up on me regularly, especially during the final days of my master's journey. Your support meant the world to me. And to my sister from another mother, Ausi TK, thank you for always being there for me. I deeply appreciate your kindness and encouragement.

To the Chemical Engineering workshop staff (Clint, Siya, and Camrien) thank you for always allowing me to take breaks in your working space whenever I needed a moment away from my own work. Thank you to the Chem Eng social club. Sharing moments of laughter and relaxation with you all provided much-needed breaks from my studies. Cheers to the good times and lasting connections. Thank you to the CPU team (Nikita, Buhle, Tawanda, Jac, and Thabo). Being part of this group allowed me to grow as a professional. And finally, thank you to my family and friends. They always called to check up on me, which was one of the things that kept me going, especially when things were tough. Thank you so much for everything you have done for me.

Abstract

Eutectic freeze crystallization (EFC) is a promising sustainable method for the treatment of hypersaline streams. However, the formation of ice scale layers on heat exchanger surfaces has hindered its industrial implementation. Previous studies have shown that smooth heat exchanger (HX) materials with low surface energy like Polypropylene Graphite (PP-GR), can help reduce ice scaling, but their anti-scaling performance in the EFC of brines with varying solute types and concentration remains unexplored. Therefore, this research aimed to study how solute concentration and type affect the ice scaling on the HX surface of PP-GR during EFC.

The study involved a continuous EFC process with a 3L column crystallizer equipped with a PP-GR heat exchanger tube, designed to observe the formation of ice scale layers and bulk crystallization. The production of ice was measured every 20 minutes for 1 hour. The amount of ice scale layer was measured after the experiment. The study was conducted in two phases: the first phase used multicomponent industrial brine from the Tweeifontein Water Reclamation Plant with Total Dissolved Solids (TDS) concentrations of 103 g/L. This brine was pre-concentrated using the cascade method to obtain concentrations of 122 g/L, and 133 g/L TDS. The second phase investigated synthetic brines of Na_2SO_4-H_2O and $MgSO_4$-H_2O at a constant molality of 0.613 mol/kg and varying $MgSO_4$ concentrations of 0.613, 1.130, and 1.47 mol/kg.

In the industrial brines, increasing the total solute concentration, from TDS of 103 to 133 g/L, reduced ice scale layer amount by 72%, from 42 g to 11 g. At 103 g/L TDS, the ice scale layer contributed 62% of the total ice yield, while at higher concentrations, it contributed less (18% at 122 g/L and 9% at 133 g/L). The ice scale layer formed within 20 minutes for the brine with 103 g/L TDS, within 30-40 minutes for 122 g/L TDS, and within 40-60 minutes for 133 g/L TDS. This reduction in ice scaling was linked to decreased interfacial interactions between the brine and heat exchanger (HX) surface, likely due to increased surface tension (from 79 to 81 mN/m) and contact angle, which weakened the attraction between the brine and HX surface. However, the role of surface tension in ice scaling could not be fully isolated due to the influence of low ice seed loading (0.5 wt.%) and low mixing intensity (Re ~700), which led to uneven supersaturation and favored surface nucleation. Future studies should increase mixing intensity and ice seed loading to better understand the impact of surface tension on ice scaling.

The differences in ice scale formation were not only due to delays in ice scale layer formation but also to variations in growth rate and delamination as solute concentration changed. Slower growth of the ice scale layer was observed in more concentrated brines, likely due to increased resistance to mass transfer of water molecules from the bulk solution to the ice scale layer. Ice scale layer from dilute brine adhered strongly to

the PP-GR surface, making removal difficult, while scales from more concentrated brines (122 g/L and 133 g/L TDS) delaminated easily. This is likely due to reduced ice adhesion strength at higher concentrations, which disrupts water molecule orientation and weakens interfacial interactions. In lower concentrations, more ordered water layers enhance adhesion. Variations in contact angle may also influence this, with lower angles in dilute brine promoting stronger adhesion, while higher angles in concentrated brines reduce it. Other factors remain unclear.

For the binary synthetic brines**,** it was found that increasing concentration (0.61 to 1.47 mol/kg) in synthetic binary $MgSO_4$ brines decreased ice scale amount by 99% (from 82 g to 0.7 g). The ice scale layer formed within 20 minutes for the dilute brine (0.613 mol/kg), within 20-40 minutes for 1.13 mol/kg, and within 40-60 minutes for the 1.47 mol/kg. The reduction in ice scaling tendency with increased concentration for this brine was also attributed to the reduced interfacial interactions between the brine and HX surface. Increasing the concentration from 0.613 to 1.47 mol/kg increased the surface tension from 77 mN/m to 79.4 mN/m. This is thought to have reduced the strength of interfacial interactions between the brine and HX surface, possibly delaying the formation of ice scaling. Slower growth of ice scale layer was also observed at higher concentrations possibly due to increased resistance to mass transfer, with Mg^{2+} ions forming a diffusive boundary layer that delayed ice scale growth.

It was also observed that the ice scale amount on the surface of PP-GR was 30% lower in $MgSO_4$ brine compared to that of Na_2SO_4 brine at the constant molality of 0.613 mol/kg While the ice scale layer formed within 20 minutes for both solutions, Na_2SO_4 brine had a faster ice scaling formation, leading to a 65% decrease in ice production rate (from 2.60 to 0.90 g/min), whereas $MgSO_4$ brine showed only a 22% decrease (from 2.04 to 1.58 g/min). Despite slower initial ice production, $MgSO_4$ brine maintained a steadier rate due to slower growth and frequent delamination of ice scale layers. Mg^{2+} ions may have disrupted hydrogen-bonded networks within the liquid-like layer on the ice surface, weakening adhesion. Additionally, Mg^{2+} ions likely neutralized surface charges on the surface of ice, further reducing adhesion. Although the exact mechanism is unclear, both disruption of hydrogen bonds and electrostatic screening are likely to contribute to delamination. These findings suggest that ions with higher charge density, like $Mg^{2+,}$ may reduce ice scaling and allow for longer freeze crystallization periods.

Overall, the current study has shown that selecting highly concentrated brine along with PP-GR would be beneficial in delaying the formation of ice scaling, reducing the growth rates of ice scale layers, and increasing the frequency of delamination of ice scale layers. Furthermore, the type of solute presents in a brine affects the formation of ice scaling as there are solutes that may have negligible or significant impact on ice scaling.

Table of Contents

List of Figures

List of Tables

Nomenclature

$U_{overall}$	Overall Heat Transfer Coefficient ($W/m^2 \cdot K$)
A	Heat transfer Area (m^2)
ΔT	Temperature Difference (˚C or K)
τ_l	Viscosity of the liquid (cP)
β	Velocity of the fluid relative to the ice (m/s)
$\dot{\mathbf{q}}$	Volumetric Flowrate of the coolant (m^3/s)
ρ	Density (Kg/m^3)
c	Concentration (wt.% or g/L)
m	Mass (kg)
M	Molar mass (kg/kmol)
T	Temperature (˚C or K)
d	Diameter (m)
Δh_{fusion}	Heat of fusion (J/kg)
C_p	Specific Heat ($J/Kg \cdot K$)
h	Heat transfer Coefficient ($W/m^2 \cdot K$)
Q	Heat flux (J/m)
$T_{coolant,\ in}$	Temperature of the inlet coolant flow (˚C)
$T_{Coolant,\ out}$	Temperature of the outlet coolant flow (˚C)
T_{Wall}	Temperature of the heat transfer wall (˚C)
T_i	Temperature at the interface between two phases (˚C)
T_s	Temperature at the surface of heat exchanger (˚C)
G	Ice Growth Rate (m/s)
δ	Boundary Layer thickness (m)
k	Thermal Conductivity ($W/m \cdot K$)
r	Radius of the cluster (m)
rc	Critical radius of the cluster (m)
ΔG	Gibbs free energy
ΔG_{volume}	Free energy for phase transformation
$\Delta G_{surface}$	Free energy change for the formation of interface
ΔG_v	Free energy change for phase transformation per unit volume

Greek Letters

$\emptyset$	Surface energy reduction factor
γ_{li}	Interfacial tension between the liquid and ice embryo (N/m)
γ_{sl}	Interfacial tension between the liquid phase and foreign solid surface (N/m)
γ_{si}	Interfacial tension between the foreign solid surface and ice embryo (N/m)
Θ	Contact angle between a liquid and foreign surface (˚)

Abbreviations

EFC	Eutectic Freeze Crystallization
EC	Evaporative Crystallization
TDS	Total Dissolved Solids
PP-GR	Polypropylene Graphite
QLL	Quasi liquid layer
HX	Heat exchanger
TWRP	Tweefontein Water Reclamation Plant
SS361	Stainless Steel
Al	Aluminum

1. Introduction

1.1 Background

The treatment and management of brines produced by South African (SA) coal mine operations are challenging. Currently, these brines are disposed of in evaporation ponds (Panagopoulos et al., 2019), which poses risks of ground-water contamination, expensive construction, and a large geographical footprint. This method provides only short-term solutions, and fail to reduce overall wastewater quantities; highlighting the need for alternative treatments (Panagopoulos & Haralambous, 2020; Ting et al., 2024).

Evaporative crystallization (EC) is a well-established method that has been shown to effectively reduce volumes of wastewater by producing pure water and salt. However, it is a costly and environmentally unfriendly solution due to the considerable energy consumption related with evaporation (Ting et al., 2024). Eutectic freeze crystallization (EFC) works by freezing a saline solution to its eutectic temperature, resulting in the formation of both ice and salt crystals simultaneously. EFC is a promising alternative due to its lower energy requirements because the latent heat of fusion of ice is approximately six times lower than the latent heat of vaporization of water (Nathoo et al., 2009; van der Ham et al., 1998). Randall et al. (2011) demonstrated the feasibility of recovering pure salts and water from coal mine-impacted waters in SA, making it viable and more sustainable option.

Given the challenges faced by South African coal mine operations regarding the treatment and management of brines, EFC presents a potential solution (Lewis et al., 2010; Panagopoulos & Haralambous, 2020; Randall et al., 2011). Despite its potential, the formation of ice scale layers on heat exchanger (HX) surface hinders its implementation on an industrial scale. Ice has a low thermal conductivity, which reduces the cooling rate. Hasan et al. (2017) and Spencer et al. (2022) reported a reduction in the heat transfer coefficient by a factor of 10-20 and a 68% decrease in heat transfer between the heat transfer surface and the bulk solution, respectively. This results in low ice production and increased downtimes, emphasizing the need to reduce ice scaling to improve productivity and availability of EFC crystallizers (Hasan et al., 2017; Spencer et al., 2022; Vaessen et al., 2004).

Ice scaling in EFC is generally mitigated using mechanical scrapers to remove the ice scale layers from the HX surface of a crystallizer (Stamatiou et al., 2005). However, these scrapers are complex, prone to mechanical breakdowns, and high investment and maintenance costs, limiting their industrial use (Stamatiou et al., 2005). Alternative methods to reduce ice scaling without mechanical scraping are needed (Hasan et al., 2017; Stamatiou et al., 2005).

Hasan et al. (2017) showed that ice scaling could be minimized in the EFC of a 4 wt.% sodium sulphate (Na_2SO_4) aqueous solution without using mechanical scrapers by selecting suitable operating conditions such as the temperature driving force and mixing intensity. In the ongoing research on finding ways to reduce ice scaling, Motsepe et al. (2022) have demonstrated that using low surface energy HX materials can reduce ice scaling in EFC. This also extends to fouling challenges in evaporative crystallization, whereby Schilling, et al. [15] reported low surface energy materials, such as Polypropylene Graphite (PP-GR), had lower scaling when compared to high surface energy materials, such as stainless steel. Although PP-GR materials are new in the heat transfer applications, and have lower thermal conductivity compared to metallic HX materials, Lewis et al. (2023) showed that they could be used as a HX materials in EFC, and actually reduce ice scaling. As a result, these materials could be used in continuous EFC applications of industrial brines, such as those from coal mines. However, using ice-scaling resistant HX materials alone may not entirely eliminate scaling since ice scaling is also affected by solution chemistry as it was shown by Leyland et al. (2019) and Vaessen et al. (2002). Furthermore, the applications of these materials in EFC have been limited to brines, such as chloride streams, at a fixed concentration (Lewis et al., 2023).

Studies by Leyland et al. (2019) and Vaessen et al. (2002) have shown that dilute brines can cause significant ice scaling for scraping crystallizer. An increase in solute concentration delayed the formation of ice scaling. However, Leyland et al. (2019) studied the influence of concentration on ice scaling only up to concentrations of 30 g/L total dissolved solids (TDS) , which are very dilute compared to some of the industrial brines produced from South African coal mines, which can reach concentrations of 240 g/L TDS. Furthermore, they did not achieve ice-scale free operations. Nonetheless, their findings showed that concentration can affect ice scaling. The influence of concentration on ice scaling can be explained by what Deshmukh et al. (2013) and Wan et al. (2021) observed on molecular level showing that the concentration of solute in water can disrupt local ordering of water molecules near the solution-HX surface interface, which could possibly delay the formation of ice heteronuclei on a solid surface

Although ice scaling from brines with varying solute type and solute concentration has been extensively as shown in studies like Chatterjee et al. (2023); (Deshmukh et al., 2013; Hasan & Louhi-Kultanen, 2015; Leyland et al., 2019; Vaessen et al., 2002; Zhang et al., 2021), there is limited data on the influence of solute concentration and solute type on ice scaling on polymer composite materials such as PP-GR particularly in a continuous EFC process. Therefore, the aim of this work was to investigate the influence of solute concentration and solute type on ice scaling formation on the surface of PP-GR during EFC.

1.2 Aims and Objectives

The overall aim of this project was to investigate the effect of brine chemistry on the anti-scaling performance of PP-GR during continuous EFC of industrial brines from typical SA coal mines. To fulfill this aim, the following objectives were formulated:

- to investigate the effect of concentration of salts, binary system, on the ice scale formation on the surface of PP-GR during freeze crystallization.
- to investigate the influence of salt type, binary system, on the ice scaling formation on the surface of PP-GR during freeze crystallization.
- to study the influence of concentration, which will be represented as TDS of industrial brine, multicomponent, sourced from coal mine processing, on the surface of PP-GR during freeze crystallization.

1.3 Scope and limitations of the study

This study investigated how both the solute type and solute concentration influence formation of ice scaling on the HX surface of PP-GR during eutectic freezing crystallization. It focused on two solute types, sodium sulphate (Na_2SO_4) and magnesium sulphate ($MgSO_4$) as well as an industrial brine sourced from the Tweeifontein Water Reclamation Plant (TWRP). The experiment setup involved EFC experiments conducted in column crystallizer (CC) equipped with a PP-GR as HX tube. Each experiment was conducted for 1 hour after seeding, and the ice scaling was only measured at the end of the experiment, without tracking the exact time scaling formed. Due to the elongated and cylindrical nature of the HX surface of PP-GR, scaling mechanisms could not be observed at all points. Therefore, observations were confined to a single point, located at the bottom section of the crystallizer.

2. Theory

This section outlines the theoretical foundation for crystallization of ice and salt in EFC. It covers the fundamentals of crystallization, focusing on nucleation and growth of crystals, and examines the role of heat and mass transfer in influencing these processes. These principles are essential for interpreting and analyzing experimental data.

2.1 Crystallization

Crystallization is described as a phase transition in which a solid with a well-defined and organized structure is formed from a solution, melt, or gas phase under appropriate thermodynamic and kinetic conditions. This process is driven by supersaturation, which can result from changes in temperature, concentration, or solvent removal (Benz, 2020). Various methods are used to crystallize materials for separation and recovery, depending on the properties of the material and the desired application. Table 2.1. summarizes common separation technologies for wastewater streams and their respective principles and disadvantages.

Table 2.1: Common separation technologies for wastewater streams: (Ali et al., 2023; Macias-Bu et al., 2023; Ting et al., 2024).

Methods	Separation Principle	Disadvantages
Cooling	Cooling the solution below its saturation temperature causing solutes to crystallize.	Low yields
Eutectic Freeze Crystallization	Freezes a saline solution to its eutectic temperature, causing the formation of both ice and salt crystals at the same time, followed by separation due to density difference between the ice and salt crystals.	High capital cost, limited investigations on multi-component brine solutions, and ice scaling issue on crystallizer surfaces.
Evaporative	Solutes are crystallized by evaporating the solvent until the required supersaturation is reached	High energy consumption, and prone to corrosion due to operating at high temperature.
Membrane	The solution is pressurized against a selective membrane, which only allows the pure solvent to pass	Prone to fouling, and limited efficiency when used as standalone method for brine treatment
Chemical Reaction	A reagent that will form a sparingly soluble product is added to the existing solution and thus precipitation is affected.	Additional chemicals, and formation of unexpected solid phase

Compared to other technologies, EFC is a promising alternative to previous technologies due to its environmentally friendliness, reduced energy intensity, and zero liquid discharge (ZLD), (Ting et al., 2024). Furthermore, in addition to water reclamation, EFC may recover other salts, making it an appropriate strategy for reaching ZLD (Randall et al., 2011; Ting et al., 2024). In conclusion, EFC presents a long-term solution for treating industrial brines. The basic principle of EFC will be detailed in the following section.

2.1.1 Basic principles of eutectic freeze crystallization

Eutectic freeze crystallization refers to the crystallization of both ice and salt together from a water-salt mixture at a certain composition and temperature referred to as eutectic point. At this point, there is an equilibrium that exists between salt, ice, and the mixture. The basic principles of EFC can be demonstrated using a phase diagram of a water-salt system as shown in Figure 2.1 (van der Ham et al., 1998).

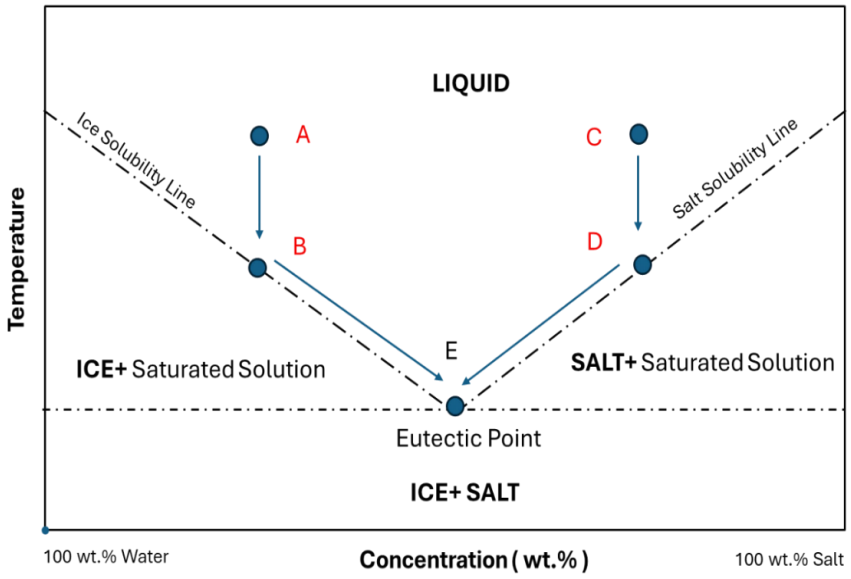

Figure 2.1: Phase diagram showing both the eutectic composition and temperature of a water-salt system. Adapted from source: van der Ham et al. (1998)

As in Figure 2.1, T and C represent the temperature and concentration of the water-salt mixture, respectively. In a case where the initial salt solution has the eutectic composition (C_E), cooling it down to its eutectic temperature will result in simultaneous crystallization of ice and salt. Due to ice ($\rho_{ice} \approx 999$ kg/m^3) being less dense than the salt solution ($\rho_{solution} \approx 1200$ kg/m^3), it floats, and salt ($\rho_{salt} > 1200$ kg/m^3) being denser than the solution, sinks, separating easily as shown by van der Ham et al. (1998). However, typically saline solutions like those from the industry operations have a salt concentration that is either higher or lower than the eutectic composition (C_E) of that solution. Thus, the following cases may take place:

- **Hypoeutectic**: the initial salt solution has a salt concentration lower than that of eutectic concentration (C_A). Cooling this solution from temperature T_A to T_B will result in the crystallization of ice only. As ice forms, the remaining aqueous solution becomes concentrated with salt, resulting to a freezing point depression point. Further cooling results in more ice crystallization until the solution reaches the eutectic point (C_E: T_E), where both ice and salt crystallize simultaneously (van der Ham et al., 1998; Yazdanpanah & Nagy, 2020).
- **Hypereutectic**: the initial aqueous solution has a salt concentration higher than that of eutectic, the opposite will occur. In this case, cooling down the solution will result in crystallization of salt only and with further cooling, the solution will reach the eutectic point where both ice and salt crystallize out simultaneously (Lewis et al., 2010; van der Ham et al., 1998). It should be noted that the eutectic points of water-salt systems may vary for different systems as this point is dependent on the type of solutes present in solution.

It should be noted, however, that industrial brines are multicomponent system, as opposed to a binary system where there are only two components (one type of salt, and solvent) (Aspeling et al., 2020; Randall et al., 2011). Therefore, EFC of multicomponent brines involves numerous solutes interacting with each other, and the solvent. This interaction affects the thermodynamic behavior of the system, influencing the solubility and eutectic temperatures of the other solutes (Benz, 2020). As the solution temperature is reducing, the first salt and ice crystallize out of solution. This causes the concentration of the non-crystallizing salts to gradually increase until a ternary eutectic point is reached, below which the second salt starts to crystallize out. When these two salts and ice are crystallizing, the concentration of the remaining salts increases, until a point is reached where all the other salts in solution, in very small quantities, crystallize out (Aspeling et al., 2020; Benz, 2020). It should also be noted that a process called nucleation initiates eutectic freeze crystallization, thus it is important to understand the theory behind this process.

In EFC, brines are generally cooled down below their equilibrium temperatures to generate supersaturation, which is the driving force for crystallization steps such as nucleation and growth as describe by Benz (2020) , which will be reviewed in the following section.

2.2 Nucleation

Nucleation is the initial stage of crystallization, where new particles form from a supersaturated solution (Mullin, 2001). This is because supersaturated system is unstable, hence changes to a stable state. There are two main types of nucleation processes: primary and secondary nucleation. Primary nucleation can happen in two ways: homogenous nucleation, which occurs in a solid-free, supersaturated liquid, and heterogeneous

nucleation, which is facilitated by foreign particles like dust or HX surface. Secondary nucleation happens when new crystals form because of the presence of existing crystals in a solution (Benz, 2020; Mullin, 2001). This study mainly focused on heterogenous nucleation because it plays a role in ice scaling formation, which is the main topic of this study. Secondary nucleation was also briefly considered as it relates to suspension crystallization.

2.2.1 Primary Nucleation Mechanisms

2.2.1.1 Homogenous Nucleation

According to nucleation theory, homogenous nucleation occurs when a nucleus forms in a crystal-free solution without any assistance from foreign particles. The total free energy change (ΔG) needed for the formation of cluster can be described by two components: volume free energy (ΔG_{volume}) and surface free energy change ($\Delta G_{surface}$), as shown in Figure 2.2 and Equation 2.1, (Mullin, 2001).

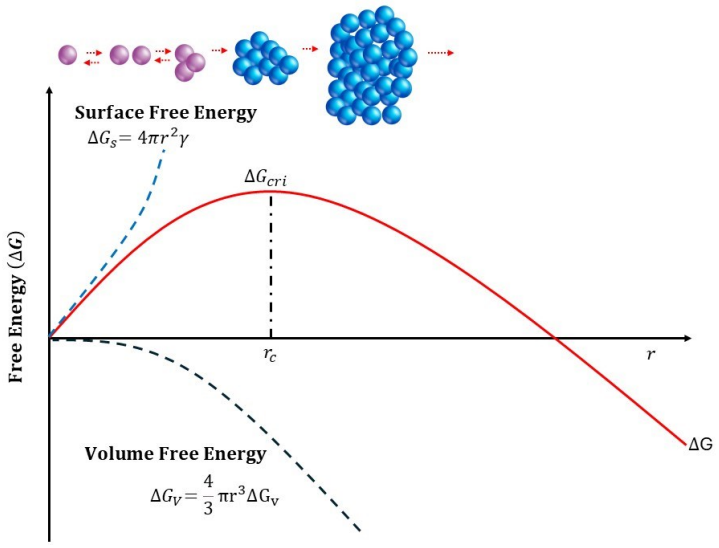

Figure 2.2: Total free energy change diagram for nucleation, adapted from (Mullin, 2001)

$$\Delta G = \Delta G_{volume} + \Delta G_{surface} = \frac{4}{3}\pi r^3 \Delta G_v + 4\pi r^2 \gamma \qquad \text{Equation 2.1}$$

where r is the radius of the cluster, γ is the interfacial tension between the developing cluster and the bulk solution, and ΔG_v is the phase transition free energy per unit volume. The "ΔG_{volume}" is proportional to r^3 and favors the cluster formation by releasing energy. The "$\Delta G_{surface}$" is proportional to r^2 and requires additional energy to form the cluster surface (Mullin, 2001). At smaller cluster sizes, ΔG_{volume} dominates, making growth thermodynamically unfavorable. As the cluster grows and reaches a critical (r_c), the total

free energy change (ΔG) decreases, favoring nucleation and the formation of a stable nucleus. The radius (r_c) is derived from the condition where the total free energy is maximized Equation 2.2):

$$r_c = \frac{-2\gamma}{\Delta G_v} \qquad \text{Equation 2.2}$$

Clusters larger than r_c lead to a decrease in ΔG, resulting in nucleation. Then, further growth of this nucleus becomes energetically favorable, and leads to the formation of a new phase in bulk, such as a crystal.

2.2.1.2 Heterogenous Nucleation

Heterogeneous nucleation occurs in the presence of a foreign body or surface such as HX surfaces, which provides nucleation sites by reducing the $\Delta G_{critical}$ for the nucleation (Mullin, 2001). This is because the interfacial energy of the new phase with this foreign surface is usually compared to the original phase, thus reducing for nucleation (Benz, 2020; Jha et al., 2016; Mullin, 2001; Yazdanpanah & Nagy, 2020). Thus, cluster formation under heterogeneous nucleation reaches the critical radii (r_c) at lower ΔG than that of homogenous nucleation and can be represented, as shown in Equation 2.3.

$$\Delta G_{critical,het} = \emptyset \Delta G_{critical,hom} \qquad \text{Equation 2.3}$$

Where $\Delta G_{critical,\ het}$ is the overall free energy changed related to the formation of a critical nuclei under heterogeneous nucleation, $\Delta G_{critical,\ hom}$ is that of the formation of a critical nucleus under homogeneous nucleation conditions, and ∅ is the surface energy reduction factor. The surface energy reduction factor is based on the contact between the embryo, the foreign surface and liquid phase, as shown in Figure 2.3, which is represented in the form of contact angle (Θ), (Benz, 2020). The contact angle describes how a liquid spread on a solid surface, often referred to as wettability (Liu et al., 2017; Mittal & Choi, 2020b).

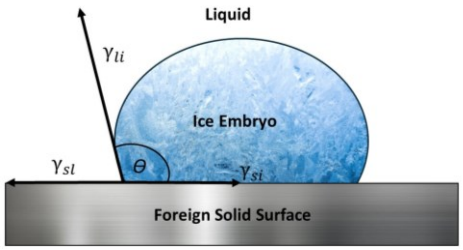

Figure 2.3: Interfacial tensions between the three phases in contact, adapted from (Mittal & Choi, 2020b)

The interactions between these phases can provide an additional energy for transformation by reducing the interfacial energy term $\Delta G_{surface}$, shown in Equation 2.1, which is related to the contact angle between the foreign surface and the cluster. The contact angle is a function of interfacial tensions between the three

phases as described by Equation 2.4, known as Young's equation. This includes the interfacial tensions between the ice-embryo and the liquid (γ_{li}), that of between the foreign solid surface and ice-embryo, γ_{si} and γ_{sl} is that between the liquid and the foreign solid surface (Mittal & Choi, 2020b).

$$\gamma_{sl} = \gamma_{si} + \gamma_{li} \cos\theta \qquad \text{Equation 2.4}$$

Or

$$\cos\theta = \frac{\gamma_{sl} - \gamma_{si}}{\gamma_{li}} \qquad \text{Equation 2.5}$$

The surface energy reduction factor Ø in Equation 2.6 can be represented as shown in equation 2.8, (Benz, 2020):

$$Ø = \frac{(2 + \cos\theta)(1 - \cos\theta)^2}{4} \qquad \text{Equation 2.6}$$

According to Equation 2.6 when the contact angle (Θ) is 0˚, Ø term is equal to 0, making the overall free energy change for nucleation 0 according to Equation 2.3. In the case of non-wettable solid surface where the contact angle (Θ) is 180˚, the surface energy reduction factor (Ø) becomes 1, resulting in the overall energy required for heterogenous nucleation being equivalent to that of homogenous nucleation. When the contact angle ranges between 0 and 180˚, the surface reduction factor is less than 1, indicating that the $\Delta G_{Critical,\,hom} > \Delta G_{Critical,\,het}$ (Mittal & Choi, 2020b; Mullin, 2001). This implies that the contact angle between the nucleus and the solid surface does influence the heterogeneous nucleation.

There are several factors that affect the contact angle, such as the temperature, surface properties of the foreign solid surface, and chemical properties of the solution (Liu et al., 2017; Lupi et al., 2014; Mittal & Choi, 2020b; Si et al., 2022; Wan et al., 2021). However, for this study, the focus was on the chemical properties of the solution due to the variations in solute type and their concentrations in industrial brines. These variations may result in varying surface tensions as described by Marcus (2016), affecting the interfacial interactions between the brine and HX surface during crystallization. As a result, this may result in different behaviors in ice heterogeneous nucleation on HX surfaces. Therefore, the theory regarding surface tension and their impact on contact angle will be explored further in the following subsection.

2.3 Surface Tension and Wettability

Surface tension is a fundamental property influencing the contact characteristics between a solid and a liquid, such as the contact angle (Marcus, 2016; Si et al., 2022). As discussed previously, contact angle plays a crucial role in heterogeneous nucleation. The behavior of a liquid's molecules differs significantly within the bulk compared to those at the surface (Faust & House, 2018; Kolasinski, 2020). In the bulk, molecules experience cohesive forces uniformly from all directions, resulting in a net force of zero.

Conversely, surface molecules, lacking neighboring molecules on all sides, only experience forces from adjacent molecules on one side. This imbalance creates excess energy at the surface, leading to stronger bonds with inner molecules and, consequently, surface tension (Faust & House, 2018).

Young's equation (Equation 2.4) provides insight into how surface tension governs interfacial interactions among the liquid's outer surface, the bulk solution, and the foreign solid surface (Benz, 2020; Kolasinski, 2020) . It is widely understood that the strength of the interactions between the liquid outer surface layer and the solid surface is determined by a balance between the cohesive forces of the liquid, which is the surface tension, and the surface energy of the solid surface, determining the contact angle (Faust & House, 2018; Kolasinski, 2020; Mittal & Choi, 2020b). Table 2.2 shows how the interfacial tensions impact the contact angle and thus the surface energy reduction factor, Equation 2.6.

Table 2.2: Influence of interfacial tensions on the contact angle and the surface energy reduction factor (Kolasinski, 2020).

Interfacial Tensions (γ)	Contact Angle	Surface Reduction Factor (Ø)
$\gamma_{li} \approx \gamma_{sl} - \gamma_{si}$	$\Theta = 0^{\circ}$	0
$\gamma_{li} > \gamma_{sl} - \gamma_{si}$	$0^{\circ} \leq \Theta \leq 90^{\circ}$	$0 \leq Ø \leq 0.5$
$\gamma_{li} >> \gamma_{sl} - \gamma_{si}$	$\Theta > 90^{\circ}$	$Ø > 0.5$

According to Equation 2.5,when the surface tension of the liquid resting on a solid surface dominates, the contact angle is larger because the liquid molecules are more attracted to each other than to the foreign solid surface (Kolasinski, 2020; Si et al., 2022) . This then leads the liquid to shrink towards itself. When the surface energy of the solid surface is dominant, the contact angle tends to be lower because liquid molecules are strongly attracted to the solid surface, allowing the liquid to spread easily (Kolasinski, 2020). This suggests that increasing the surface tension of the liquid and while keeping the surface energy of the HX surface as low as possible such as using low surface energy HX surfaces, may result in an increasing in the contact angle, as shown in Equation 2.5. This may reduce the strength of the interfacial interactions between the brine and the solid surface, making it difficult for water molecules to attach to the HX surface and form ice on it.

Various substances can alter the surface tension of a liquid (Mullin, 2001; Pegram & Record, 2007; Si et al., 2022). This change depends on the molecular attraction within the liquid and is determined by how molecules are attracted to each other in a specific liquid (Kolasinski, 2020; Mullin, 2001). Surfactants, for example, attract each other weakly. When these compounds are introduced in liquid, some of their molecules move to the interface of water, forming a layer of weakly attracted molecules at the interface.

Then it reduces the surface tension of the liquid. This helps substances, such as paint, to spread easily and adhere to solid surfaces. On the other hand, inorganic salts such as NaCl and Na_2SO_4 can increase the surface tension of a liquid (Faust & House, 2018; Si et al., 2022). This is because inorganic salts exist as ions in a solution, and the attraction between these ions and the water molecules pull the surface water molecules into the bulk solution (Kolasinski, 2020; Marcus, 2016; Pegram & Record, 2007). When combined with the hydrogen bonding that already exists between water molecules, additional force is exerted onto the water molecules at the surface, increasing the surface tension of the solution. The force exerted on the water surface molecules increases with as the concentration of these ions increases (Si et al., 2022).

Figure 2.4 shows how NaCl salt affects the surface tension of water, and its interfacial interactions with a solid surface. Si et al. (2022) shown that the presence and concentration of inorganic salts such as NaCl, Na_2SO_4, $CaCl_2$, NH_4Cl, and $NaHCO_3$ influences the surface tension of water, ultimately affecting the contact angle between the salt solution and the coal surface. Pure water showed a lower contact angle on the solid surface, indicating poor wettability. However, adding NaCl salt caused ions to bond with water molecules, increasing the contact angle, as a result reducing wettability of the solid surface.

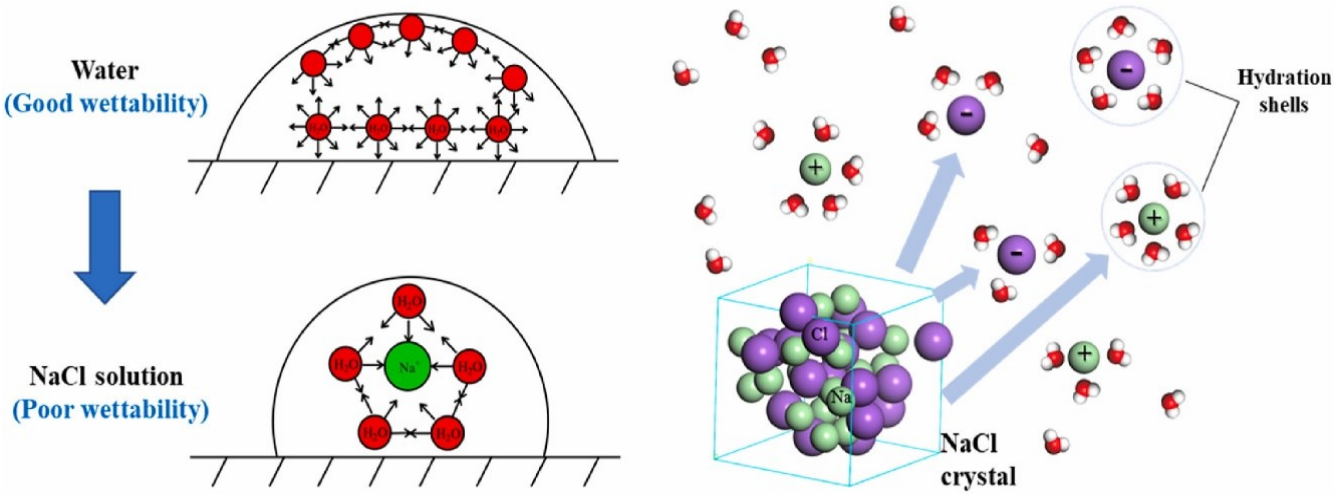

Figure 2.4: Effect of inorganic salt on surface tension (Si et al., 2022).

Industrial brines treated in FC and EFC typically contain dissolved inorganic salts at varying concentrations, the strength of interfacial interactions between these brine solutions and HX surface of the crystallizer may vary. These variations could lead to different behaviors in ice scaling on the HX surface of the crystallizer.

2.4 Secondary Nucleation

Secondary nucleation is the formation of new crystals nuclei because of the presence of existing crystals in a solution. Unlike primary nucleation, which occurs spontaneously, secondary nucleation is induced by interactions between the existing crystals and the surrounding supersaturated solution. This process is especially important in industrial crystallization because it offers control over the crystallization process by adding seeds into a supersaturated solution (Aspeling et al., 2020; Benz, 2020; Mullin, 2001). For instance, introducing ice seeds into a supersaturated brine solution initiate ice crystallization by providing surfaces for water molecules to deposit, ensuring controlled growth (Mullin, 2001).

Secondary nucleation can be categorized into three main types: true, apparent, and contact secondary nucleation. True secondary nucleation occurs at low supersaturation when subcritical nuclei survive and trigger nucleation through dendritic or polycrystalline breeding (Mullin, 2001). Apparent secondary nucleation occurs when small fragments are dislodged from the surface of a crystal and reintroduced into the solution. Known as initial or dust breeding, this process is particularly prominent in industrial crystallization systems (Lewis et al., 2015). Contact nucleation, also referred to as collision breeding, is the most impactful mechanism, driven by crystal collisions with each other or with vessel surfaces, influenced by operational parameters (Benz, 2020).

The energy barrier for secondary nucleation is significantly lower than that of primary or heterogeneous nucleation due to the presence of existing crystals (Aspeling et al., 2020; Lewis et al., 2015). These crystals act as templates, reducing the energy required to form new nuclei by eliminating the need for critical nucleus formation. For instance, the presence of ice seeds in a supersaturated solution facilitates rapid and controlled nucleation by providing stable sites for molecular deposition. In contrast, heterogeneous nucleation, though it also reduces the energy barrier compared to homogeneous nucleation, requires stabilization through external surfaces or interface defects (Lewis et al., 2015). This additional stabilization makes heterogeneous nucleation less efficient in systems with abundant seed crystals.

In industrial water crystallization systems, such as those involving heat exchangers (HX), secondary nucleation principles are critical in addressing ice scaling (Mittal & Choi, 2020b; Spencer et al., 2022). Ice scaling can occur when ice fragments detach due to collisions, re-enter the solution, and promote further growth (Motsepe et al., 2022) . This leads to the accumulation of a scale layer on HX surfaces, reducing their effectiveness in cooling the bulk solution. While introducing sufficient ice seeds can promote bulk nucleation by lowering the energy barrier, addressing ice scaling requires more than delaying heterogeneous nucleation (Spencer et al., 2022). It is also necessary to control the growth of the scale layer, as its thickness

determines the rate at which HX surfaces become covered, thereby impacting overall system efficiency (Hasan et al., 2017).

In conclusion, secondary nucleation plays a vital role in crystallization by significantly reducing the energy barrier and enabling controlled crystal growth (Aspeling et al., 2020; Yazdanpanah & Nagy, 2020). However, in industrial applications like water crystallization, managing both nucleation and the subsequent growth of crystal layers is also essential to optimize performance and mitigate challenges such as ice scaling.

2.5 Crystal Growth

Crystal growth occurs after the formation of a stable nuclei and can be defined as a deposition of solute or solvent molecules onto an existing crystal surface (Benz, 2020; Mullin, 2001). Ice growth on the surface of a solid surface, such as a HX surface, can be a planar growth, growing normally from the HX surface, as shown in Figure 2.5 (Pronk et al., 2006). This type of growth of ice on a subcooled heat transfer from a dilute electrolyte (salt) solution involves three main steps as described by Mullin (2001): Mass transfer involves the movement of solutes away from the growing ice crystal surface to the bulk to allow growth. Heat transfer of the heat of crystallization from the growing ice-solution interface to maintain the supersaturation of the ice with respect to its solubility. Surface Integration of water molecules into the ice lattice structure.

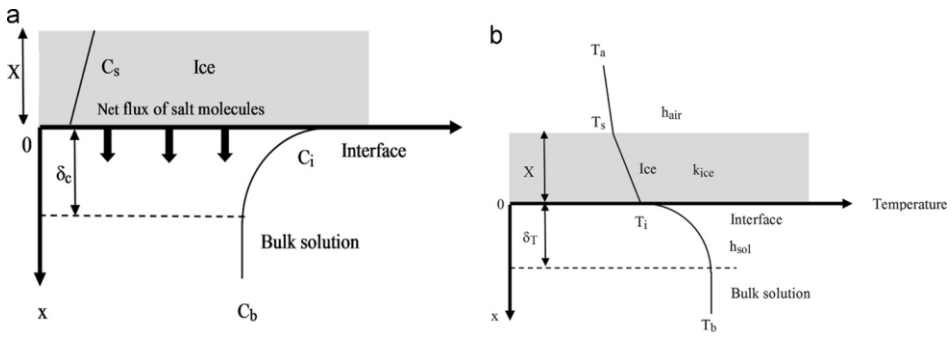

Figure 2.5: A schematic representation of both the concentration (a) and temperature(b) profiles during ice crystallization by natural freezing from solution (Hasan & Louhi-Kultanen, 2015).

Any of the three steps involved in the growth of an ice layer on cooled heat transfer surface could be the limiting factor. However, Hasan and Louhi-Kultanen (2015) and Pronk et al. (2006) reported that in ice crystallization, surface integration kinetics are generally faster due to smaller molecular size of water molecules. Thus, heat transfer and mass transfer are the main factors that affect the growth rate of ice.

In the case where growth of ice is dominated by the heat transfer from its surface to the bulk solution, its growth rate can be represented, as shown in Equation 2.7. The heat transfer resistance is conductive because the heat of crystallization is transferred through the ice layer to the HX of surface of the crystallizer (Pronk et al., 2006; Yazdanpanah & Nagy, 2020).

$$G = \frac{k_{ice}}{\rho_{ice} X_{ice} \Delta h_{fusion}} (T_i - T_s) \qquad \text{Equation 2.7}$$

k_{ice} (W/m·K) represents the thermal conductivity, ρ_{ice} (kg/m^3) is the density of ice, T_i (˚C) and T_s(˚C) is the temperature at the ice-liquid interface and is the temperature at the wall, Δh_{fusion} is heat of fusion of ice. The growth of ice under these conditions is being limited by only the difference between the temperature at the interface (T_i) and the heat transfer surface of the crystallizer. This generally occurs in pure water systems.

In electrolyte solutions, the growth of ice involves the bulk diffusion of hydrated ions or solvent molecules to the ice front, and the counter-diffusion of rejected ions away from the ice-solution front, as shown in Figure 2.5. This creates a stagnant ion-rich layer, called diffusion boundary layer, at the ice front, denoted by "δ_C" in Figure 2.5. As a result, this slows the diffusion of water molecules from the bulk solution to ice interface, thus affecting its growth rate (Mullin, 2001). This phenomenon can be described as transport of water molecules through a semi-permeable membrane (diffusion boundary layer), and can be modelled, as shown in Equation 2.8. (Pronk et al., 2006).

$$G = \frac{dm}{dt} = \frac{k_d}{C_b} \frac{\rho_{solution}}{\rho_{ice}} \frac{M_{H_2O}}{M_{solution}} (C_i - C_b) \qquad \text{Equation 2.8}$$

Here k_d is the mass transfer coefficient (m/s), C_b and C_i (wt.% or g/L) is the solute mole concentration in the bulk solution and ice-solution interface, ρ_{ice} and ρ_{liquid} (Kg/m^3) are the density of ice and liquid respectively, M_{H_2O} and $M_{solution}$ (kg/kmol) are the molar mass of water and solution respectively. In this case, the concentration of the solutes affects the growth rate of ice.

Kapembwa et al. (2014) noted that in pure water system, the growth rate of ice is mainly governed by heat transfer from the ice-solution interface to the bulk solution. However, in electrolyte solution, the growth rate is governed by both the mass transfer and heat transfer. Interestingly, Pronk et al. (2006) found that above 1 mol% solute concentration, the mass transfer resistance mainly governs ice growth, as shown in Figure 2.6. This relationship was modelled using a combination Equation 2.7 and Equation 2.8.

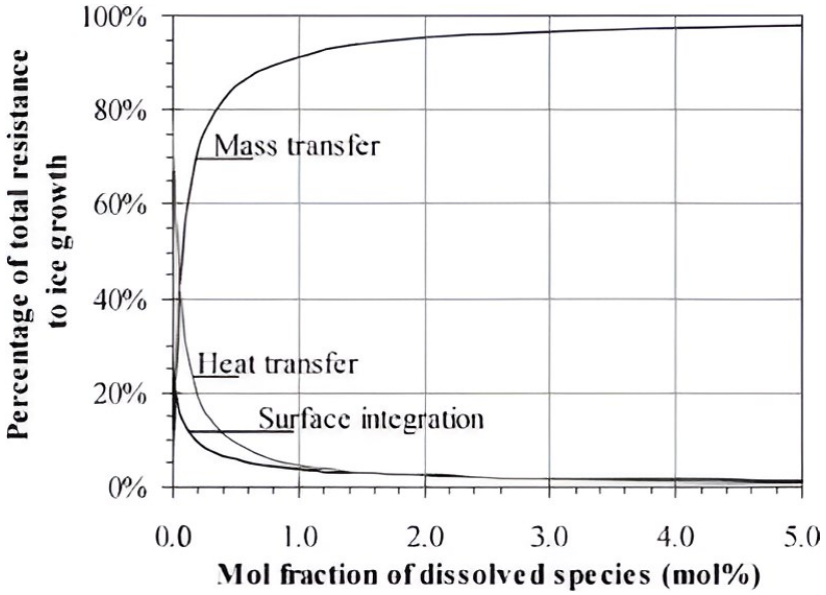

Figure 2.6: Contributions to the resistance to the growth of ice crystals on the wall for NaCl solutions for a total temperature difference of 1.0 K (Pronk et al., 2006).

Since industrial brines are generally electrolyte solutions at varying concentrations, this suggests that the growth of ice in this brine may be limited by either mass transfer or heat transfer from bulk solution the growing ice front. For example, brines from coal mining-impacted water treated by Randall et al. (2011) had a TDS of 27 g/L, whereas the ones treated by Dondo et al. (2022) had a TDS level of 46 g/L , as shown in Table 2.3.

Table 2.3: The concentration of the major species in brines studied by Randall et al. (2011) and Dondo et al. (2022).

Species	Na	K^+	Ca^{2+}	Mg^{2+}	SO_4^{2-}	Cl^-	NO_3^-	Study by:
Concentration	6 700	1 810	1 340	75	16 000	955	398	Randall et al. (2011)
(mg/L)	6 300	550	1 000	6 700	29 800	2 300	-	Dondo et al. (2022)

However, these brines have significantly higher concentrations than that of Pronk et al., 2006, suggesting that the growth of ice from these brines will likely be governed by mass transfer. Although the growth of ice from industrial brines, such as by Dondo et al. (2022), may be limited by mass transfer, the extent to which mass transfer affects it may depend on the concentration of the brine. For example, the brine treated by Dondo et al. (2022) had a higher TDS level by 41% than that of Randall et al. (2011), suggesting that it could have relatively a greater resistance to mass transfer. As result, it slows the growth rate of ice scale layers on HX surfaces and overall ice formation from the bulk solution. A slower growth rate of ice scale layers can result in low amounts of ice scale layers covering the HX surface, thereby prolonging the

availability of crystallizers. Therefore, understanding and controlling solute concentration is crucial in managing ice scaling on HX surfaces in EFC and FC applications.

It should however be noted that growth of ice scale layer is not the only factor that contributes to the ice scaling and is affected by solute concentration and solute type. Adhesion of ice crystals from the bulk solution can also contribute to the ice scaling. Thus, the following section will focus on ice adhesion.

2.6 Physical mechanism of Ice Adhesion

In the context of EFC, the adhesion of ice affects the formation and accumulation of ice scale layers on heat exchanger (HX) surfaces. Ice crystals suspended in the crystallizer can adhere to the HX surface, contributing to the growth or initiation of ice scale layers. Weaker adhesion between the HX surface and ice facilitates the removal of ice scale layers by scrapers or the force exerted by the flowing brine solution (Chatterjee et al., 2023; Matsumoto et al., 2010; Mittal & Choi, 2020b). This detachment can prolong the availability of ice-scale-free HX surfaces, thereby extending production time. Thus, to mitigate strong adhesion of ice to the HX surface, it is essential to understand the mechanisms by which ice crystals adhere to solid surfaces and the factors influencing these interactions.

Adhesion is a physical process that involves covalent bonds, van der Waals forces, and electrostatic interactions. The chemical bonding theory of adhesion describes the development of covalent, ionic, or hydrogen bonds across the interface that are unique to the nature of the contacting medium and act over very short distances of 0.1-0.2 nm. Water molecules or ice can strongly adsorb on some surfaces, whereas others have no affinity Van der Waals forces, on the other hand, act across longer-range across all types of materials. However, it was discovered that van der Waals forces were not the primary cause of adhesion in these cases. According to electrostatic theory, when two metals contact, electron transfer forms an electrical double layer, which creates attractive forces. This theory, proposed by Stoneham and Tasker in 1985, indicates that the presence of charge layers on the surface of ice, depending on the contact conditions, may lead to higher adhesion due to electrostatic forces (Petrenko & Whitworth, 2002). Thus, the adhesion process is governed by the interactions of three forces, covalent, van der Waals, and electrostatic, whose dominance varies based on the specific materials and conditions involved.

(Petrenko & Whitworth, 2002); Ryzhkin and Petrenko (1997); (Vaessen et al., 2002) discovered that different ions had different abilities to screen the ice surface, decreasing the partial positive charge and, as a result, the adhesive ability of ice on the HX surfaces to varying degrees. Given that the brines treated in EFC often contains impurities and at varying concentrations, this suggests that adhesion of strength of ice

onto HX surface may differ, leading to different amounts of ice crystals adhering to or delaminating from the HX surface.

2.7 Heat transfer in EFC crystallizers

Heat transfer is fundamental to the EFC process, which is driven by lowering the solution temperature below freezing point, inducing supersaturation, and removing the heat of crystallization from the solution (Chivavava et al., 2014; Yazdanpanah & Nagy, 2020). Previously, eutectic crystallizers cooled the solution directly with the coolant, but this approach was abandoned due to contamination of the crystals and equipment. Indirect cooling was then adopted. In indirect cooling EFC, heat is transferred from the solution to the cold HX surface of the crystallizer through forced convection. Subsequently, this heat is conducted through the wall and transferred to the coolant, as shown in Figure 2.7 (De Goede & De Jong, 1993; Hasan et al., 2017).

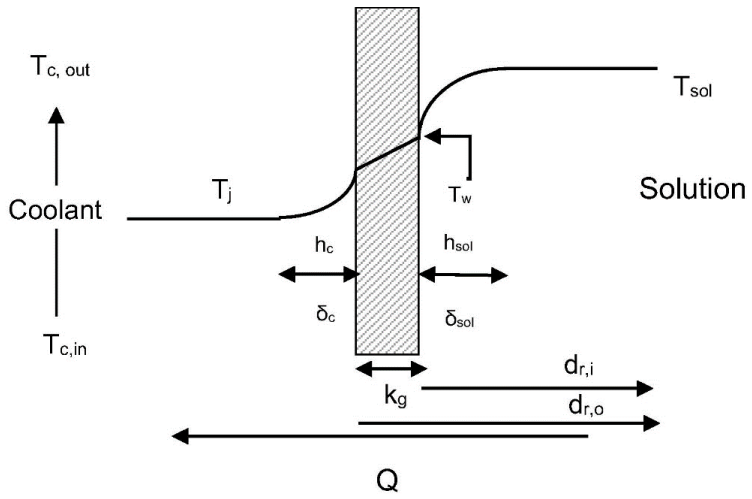

Figure 2.7: Temperature profile across a heat exchanger surface, showing the temperatures of both inlet and outlet coolant inside the jacket side and the average temperature of bulk solution in the crystallizer (Hasan et al., 2017)

In a continuous cooling crystallization process the sensible heat of the feed brine solution and heat of crystallization are both transferred to the coolant. Furthermore, there is also heat gained by coolant from the environment, hence crystallizers are insulated to minimize that. The total heat removed from the bulk solution to the coolant can be estimated using Equation 2.9.

Equation 2.9

$$Q = \dot{q}\rho_{coolant}C_{p,coolant}\left(T_{coolant,out}-T_{coolant,in}\right) = U_{overall}UA\Delta T_{LMTD}$$

Where, Q(W) represents the total heat transferred to the coolant from both the environment and the solution, $\dot{q}(m^3/s)$ is the volumetric flow of the coolant, $\rho_{coolant}$ (kg/m^3) is the density of the coolant, $C_p(J/kg\cdot K)$ is the specific heat capacity of the coolant, $T_{Coolant,\ out}$ and $T_{Coolant,\ in}$ (˚C) are the inlet and outlet temperature of the coolant, respectively, $U_{overall}(W/m^2\cdot K)$ is the overall heat transfer coefficient $(W/m^2\cdot K)$ across the crystallizer, A (m^2) is the area of the heat transfer surface, and ΔT(˚C) is the temperature difference between the solution and the coolant. The heat transfer in this study was in a co-current flow, and its "ΔT(˚C)" term can be expressed as shown in Equation 2.10.

Equation 2.10

$$\Delta T_{LMTD} = \frac{\left(T_{Coolant,out} - T_{Solution,out}\right) - \left(T_{Coolant,in} - T_{Solution,out}\right)}{\ln\left(\frac{T_{Coolant,out} - T_{Solution,out}}{T_{Coolant,in} - T_{Solution,out}}\right)}$$

Where, $T_{coolant,\ in}$, $T_{coolant,\ out}$, $T_{solution,\ in}$, $T_{solution,\ out}$ represent the temperatures of the inlet coolant flow, outlet coolant flow, inlet solution flow and outlet solution flow, respectively. The overall heat transfer coefficient (U) across the crystallizer can be described using Equation 2.11. It quantifies the efficiency of the heat exchange between these mediums, which in this case are the solution, heat transfer surface of the crystallizer, and the coolant.

Equation 2.11

$$\frac{1}{U_{overall}} = \frac{1}{h_{coolant}}\cdot\left(\frac{d_{outer}}{d_{inner}}\right) + \frac{d_{outer}\ln\left(\frac{d_{outer}}{d_{inner}}\right)}{2k_{wall}} + \frac{1}{h_{solution}}$$

Here, $h_{solution}$ and $h_{coolant}$ $(W/m^2\cdot K)$ show the individual heat transfer coefficients of the bulk solution side and coolant side, respectively. d_{inner} (m) and d_{outer} (m) are the inner and outer diameters of the tube wall (m) between the solution side and coolant side, while k_w is the thermal conductivity of the material of the tube wall. The degree of thermal resistance that each medium gives to heat transfer is measured by heat transfer coefficients. The lower the resistance, the greater the heat transfer between two mediums, for example, between solution and coolant. When an ice scale layer forms on the HX surface of the crystallizer, additional thermal resistance is added to the heat transfer from the solution to the coolant. This consequently lowers the heat transfer rate because ice has a comparatively poor thermal conductivity (2.2 W/m· K) in comparison to that of the commonly used material of construction, such as SS316 (12-45 W/m·K), for HX surfaces (Vaessen et al., 2004; Yazdanpanah & Nagy, 2020). The impact of this additional thermal resistance induced by ice scale layer on the overall heat transfer coefficient can be represented using Equation 2.12.

$$\frac{1}{U_{overall,scale}} = \frac{1}{U_{overall}} + \frac{1}{h_{scale}} = \frac{1}{U_o} + \frac{dscale}{2k_{scale}}$$ Equation 2.12

Where h_{scale} (W/m^2·K) is the heat transfer coefficient of the scale layer. The reduction in the overall heat transfer coefficient makes the cooling between the solution and coolant to be inefficient. As less heat is removed from the solution, the temperature of the solution increases, reducing the degree of supersaturation. Consequently, decreasing the overall productivity of the crystallization process (Vaessen et al., 2004). Figure 2.8 exemplifies this phenomenon, showing the overall heat transfer coefficient and temperature profile across the fluidized bed crystallizer over time, with and without the ice scale layer on a heat transfer surface.

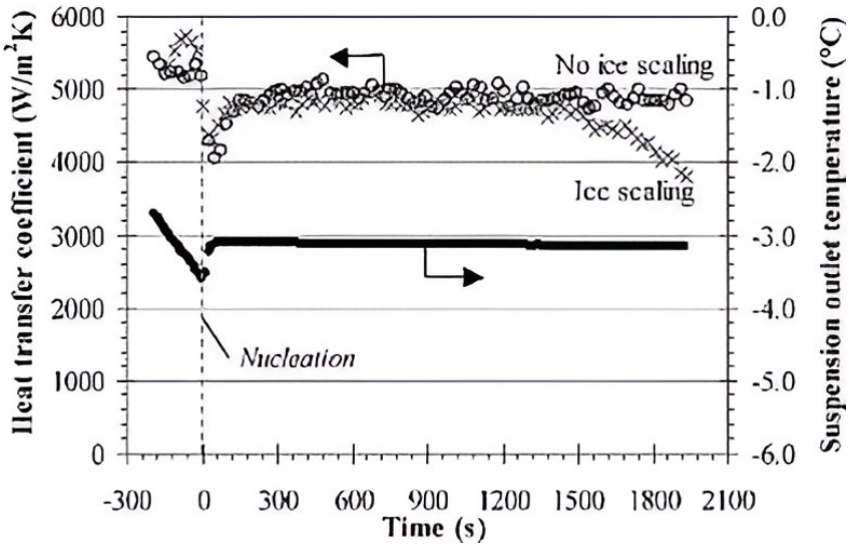

Figure 2.8: Heat transfer coefficients profile across a fluidized bed during ice crystallization from a 5.0 wt.% sodium chloride solution (Pronk et al., 2006).

As seen in Figure 2.8, the overall heat transfer coefficient remains constant when there is no ice scaling. However, in the presence of ice scaling, there is a decline in the heat transfer coefficient due to increased thermal resistance. Therefore, minimizing the formation of ice scale layers on heat transfer surfaces is crucial to maintain desired heat transfer coefficient over extended periods, consequently improving efficiency and productivity of the crystallization process.

3. Literature Review

3.1 History and applications of Eutectic Freeze Crystallization (EFC)

Extensive research has demonstrated the feasibility of using eutectic freeze EFC to treat a wide range of wastewater streams (Ting et al., 2024). EFC dates back to the 1950s when Nelson and Thompson investigated the crystallization of salt from seawater, as it was reported by Ting et al. (2024). Then other researchers further explored EFC and discovered that gradual cooling and seeding efficiently separated salt solutions into two solid phases. Stepakoff et al. (1974) then proposed using continuous EFC for treating brines through direct cooling. However, this method was abandoned due to product contamination, resulting in further research to improve EFC (Ting et al., 2024).

van der Ham et al. (1998) re-initiated EFC research using cooling disk column crystallizer to recover $NaNO_3$ and Na_2SO_4 salts. Ma et al. (2022) studied the recovery of $NiSO_4$ and $CoSO_4$ hydrates from aqueous metal sulfate solutions. The feasibility of EFC of using EFC to recover potable water and other pure salt products from coal mine wastewater streams has also been investigated (Aspeling et al., 2020; Chivavava et al., 2014; Hasan et al., 2017; Lewis et al., 2023; Lewis et al., 2010; Randall et al., 2011; van der Ham et al., 1998). Lewis et al. (2010) for example, demonstrated the recovery of nearly pure (99%) $Na_2SO_4.10H_2O$, $CaSO_4.5H_2O$ and potable water from wastewater stream generated by reverse osmosis at the EMalahleni Water Reclamation Plant (EWRP), through several stages. Himawan et al. (2006a) also shown the recovery of $MgSO_4.7H_2O$ and ice from a $MgSO_4$-industrial stream generated from flue gas desulphurization. Later Aspeling et al. (2020) demonstrated the recovery of several salts ($MgSO_4.7H_2O$ and $Na_2SO_4.10H_2O$) and ice a single stage from a multicomponent aqueous solution, similar to industrial brines. Recently, Dondo et al. (2022) demonstrated the recovery of $Na_2SO_4.10H_2O$ from a multicomponent brine generated by reverse osmosis at Tweefontein Water Reclamation Plant (TWRP).

Given the challenges faced by South African coal mine operations regarding the treatment and management of brines, EFC presents a potential solution. Employing EFC as a treatment method for brines generated from coal mines may not only treat these brines but do so in a sustainable manner. Bibliometric analysis of EFC research conducted by Ting et al. (2024) revealed that EFC is a sustainable solution for treating saline wastewater compared to other methods. EFC also has the potential to achieve zero liquid discharge, as it was shown by Randall et al. (2011), converting 99% of liquid waste stream from RO plant into potable water and viable salt products. This demonstrates the significant potential of EFC recovering various salts and potable water from wastewater streams from South African coal-mine operations, which are currently producing large volumes of brine solutions on an industrial scale.

Despite the potential benefits of EFC for the wastewater treatment industry, several challenges have hindered its industrial implementation. One of the major challenges is the formation of ice scale layers on the HX surface of eutectic freeze crystallizers. The formation of an ice scale layer on a HX surface is undesirable because ice has a relatively low thermal conductivity, i.e., 2.14 W/m·K (Hasan et al., 2017). This then reduces the cooling rate between the refrigerant and the brine suspension in the crystallizer by reducing the overall heat transfer coefficient and in turn, productivity (Spencer et al., 2022; Vaessen et al., 2002). Hasan et al. (2017) reported that the ice scaling reduced the heat transfer coefficient by a factor of 10-20. Spencer et al. (2022) also reported that the formation of ice scaling reduced the heat transfer between the heat transfer surface and the bulk solution by 68%. These reductions emphasize the need for controlling and mitigating the ice scaling in EFC processes. However, the studies did not specify the thickness of the ice layer under which these reductions were observed, and since thicker ice layers result in higher thermal resistance, this makes it more difficult for heat to transfer. Despite this lack of specific detail, their results clearly demonstrated that ice scaling can significantly reduce the heat transfer coefficient.

In EFC, cooling generates supersaturation, which drives the crystallization process (Chivavava et al., 2014; Lewis et al., 2023; Spencer et al., 2022). Therefore, reducing ice scaling is crucial to maintaining the desired heat transfer coefficient over extended longer periods. This ensures that the required cooling is continuously applied, which in turn promotes and maintains supersaturation for longer duration, facilitating crystallization. Maintaining these conditions is important for improving the overall efficiency of the freeze crystallization process. Addressing ice scaling is key to improving the performance implementation of EFC in industrial applications.

3.2 Methods of mitigating ice scaling

Numerous approaches have been explored to reduce the severity of ice scaling in FC and EFC processes (Ting et al., 2024). This includes using mechanical scrapers to remove the ice scale layer from the heat transfer surface of a crystallizer. While mechanical scrapers can partially mitigate the severity of ice scaling, their complex design, susceptibility to mechanical breakdown, high investment and maintenance costs limit their application on an industrial scale (Hasan et al., 2017; Stamatiou et al., 2005). Pronk et al. (2006) investigated the use of liquid-solid fluidized bed heat exchangers as an alternative to scraped wall crystallizers. Their findings demonstrated a reduction in ice scaling and improved heat transfer efficiency, but this approach required an additional step for the recovery of ice and salt from the solution.

Hasan et al. (2017) showed that ice scaling could be minimized from a 4 wt.% Na_2SO_4 aqueous solution without using scrapers by selecting suitable operating conditions. Their findings showed that operating at lower temperature driving forces can delay the onset of ice scaling. In addition, they showed that increasing

mixing intensity can also delay the onset of ice scaling as it disrupts the build-up of supersaturation near the HX surface.

Expanding upon the understanding of ice scaling behavior during EFC within the same brine system and using non-scraped crystallizer, Motsepe et al. (2022) explored the effect of surface properties of HX material of a crystallizer on ice scaling. Ice scaling on stainless steel (SS316), aluminum (Al), copper, and brass, with properties shown in Table 3.1, was studied using in-situ and in real-time differential interference contrast (DIC) optical method.

Table 3.1: Properties of the metals used by Motsepe et al. (2022).

Material	Surface Energy (mJ/m^2)	Roughness (Rq)
Copper	50	63.6±6
Al	48	18.5±4
Brass	35	69.6±9
SS316	40	120.5±3

The results showed that brass, which has low surface energy, showed the highest anti-scaling performance, as shown in Figure 3.1.

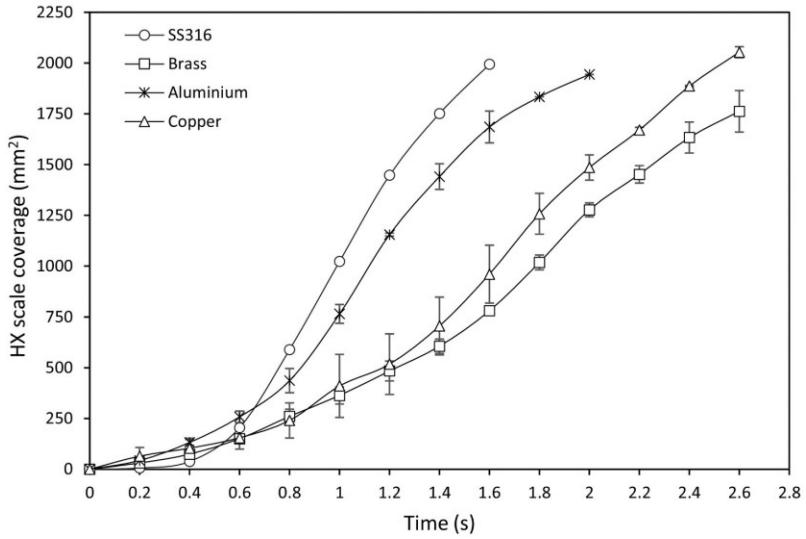

Figure 3.1:The cumulative ice scale layer coverage on different HX materials at comparable heat fluxes. (Motsepe et al., 2022).

This was attributed to low wettability of the brass HX surface, therefore reducing the strength of solution-solid material interactions. These findings align with findings from previous work by Benz (2020); (Fitzner et al., 2015; Förster et al., 1999; Kazi et al., 2015; Lupi et al., 2014; Zou et al., 2011). SS316 had faster ice

scale coverage than Al and this was attributed to its rougher surface than Al. This resulted in ice scaling being predominantly through nucleation due to providing more nucleation sites for ice scaling.

These findings suggest that it is important to minimize both the surface energy and roughness to reduce ice scaling. Thus, smooth HX materials with low surface energy have the potential to reduce ice scaling in continuous EFC of industrial brines. Although brass has a lower ice scaling tendency compared to the studied HX materials, it has a higher surface energy (35 mJ/m^2) (Motsepe et al., 2022) and rougher surfaces than most polymer composite materials, such as PP-GR (surface energy of 22.4 mJ/m^2) (Lewis et al., 2023). Therefore, the following section will identify polymer composite HX materials that have the potential to reduce ice scaling in industrial brine EFC applications.

3.3 Effect of surface chemistry of HX materials of construction on ice scaling

Polymer composite materials are among the HX materials that have both lowest surface energy and lowest surface roughness (Cevallos et al., 2012; Schilling et al., 2022). The reduction in surface energy increases the contact angle between the solid surface and liquid, lowering strength of the interfacial interactions (Memon et al., 2020; Zou et al., 2011). As widely understood, the reduction in interfacial interactions increases the total free energy required for the formation of heteronuclei (Lupi et al., 2014; Motsepe et al., 2022; Mullin, 2001), which in EFC would be the initiation of the ice scale layer. Furthermore, the reduction in surface roughness limits the number of locations where liquid molecules can adhere, reducing the possibility of heterogenous nucleation (Förster et al., 1999; Motsepe et al., 2022). Thus, this suggests that polymer composite materials as HX materials for EFC crystallizers can limit ice scaling by inhibiting heterogeneous nucleation and adhesion of ice, ultimately reducing the severity of scaling on HX surfaces.

Schilling et al. (2022) studied crystallization fouling on heat exchanger tubes made of Polypropylene Graphite (PP-GR), Polyphenylene Sulfide Graphite (PPS-GR), Polyphenylene Sulfide Graphite Modified (PPS-GR-M) and stainless-steel (Duplex), as shown in Figure 3.2. The term “trd” in Figure 3.2 refers to the surface-treated tubes. Fouling induction periods for polymer composite materials (PPS-GR-M, PPS-GR, PP-GR) and stainless steel were 9.9, 10.4, and 15.7 and 1.9 hours, respectively. Furthermore, the asymptotic fouling resistance was higher for SS316 than for PPS-GR and PPS-GR-M, and it was the lowest for the PP-GR tube. The low fouling tendency in polymer composite materials was attributed to their low surface energy and smooth surface, which resulted in low strength of the interfacial interactions between the solid surface and $CaCO_3$/$CaSO_4$ solid particles. Accordingly, polymer composite materials may be potential alternatives to common HX materials in heat transfer applications, such as SS316, for FC and EFC applications. However, a major drawback of polymer novel composite materials is their relatively low

thermal conductivity (0.1-3 W/m·K),(Schilling et al., 2022). Nevertheless, these polymer composite HX materials have potential to significantly reduce the ice scaling in EFC applications.

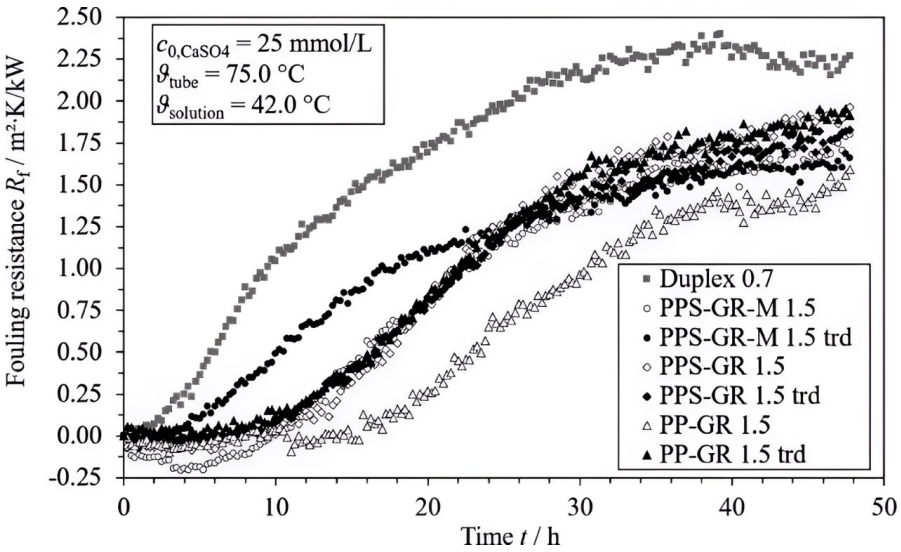

Figure 3.2:Fouling resistance of different tube materials with $CaSO_4$ solution in the stirred vessel test rig, (Schilling et al., 2022).

Lewis et al. (2023) recently extended on the existing polymer materials research by evaluating the feasibility of using graphite (PP-GR) as a HX material in freeze crystallization of a multicomponent brine, dominated by NaCl. The study compared the scaling mechanisms of ice on the HX surface of PP-GR tube to commonly used HX materials, such as Al and SS316. The findings showed that PP-GR delayed the formation of ice scale layer 77% and 79% longer than Al and SS316, respectively, as shown in Figure 3.3.

These findings are similar to those reported by Schilling et al. (2022), in which PP-GR delayed fouling longer than SS316. Lewis et al. (2023) also observed that the ice nucleated on the HX surface of Al did not delaminate, and continued to grow, whereas on SS316, ice scale layers would delaminate into the bulk solution. The delamination of ice scale layers from a HX surface can increase the availability of the HX surface cooling, ultimately increasing the production time.

Lewis et al. (2023) attributed the differences in ice scaling mechanisms and induction times to the variations in the surface energies of the materials. The Al has a surface energy of 48 mJ/m^2, SS316 has 40 mJ/m^2 and PP-GR has 22.4 mJ/m^2. It is believed that the higher surface of Al material facilitated stronger attraction of water and ice molecules to its surface, lowering the changes of delamination, and resulting in faster ice scaling rates. Zou et al. (2011) showed that the adhesion strength of ice on surfaces with higher surface energy tend to be stronger. This may support the observations by Lewis et al. (2023) on low probability of delamination and faster ice scaling rates on high surface energy materials.

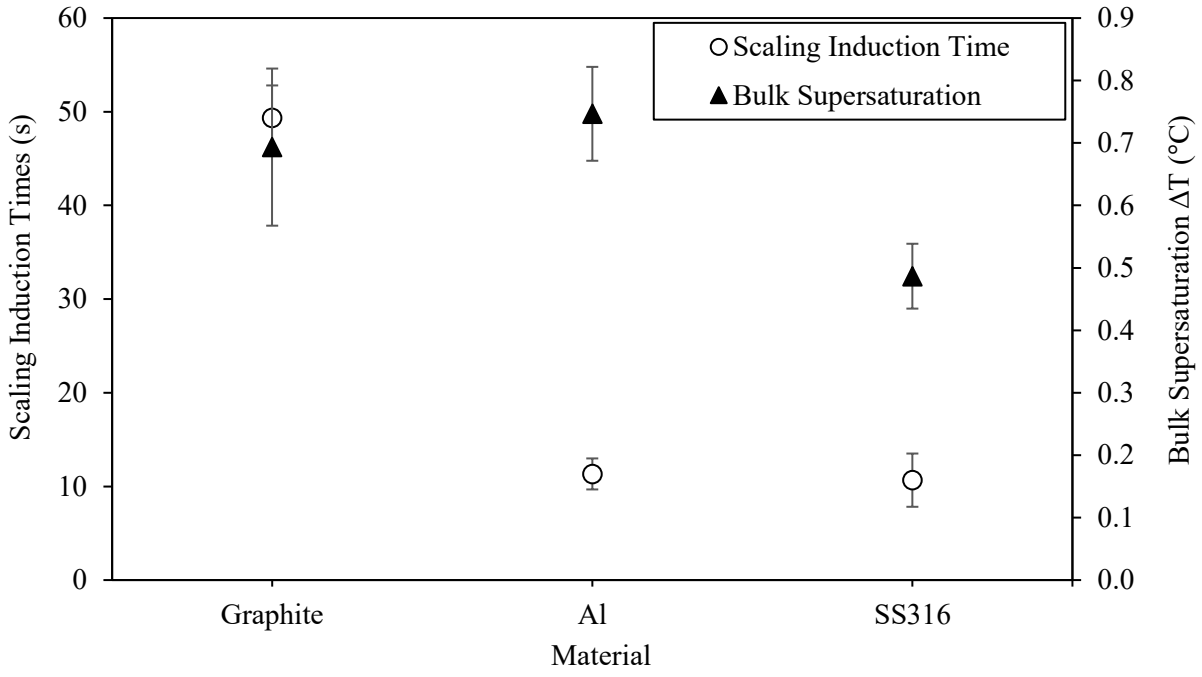

Figure 3.3: Ice scaling induction times and bulk supersaturations for different HX materials *(*Lewis et al., 2023*)*.

Although Motsepe et al. (2022) did not measure the adhesion strength of ice, their findings showed that the material with the lowest surface energy, brass (35 mJ/m^2) had the lowest scale coverage over time compared to other materials such as SS316 (40 mJ/m^2), and copper (50 mJ/m^2). These studies align with the findings from the ongoing research, Förster et al. (1999); (Kazi et al., 2015; Memon et al., 2020; Motsepe et al., 2022; Schilling et al., 2022; Zou et al., 2011), on modifying the surface properties of HX materials to reduce scaling. Thus, it can be concluded from the studies that extensively investigated scaling on different materials that low surface energy can resist or delay the formation of scaling. Therefore, PP-GR was selected as the HX materials for freeze crystallization applications in our study due to having low ice scaling tendency.

3.3.1 Influence of contact angle on ice formation on solid surfaces

Liu et al. (2017) investigated the ice patterns on solid surfaces with different wettability as shown in Figure 3.4. The contact angle between ice and the hydrophilic materials was 14.5° and hydrophobic was 107.3°. Although ice nucleation was allowed to occur at the same time and temperature, the ice growth patterns differed based on the contact angle. On the material with a lower contact angle, it was observed that the growth of ice was along the surface, whereas on the material with a higher contact angle, it was off surface. The growth along the surface shows stronger affinity between water and material. It also indicates that the rate at which this material will be covered by ice will be higher. In EFC, this would lead to a significant

reduction in heat transfer rate between the HX surface and brine solution. The growth off surface shows weaker attraction between the material and ice, meaning this ice scale layer could be removed easily by scrapers or a moving solution, reducing the accumulation of ice on the HX surface. These findings show that the contact angle can change which direction the ice crystal grows in.

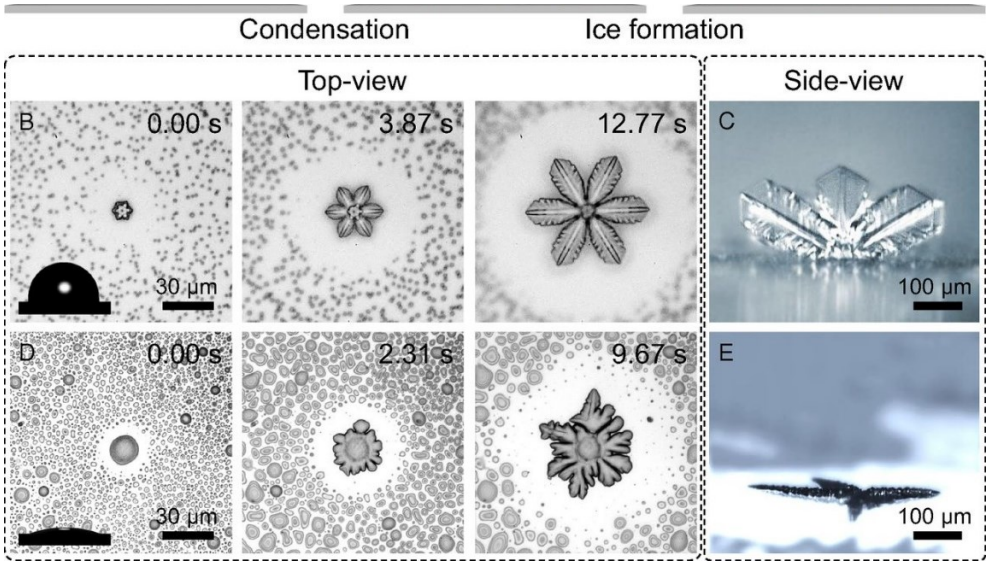

Figure 3.4: Two ice growth modes on hydrophilic(D & E) and hydrophobic surfaces (B and C), with contact angles of 14.5 and 107.3, respectively (Liu et al., 2017)

Given that solute concentration can affect the contact angle between water and a solid surface, it can be suggested that treating brines with varying solute concentration can lead to different ice scaling behaviors. Thus, it is hypothesized that as the concentration of inorganic salts in brines increases, ice scaling is going to grow normal to the surface due to reduced interfacial interactions between the brine and the HX surface, making it prone to delamination.

3.4 Influence of brine chemistry on ice scaling

Using scaling resistant HX materials in EFC processes alone will not mitigate the scaling altogether. This is because crystallization on a solid interface is also a function of solution chemistry. The formation of ice or attachment of water molecules on a solid surface is determined by the hydrogen bonds between the water molecules, and by water-solid interfacial interactions (Benz, 2020; Fitzner et al., 2015; Lupi et al., 2014). These interactions determine the layering and ordering of water structures that are formed at the solid interface (Kolasinski, 2020). Furthermore, these interactions depend on the chemistry of solid surfaces and the surface tension of water. Since the surface properties of the HX surface are fixed in this study, only the

properties of the solution that influence the formation of water structures at the interface of a solid surface will be reviewed.

3.4.1 Influence of impurities on interfacial water structures during ice formation

When inorganic salts dissolve in the water, ions become solvated (Faust & House, 2018; Kolasinski, 2020; Marcus, 2009, 2016). These solvated ions influence functional roles in charge screening or transporting, influencing the kinetics of ion-water and water-water hydrogen bonding (HB) breaking, as well as structural relaxation in aqueous solutions. The orientation and characteristics of hydrogen-bonded networks near the interface have a significant impact on the chemical and physical attributes of water (Kolasinski, 2020). The unique effects of ions on water structure have been characterized by "structure-making" and "structure-breaking", which are also applied to explain a variety of phenomena in electrolyte systems. Chu et al. (2024) studied the influence of ions on the solid-liquid transition behavior at different temperatures as shown in Figure 3.5.

It was observed that ions affected the behavior of water differently. The fraction of ice-like water increased in the following order: $Zn(ClO_4)_2 < ZnBr_2 < ZnCl_2 < ZnSO_4$, showing that SO^{-2}_4 is a better water structure-maker than other ions (Chu et al., 2024). This can also be explained by using electric field induced by the solvated ions, which can affect the rearrangement of dipolar water molecules, ultimately affecting the formation of ice (Kolasinski, 2020; Petrenko & Whitworth, 2002; Ryzhkin & Petrenko, 1997). On molecular level, Deshmukh et al. (2013) investigated the influence of chloride ion concentration on the structure of water near its interface. At low concentrations, ordered structures, unlike typical bulk water, were formed. Interfacial water layers exhibited a high degree of translational order, indicating mobility of water molecules. However, with increased concentration, a decrease in translational order was observed, accompanied by a loss of ordering of water molecules near the interface.

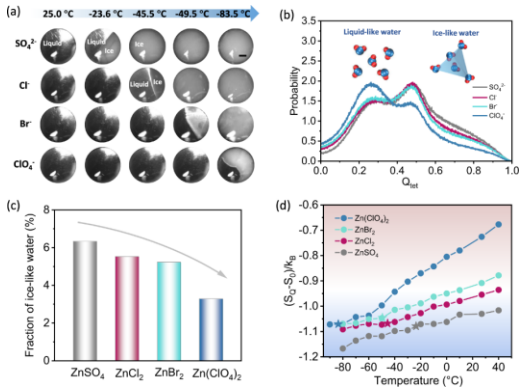

Figure 3.5: Optical microscopic observations of four electrolytes. b) the probability distributions of the tetrahedral order for water molecules in electrolytes, and the schematic models of liquid-like and ice-like

water. c) a fraction of ice-like water for four electrolytes. d)tetrahedral entropy of water molecules in the four electrolytes (Chu et al., 2024).

Near the solid surface interface, the translational and vibrational movements of water molecules, as well as hydrogen-bonded networks, encountered hindrance or restriction (He et al., 2009). Poor interfacial water layers on a solid surface can delay or affect the formation of ice scaling. This phenomenon can be partially explained by the findings of Zhang et al. (2021), who used molecular dynamics (MD) simulations to study ice formation on solid surfaces in the presence of various solutes (NaF, NaCl and NaBr). Their results showed that the number of water molecules incorporated into ice was higher in NaCl and NaBr compared to NaF system as shown in Figure 3.6. Additionally, the solutes were found to uniquely influence the structure and dynamics of ice formation.

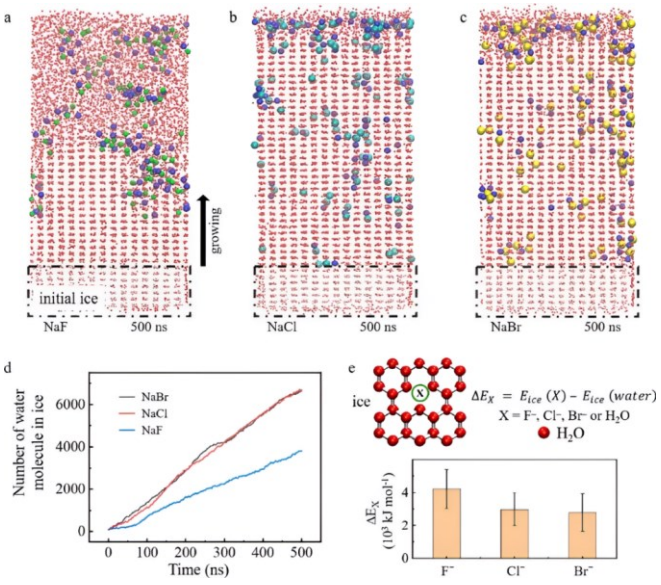

Figure 3.6: Snapshots of Molecular dynamics simulations for ice growing in NaF, NaCl, and NaBr solutions at 245 K (Zhang et al., 2021).

These findings highlight the importance of solute type and concentration in industrial brines, which this thesis examines as factors affecting ice scaling. The unique interactions between solutes and water molecules near solid surfaces can either promote or disrupt the formation of structured water layers necessary for ice nucleation (Deshmukh et al., 2013; Faust & House, 2018; He et al., 2009; Z. He et al., 2016; Kowacz & Putnis, 2008; Marcus, 2009; Shi et al., 2023). For example, ions like NaCl may stabilize these water layers, facilitating ice scaling, while others like NaF or similar ions to those typically found in industrial brines may hinder it. These behaviors are important for understanding and mitigating ice scaling in heat exchanger systems under varying brine.

3.4.2 Influence of solute concentrations and solute type on contact angle

It is widely known that the contact angle between the water liquid droplet and the solid surface, such as HX surface, affects the formation of ice on those solid surfaces (Liu et al., 2017; Mullin, 2001). This contact angle can be affected by several factors such as temperature, surface properties of the HX surface, solute concentration and solute type (Al-Zaidi & Fan, 2018; Gribanova et al., 2016; Liu et al., 2020). For this study, the focus was on the influence of solute concentration and type due to its relevance in industrial brines, which are known to have varying solute concentrations and type.

Si et al. (2022) demonstrated that increasing inorganic salt concentration led to higher contact angle between the solid surface and liquid phase, resulting in low contact area between the surface and liquid phase. Although their study was not focused on the formation of scale layering, their findings provide insight into how salt concentration can affect the interfacial interactions between a solution and a solid surface. Al-Zaidi and Fan (2018) also observed that as the concentration increased the contact angle increased. It was also observed that the extent to which the contact angle increased was different for various ions. The increase in contact angle as the concentration increased was attributed to the increase in surface tension of the liquid induced by the increase in the concentration of ions. Industrial brines contain a variety of salts at varying concentrations. This variation can affect the interfacial interactions between the brine and the HX surface. It is thought that as the strength of interfacial interactions is affected, the energy required for nucleation to occur on a particular solid surface is also affected as described by Table 2.2.

3.4.3 Influence of impurities on ice adhesion

In the context of EFC, the adhesion of ice plays a critical role in the formation and accumulation of ice scale layers on heat exchanger (HX) surfaces. Ice crystals suspended in the crystallizer can adhere to the HX surface, contributing to the growth or initiation of ice scale layers. Impurities can affect the properties of the ice-solid surface significantly, consequently impact the strength of ice adhesion (Mittal & Choi, 2020b). According to several researchers like (Petrenko & Whitworth, 2002), (Chatterjee et al., 2023), the presence of impurities in a solution or on the surface of ice adhesion strength. This is can be explained by the properties of the liquid layer formed at the interface of ice-solid surface (Jha et al., 2016; Mittal & Choi, 2020b). Ice surfaces are thought to have melted layers around them, known as quasi-liquid layers (QLL), which play a role in ice growth and its interactions, such as adhesion, with foreign surfaces. The term "quasi-liquid layers" refers to the liquid film layer on the surface of an ice crystal that shows properties similar to those of a liquid, as seen in Figure 3.7(B) (Asakawa et al., 2016; Mittal & Choi, 2020a; Petrenko & Whitworth, 2002). These layers are thought to play a role in the adhesion strength between solids.

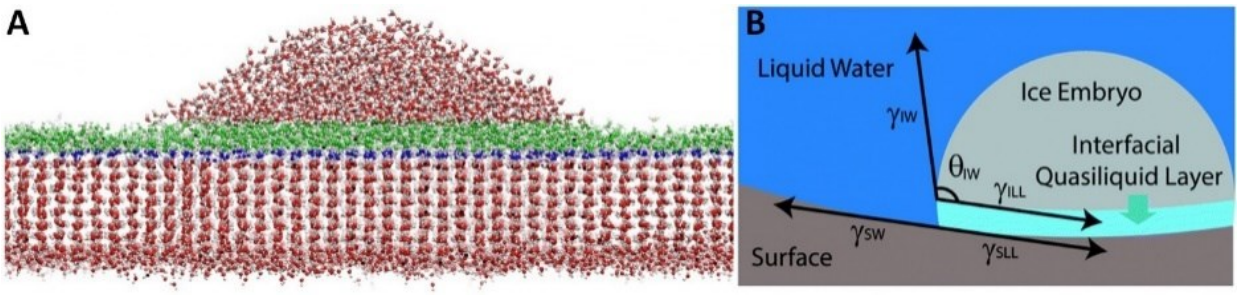

Figure 3.7: a) Pre-melting QLL at the ice-water interface; b) Heterogeneous nucleation showing ice embryo and interfacial QLL (Jha et al., 2016).

The presence of quasi-liquid layer on ice surfaces was first explained by Faraday that when two ice cubes are brought into contact, they fused (Mittal & Choi, 2020b). It was concluded that this was based on the quasi-liquid layer that exists on the surface of ice. Other researchers like Thomson and Reynolds expanded on further on this layer (Mittal & Choi, 2020b). Jameson proposed the pressure melting theory to explain the phenomenon of ice skating. The presence of this layer on the ice reduces the frictional force of ice, hence ice skating is possible. It is believed that this quasi-liquid layer on the surface of solid surface plays a role in the adhesion of ice to other solid surfaces (Jha et al., 2016; Memon et al., 2020; Ryzhkin & Petrenko, 1997; Y. J. Zhang et al., 2022). Several studies including those by Asakawa et al. (2016) and Y. Zhang et al. (2022) have also shown that ice has this quasi-liquid layer on its surface. It is assumed that the thicker this layer is, the lower the friction force between the surface and ice, suggesting weaker adhesion. The thickness of this layer affects the solid-solid contact between surfaces. With an increase in the thickness of this layer, the lesser the contact (adhesion) is between the ice surface and the foreign surface (Mittal & Choi, 2020b).

Several studies, such those conducted by Chatterjee et al. (2023), reported that the presence and concentration of impurities can cause and affect the thickness of this quasi-liquid layer on the surface of ice, thereby affecting the adhesion strength of ice. Although not directly related to the quasi-liquid layer, Petrenko and Whitworth (2002) and Vaessen et al. (2002) found that different ions have varying abilities to screen the ice surface, reducing the partial positive charge and, as a result, the adhesive force of ice on the cooled wall varying extents. Given that the brines treated in EFC often contains impurities and at varying concentrations, this suggests that the adhesion strength of ice onto HX surface may differ, leading to different amounts of ice crystals adhering from or delaminating from the HX surface, Therefore, understanding how solute type and solute concentration influences ice scale formation and growth through adhesion on various HX materials is also crucial for effectively reducing ice scaling in EFC processes.

3.4.4 Effect of solute concentration on ice scaling induction time

Leyland et al. (2019) studied the influence of solute concentration on ice scaling induction time in a Na_2SO_4-H_2O system. The scaling induction time in their study was defined as the period between the initial ice nucleation and the onset of ice scale layer on the HX surface. It was observed that as the concentration of various solute types, $CaSO_4$, $MgSO_4$, and NaCl, increased the ice scaling induction time was prolonged, as shown in Figure 3.8.

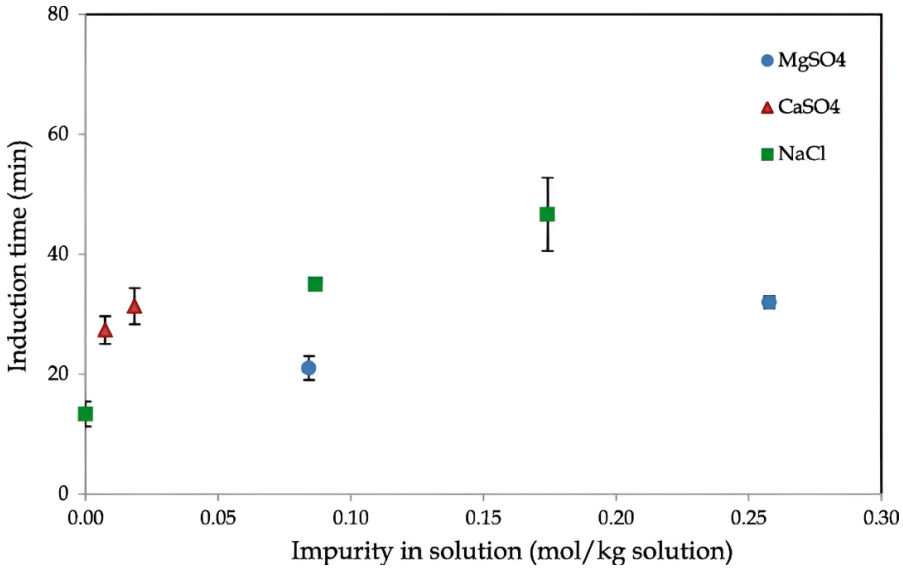

Figure 3.8: Induction time for the ice scale layer formation at varying impurity content in a binary Na_2SO_4 solution (Leyland et al., 2019).

The ice scaling induction time for the NaCl solution increased from just under 40 minutes to more than 40 minutes after the concentration was increased from 0.019 to 0.17 mol NaCl/kg, while it increased slightly for $MgSO_4$ when the concentration was increased from 0.08 to 0.26 mol /kg solution. The increase in induction time observed between 0.01 mol and 0.02 mol $CaSO_4$/kg brines was statistically insignificant when considering the error bars. However, this could also result from the limited concentration range examined. Expanding the concentration range in future studies may help determine if a significant variation in induction time emerges with increasing concentration.

For $MgSO_4$, a slight difference in induction time was observed between a concentration of 0.08 to 0.26 mol/kg as shown in Figure 3.8. This limited difference could be attributed to higher temperature driving forces, which may overshadow the influence of concentration on ice scale formation. Therefore, conducting such studies under lower temperature driving forces might provide more insight into concentration-dependent behavior of induction time. Additionally, the extent to which induction time increased with

increase in solute concentration appeared to depend on the nature of solute. Nevertheless, the results suggested a general trend where the induction time for ice scaling demonstrated potential for increase as the concentration was increased.

Leyland et al. (2019) attributed the increase in induction time for ice scale formation on the HX surface as the solute concentration increases to an enhanced mass transfer resistance to water molecules moving from the bulk to the water-clusters forming on the HX surface. Electrostatic interactions are also thought to increase at higher impurity concentrations. Vaessen et al. (2002) also observed a similar trend, where the induction time for ice scaling from electrolyte solutions (HNO_3 and $CaCl_2$) on a scraped surface increased as the concentration increased. It is believed charges of ions in solution can induce ice adhesion effects as it was described by (Ryzhkin & Petrenko, 1997). At higher concentrations, the electrostatic interactions between ions and the surface of ice become stronger, reducing the adhesion abilities of ice.

Ice forms by rejecting foreign ions to the bulk solution, resulting in the formation of water clusters (Mullin, 2001). The attraction between the ions and water molecules result in the formation of a liquid layer rich in ions surrounding the developing water clusters (Zhang et al., 2021). Ions around these water clusters have the ability to lower the freezing point of water (Vrbka & Jungwirth, 2005; Wan et al., 2021), which may delay the formation of ice. At higher concentrations, the presence of ions around the forming water clusters may increase, consequently delaying the formation of ice scaling. However, there could be other reasons for the influence of ions on ice heterogenous nucleation. For instance, when the concentration of the solutes in a brine increases, the surface tension also increases. The strength of interfacial interactions between the brine and the HX surface could decrease with increasing surface tension, consequently delaying the formation of ice scaling on a HX surface. Nonetheless, the concentration of ions does affect the induction time for ice scaling. It should be emphasized, however, that the amount of ice scale layer on a HX surface is not determined solely by the induction time for ice scaling. Growth also influences the amount of ice scale layer forming on a HX surface.

3.4.5 Effect of solute concentration on crystal growth

Understanding the growth rates and mechanisms of ice on HX surfaces is essential as higher growth rates of ice scaling indicate that the heat transfer rate would decrease faster possibly resulting in downtimes. On the other hand, slower growth and coverage of ice scale on HX surface may extend the availability of crystallizers, potentially increasing the production time (Motsepe et al., 2022). Thus, using appropriate brine solutions with ice scaling resistant HX materials may significantly prevent ice scaling from covering the entire HX surface. Solute concentration is one of the parameters that affect the growth rates of ice (Matsumoto et al., 2012; Zhang et al., 2021). Since industrial brines contain solutes at varying

concentrations, it is important to investigate how the changes in solute concentrations influence the growth rate of ice scaling, and crystallization.

Matsumoto et al. (2012) studied the growth of ice on a solid surface over time at a varying solute concentration (10 wt.%, 20 wt.%, 22.5 wt.%, 30 wt.%, and 35 wt.%) of trehalose solution, as seen in Figure 3.9.

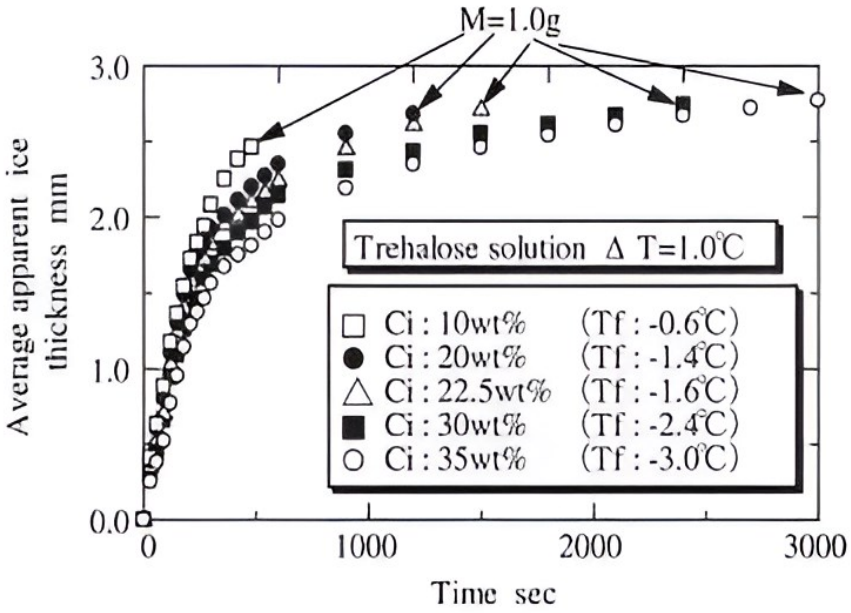

Figure 3.9: The relationship between time and average apparent ice thickness from trehalose solution with a varying concentration *(*Matsumoto et al., 2012*)*.

Figure 3.9 shows that although the ice layer on the solid surface formed approximately around similar times within 500s, the time it took for these ice layers to reach a mass of 1.0 g differed with the concentration of the solution. The trehalose solution with concentrations of 10 wt.%, most dilute, reached a mass of 1.0 g, within 500s, which was faster than the trehalose solutions with concentrations equal to/above 30 wt.%, reaching the same mass of ice after 2 500s. This suggests that the rate at which this ice layer grew over time decreased as the concentration of trehalose increased. Such phenomenon can be attributed to the increase in the mass transfer induced by the solutes to transport water molecules to the surface of a growing front of ice layer, as it was explained by Pronk et al. (2006). This is based on a widely accepted theory that solutes must diffuse away from the from interface of ice to allow growth. However, due to the diffusion of solutes away from the ice layer, a liquid layer rich in these solutes form around the ice-brine interface. This liquid layer can interfere with the incorporation of water molecules into the ice crystal lattice, affecting its growth rate (Kapembwa et al., 2014).

On a molecular level, Zhang et al. (2021) simulated the growth rate of ice from NaF solution with different concentrations at varying temperature driving forces. The findings showed that, under similar temperature driving forces, the growth rate of ice from NaF solution with a higher concentration was always the slowest. The high presence of rejected foreign ions near the ice-solution interface reduced growth rates of ice. This was thought to have slowed the incorporation of additional water molecules into the ice crystal lattice. The study by Pronk et al. (2006) found that in NaCl solutions with varying concentrations, the growth of the ice scale layer is influenced by mass transfer, especially at higher concentrations, compared to heat transfer and surface integration.

Stocking and King (1976) observed that in highly concentrated sucrose solutions, the rate of crystal growth decreased due to increased viscosity caused by high concentrations of sucrose. This may apply to $MgSO_4$ brine solutions, which have higher viscosity at higher concentration. Although Hasan and Louhi-Kultanen (2015) investigated ice layer growth in dilute (1 wt.%, 2 wt.%, 3 wt.%, and 4 wt.%) Na_2SO_4 solutions, they observed that for all values of temperature driving forces, the growth of ice layer decreased linearly over time as the concentration was increased. However, for a 4 wt.% Na_2SO_4 solution, the growth rate of the ice layer did not decrease significantly after freezing time of 5 hours. This was attributed to the simultaneous crystallization of salt and ice. It appears that increasing the concentration of the non-crystallizing component has a significant effect on ice growth. Once other components start to crystallize out, their influence on the growth of ice is limited. Meewisse and Ferreira (2003) observed a similar phenomenon in which NaCl reduced the ice scaling over a specific range of concentrations, but this effect began to diminish at the eutectic point due to NaCl crystallization. This suggests that, while increasing solute concentration may decrease the ice scaling growth, eutectic solutions may show different ice scaling behavior.

3.4.6 Effect of solute concentration on ice adhesion strength

The presence of ions or solutes can also influence the behavior of ice by affecting the adhesive properties of ice surface via screening of the surface charge of ice which reduces both its partial positive charge and adhesive force of ice to the surface (Chatterjee et al., 2023; Chernyy et al., 2014; Jha et al., 2016; Metya & Singh, 2018; Petrenko & Whitworth, 2002; Ryzhkin & Petrenko, 1997; Y. Zhang et al., 2022). Ice crystals from bulk solution can adhere to HX surfaces, contributing to ice scaling, due to attractive forces between these HX surfaces and the ice surface. This phenomenon was observed by Lewis et al. (2023) whereby PP-GR only scaled through adhesion of ice crystals from the bulk whereas other HX materials scaled through heterogenous nucleation. Thus, since PP-GR will be used in the EFC of brines with different impurities, the adhesion strength between ice scale layer and the PP-GR may vary, ultimately affecting the amount of ice crystals that may adhere and accumulate on this HX material.

Boinovich et al. (2022) described the influence of solute on adhesion strength, stating that accumulation of solutes at the interface of ice and solid may affect the ice adhesion strength. It has also been proposed that a thin layer of disordered ice, known as the quasi-liquid layer (QLL), forms next to a surface when the water freezes and plays an essential role in the adhesion strength of ice. Vrbka and Jungwirth (2005) demonstrated that at low concentrations more ordered water layers than normal bulk water formed at the interface. However, at higher concentrations the water layers on the surface of ice were disordered. Disordered water layers on the surface of ice result in low adhesion strength. Thus, this suggests that high concentrated brine may induce disordered water layers on the surface of ice, resulting in low adhesion strength of ice. As a result, the ice scale layers formed from higher concentrated brines may have low adhesion strength, subsequently be prone to delamination.

Chatterjee et al. (2023) studied the influence of concentration of several impurities (salt, surfactant, and solvent) on the adhesion strength of ice on three different solid surfaces; copper, glass, silicon, as shown in Figure 3.10.

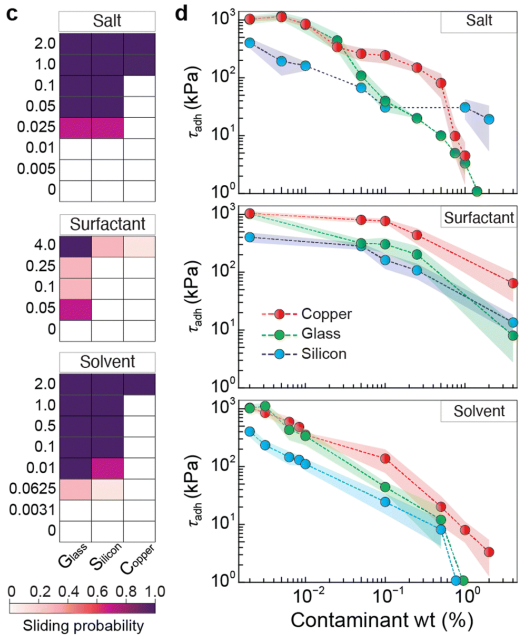

Figure 3.10: Adhesion strength of impure ice on surfaces. (c) Probability of the failure mechanism of contaminated ice on variations *(*Chatterjee et al., 2023*)*

As seen in Figure 3.10, Chatterjee et al. (2023) observed that as the concentrations of the impurities were increased, the adhesion strength of ice decreased. Interestingly, at low solute concentrations (< 0.031 wt.% solvent, < 0.05 wt.% surfactant, < 0.01 wt.% salt) the adhesion strength of ice was extremely strong, showing no sliding probability. However, as the solute concentration increased, the sliding behavior was

observed. The loosened frozen ice was covered in a thin liquid film. This was attributed to the presence of QLL on the surface of ice, which was induced by high concentration of ions around the surface of ice. This liquid layer is said to lubricate the ice surface, consequently reducing the coefficient of friction, which possibly results in reduced adhesion strength (Mittal & Choi, 2020a).

To understand how solute concentration affects the adhesion strength through liquid-like layer, Chatterjee et al. (2023) conducted further investigations using simulations to evaluate the influence of concentration on the thickness of liquid-like layer on the surface of ice. The results showed that the thickness of the liquid-like layer increased as the concentration of NaCl increased. It is believed that abundance of solutes at the ice-solution interface disrupted the hydrogen-bond networks of water molecules and their lifetime. This then caused the order-to-disorder transition of hexagonal ice into bulk-like water, which prompted shorter hydrogen bonding lifetime, which was thought to have influence on the adhesion strength of ice. The presence of solutes at the interface of ice-solution seems to affect the properties of the liquid layer between the interface of ice and solid surface, which in turn affects the adhesion strength of ice. Furthermore, an increase in impurities in this layer may lower the surface tension of the liquid around ice, resulting in less contact between the ice and the foreign surface as was reported by Kolasinski (2020). Nonetheless, this shows that the presence of the liquid-like layer on the surface of ice affects its adhesion strength.

Although there are different explanations for how concentration affects adhesion strength, it is widely agreed that increasing the concentration reduces the adhesion strength of ice. The low ice adhesion strength may be beneficial for EFC processes as these ice scale layers could be removed easily from the HX surface by the moving brine solution, increasing the availability of crystallizers. This could also be beneficial for processes that use mechanical scrapers as the scraping force needed to remove the ice scale layers from a HX surface may be reduced. This is supported by the findings by Matsumoto et al. (2012), where it was observed that scraping force required to remove the ice scale layer from a the HX surface decreased as the solute concentration (10, 20, 22.5, 30 and 35 wt.%) was increased. However, above the concentration of 22.5 wt.%, the scraping force required remained nearly constant. Nonetheless, the increase in solute concentration has been shown to reduce the ice adhesion strength.

3.4.7 Effect of solute type on ice scaling induction time

Randall et al. (2011) showed that South African industrial brines from coal mines can contain various ionic species, such as Mg^{2+}, Na^{+}, K^{+}, Ca^{2+} and Cl^{-}. Treating such brines with variations in types of solutes can lead to different behaviors in ice scaling during EFC. This is because impurities can influence the layering, stability, and adhesive properties of water structures through electrostatic interactions. These interactions affect how ice forms on solid surface (Asakawa et al., 2016; Benz, 2020; Fitzner et al., 2015; Kowacz &

Putnis, 2008; Memon et al., 2020; Metya & Singh, 2018; Pegram & Record, 2007; Ryzhkin & Petrenko, 1997; Si et al., 2022; Vaessen et al., 2002). Mullin (2001) showed the colloidal materials, such as gelatin, can suppress nucleation in electrolyte solutions, while surfactants promote the formation of ice nuclei. The promotion of ice heterogenous nucleation by surfactants is attributed to the reduction of surface tension of the liquid at the solid-liquid interface, increasing the contact area between the solid and liquid phase. In the case of liquid water resting on a cold solid surface, increasing the contact area may reduce the energy needed to form ice, provided that the liquid is at or below its freezing point. Conversely, certain impurities or solutes may decrease the contact area between the water molecules and a foreign solid surface, resulting in poor wettability, ultimately hindering ice heterogenous nucleation.

Although a study by Si et al. (2022), did not study ice heterogenous nucleation, it was shown that various inorganic salts affected the contact area between salt solution and coal surface. Since the contact area between surface and liquid phase plays an essential role in heterogenous nucleation, it can be suggested that the presence of inorganic salts like $MgSO_4$, NaCl, and so on, in brines could influence ice heterogenous nucleation during EFC of coal-impact impacted waters. Such phenomenon was observed by Leyland et al. (2019) whereby introducing small quantities of impurities in the Na_2SO_4-H_2O system delayed the formation of ice scaling, unique to each dissolved ionic impurities. The Ca^{2+} delayed ice scale formation more compared to Mg^{2+} ions although Mg^{2+} was slightly at a higher concentration. This was attributed to Mg^{2+} having a higher charge density, which possibly prevented it from screening the surface of ice, thereby suppressing the effect of Mg^{2+} on scaling behavior. However, it was not reported on these ions affected the scaling before it formed, only after it had formed. There are studies, such as by Chu et al. (2024) and Deshmukh et al. (2013) that report that impurities affect the local ordering of water layers at the interface. This could be used to explain the influence of impurities on ice nucleation.

Z. Y. He et al. (2016) studied the influence of various ions on induction time for ice heterogenous nucleation on polyelectrolyte brush (PB)-water interface at a freezing point of -20 ˚C. Z. He et al. (2016) found that the induction time on ice nucleation in the presence of various cations were in the decreasing order of Ca^{2+} > Mg^{2+}, Gdm^{+}, K^{+}, Na^{+}, Cs^{+}, TMA^{+}, Li^{+} and NH_4^{+}. The Ca^{2+} had a stronger impact on the induction time, attributed to its ability to disrupt the hydrogen-bonded networks at the water interface. For the anions, the delay followed the order of SO_4, F^{-}, Ac^{-}, HPO_4^{2-}, Cl^{-}, Br^{-}, SCN^{-}, NO^{-}_3 and I^{-}. The results align with the findings by Leyland et al. (2019), who also reported that that Ca^{2+} had a greater impact on ice nucleation compared to Mg^{2+}.

However, it is important to note that the aqueous solutions tested by Z. He et al. (2016) were not at equivalent molality, limiting the ability of the study to fully investigate the influence of solute type on ice

formation. Interestingly, Leyland et al. (2019) observed that despite Ca^{2+} having a lower charge density and its solution being at a lower molality, it had more impact on the ice scaling than Mg^{2+}. It is believed that the higher charge density of Mg^{2+} may have inhibited its ability to screen the ice surface, thereby reducing its effect on the scaling behavior. However, it is worth noting that Leyland et al. (2019) investigation involved these ions as impurities in a Na_2SO_4-H_2O brine system, which might behave differently in their own binary systems. Nonetheless, their findings demonstrated that the nature of solutes can affect the formation of ice scaling.

Considering that Mg^{2+} and Na^{+} are dominant cations in industrial brines from SA coal mine operations and have different charge densities, their impact on the formation of ice scaling in EFC of industrial brines is expected to vary. However, in this study, it is hypothesized that brines containing Mg^{2+} will have a greater impact on the formation of ice scaling than those containing Na^{+} ions. This is due to Mg^{2+} having a higher charge density, which allows it to disrupt hydrogen-bonded networks between water clusters more effectively. As a result, delay the formation of ice scaling.

Furthermore, while the aforementioned findings highlight the importance of impurities on ice heterogeneous nucleation, it is equally essential to understand their influence on the growth of ice scaling. This understanding becomes important for continuous processes, where faster growth rates of ice scale layer can lead to shorter production times. Thus, this study aims not only for the heterogenous nucleation of ice but also its growth mechanisms in the presence of various cations, with the focus on Mg^{2+} and Na^{+}.

3.4.8 Effect of solute type on growth and structure of a crystal

Zhang et al. (2021) studied the influence of various cations and anions on the growth rates and shapes of single ice crystals. They first focused on comparing these anions; F^{-}, Cl^{-}, Br^{-} while keeping cation, Na^{+}, fixed, and with pure water at different temperature driving forces. The findings showed that the growth rate of ice was lower in NaF solutions than in NaCl and NaBr solutions, as shown in Figure 3.11. To further under these differences, Zhang et al. (2021) conducted classical Molecular Dynamics (MD) simulations to understand this phenomenon on a molecular level. It was observed that the F^{-} ions were almost rejected to the ice-solution interface during ice growth whereas NaCl and NaBr partly incorporated into the ice crystal. The rejection of F^{-} from the growing ice front led to aggregation of F^{-} molecules around the ice-solution interface, inducing the ice crystal to form hexagonal shapes and slowing the attachment of additional water molecules to surface of ice (Zhang et al., 2021). The rejection of F^{-} from the bulk ice was attributed to higher increase in the potential energy of bulk ice when F^{-} ion was incorporated, suggesting that F^{-} ion was the least likely to be incorporated into ice. However, some studies, such as Astilleros et al. (2003), reported

that the incorporation of impurities into the structure of a crystal can reduce the growth rates by increasing its solubility, thus reducing the step velocity.

Zhang et al. (2021) also observed that in the case of various cations (Na^+, NH_4^+, K^+ and Cs^+), slower growth rates were observed in the cation with a higher charge density, which in this case was NH_4^+, followed by Na^+, K^+ and Cs^+. The Na+ has a higher charge density than K^+. It is believed that cations with higher density charge restrict the rotation and orientation of water molecules near the interface of water structures, slowing their incorporation into the ice lattice. The lower charge densities do not coordinate water dipoles strongly to break water structures, thus have less impact on the stability of water clusters . Sei et al. (2002) observed that trehalose was more effective in reducing the growth rate of ice crystals than sucrose. This was attributed to trehalose molecules binding more on water molecules than sucrose does to water molecules. This probably decreased the incorporation of water molecules into the ice lattice.

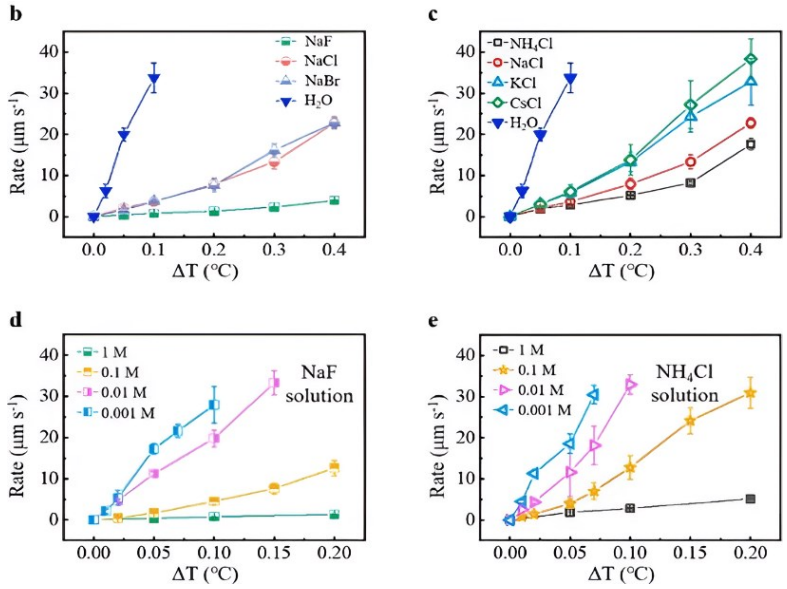

Figure 3.11: Growth of ice crystal from pure water and salt solutions (Zhang et al., 2021)

Matsumoto et al. (2012) also observed different ice growth behaviors on a HX surface from trehalose and Ethylene-Glycol (EG) solutions at a fixed freezing point of -1.6 ˚C. The growth of ice on a solid surface from a trehalose solution was dominantly perpendicular to the HX surface, whereas from the EG solution was dominated by parallel growth. The author did not state the reasons behind the differences in this behavior. Nonetheless, these findings showed that various solutes can lead to different ice growth patterns on an HX surface. These findings show that impurities can affect the growth of the ice scale layer depending on their nature. For instance, Mg^{2+} ions bond more strongly to water molecules than Na^+ ions, suggesting that the resistance to the ice crystal growth may differ for both ions at the equivalent molality.

3.4.9 Effect of solute type on ice adhesion strength

Investigations by Petrenko and Whitworth (2002) indicated that $CaCl_2$ and $MgCl_2$ were more effective than NaCl in reducing ice adhesion due to their ability to create a thicker brine layer and induce a greater disruption in the ice lattice. Organic solutes, such as glycol and ethanol, also affect ice adhesion. These compounds lower the freezing point and disrupt hydrogen bonding, but their effectiveness varies with concentration and type of substrate.

Chatterjee et al. (2023) demonstrated that just a 0.00625 wt.% ethanol aqueous solution could reduce ice adhesion strength on copper surface by up to 50%, whereas for the surfactant solution, concentrations of about 4 wt.% were needed to reduce ice adhesion strength such that it triggers sliding of ice from the copper surface. Chatterjee et al. (2023) attributed the negligible decrease in adhesion strength of ice with increasing surfactant concentration to the decrease in the surface tension that resulted from the attachment of surfactant molecules on the hydrophilic surfaces. Given that the industrial brines contain various solute types, this suggests that some solutes may have significant impact on the adhesion strength of ice scale layer, whereas others may have insignificant impact, leading to variations in the amount of ice scale layer adhering strongly on HX surfaces during freeze crystallization.

Vaessen et al. (2002) studied ice scale formation from electrolyte solutions on scraped surfaces. It was observed that there was dissimilar ice scaling behavior between HNO_3 and KNO solutions. This was attributed to electrostatic forces between the ions and ice surface, causing adhesion effects. It is believed that ions can screen the surface charges on ice, consequently affecting its adhesion abilities. Hence, Vaessen et al. (2002) assumed that the reason HNO_3 had more impact on the ice scaling behavior was that H^+ ions are better capable of screening surface charges on ice than K^+ ions.

Chernyy et al. (2014) studied the influence of ions on the adhesion strength of ice at two temperatures (-10 ˚C, -18 ˚C), as shown in Figure 3.12. These ions were incorporated into the polyelectrolyte brush layers, which was in between the ice layer and glass slide. As seen in Figure 3.12, Li^+ ions recorded a decrease about 70% at -10 ºC, and 40% at 18 ºC, in adhesion strength of ice. Whereas Na^+ ions recorded a decrease of about 50% at -10 ºC. Although ions such as, K^+ and F^- showed a decrease in adhesion strength of ice at temperatures of -10 ºC, they did not have any impact on adhesion strength of ice when the temperature was reduced to -18 ºC. The maximum reduction (25-40%) in ice adhesion strength at -18 ºC was observed by polyelectrolyte brush layers with these ions in this descending order: $Li^+ > Na^+ > Ca^{2+}$.

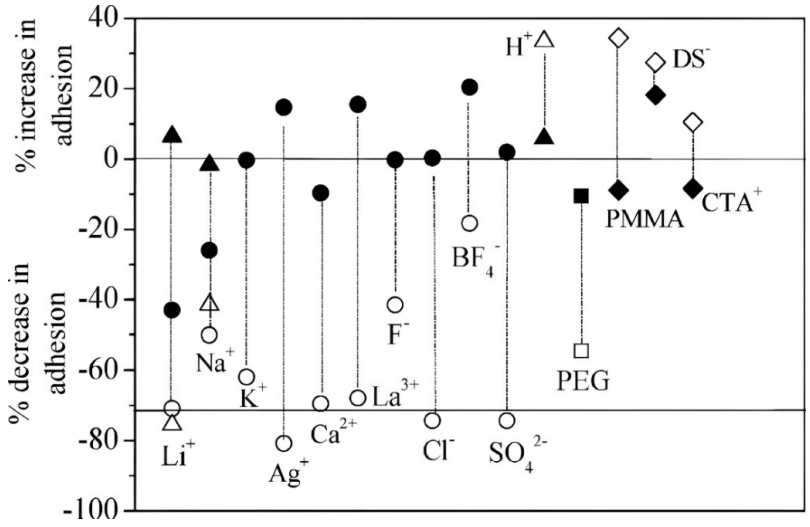

Figure 3.12: Changes in ice-adhesion for different ions incorporated in polyelectrolyte brushes. Filled symbols represent measurements at −18 °C. *(*Chernyy et al., 2014*)*

Ions such as, Li^+, Ca^{2+}, and La^{3+}, are known as structure-breaker ions due to their larger charge density, meaning they tend to disrupt water hydrogen bonds, while ions with lower charge densities such as K^+ and Cl^- with lower charge densities do not coordinate water dipoles strongly to break water structures (Chernyy et al., 2014; Marcus, 2009). Li^+ ions have negative structural entropy of -54 J/K·mol, Na^+ [-14 J/K·mol], suggesting water structure making, whereas Cl^- and SO_4^{2-} have positive structural entropy making them less favorable to stabilize water structures. However, this seems to not have affected ice adhesion strength. Nonetheless, these findings showed that the type of ion can affect the adhesion strength of ice. Thus, since Na^+ and Mg^{2+} ions have dissimilar sizes and charges, their presence during FC and EFC of industrial brines may affect the adhesion strength of ice onto HX surfaces differently, resulting in different amounts of ice accumulated on the HX surface of the crystallizer. Murase and Nanishi (1985) showed low ice adhesion strength on a material containing Li^+ ions. This was attributed to the Li^+ ions having hydrogen bond breaking properties which then disrupt the water molecules on the liquid-like layer on the surface of ice.

Matsumoto et al. (2012) also observed that when comparing trehalose solution with that of EG solution, the scraping force required to remove a specific amount of ice from the HX surface was always greater in EG solution. The authors did not state any reasons for these differences. However, it is thought that these differences were due to the variations in the properties of the liquid-like layer on the surface of ice. The trehalose may have reduced the adhesive properties of ice significantly than EG.

3.5 Summary and Gap Analysis

While EFC has shown the feasibility to treat brines from coal-impacted waters on laboratory scale in SA, its industrial implementation has been hindered by ice scaling (Hasan et al., 2017; Lewis et al., 2023; Leyland et al., 2019; Motsepe et al., 2022; Randall et al., 2011). Ice scaling reduces heat transfer rates in EFC due to its low thermal conductivity, resulting in low availability of crystallizers and decreased ice productivity (Bonales et al., 2017). Therefore, reducing ice scaling is essential to increase the availability of crystallizers and ice productivity.

Several studies such as by Motsepe et al. (2022) have shown that low surface energy HX materials for EFC crystallizers can mitigate ice scaling in EFC of 4 wt.% Na_2SO_4. Furthermore, Lewis et al. (2023) investigated the influence of various HX materials on ice scaling in a NaCl system, reaffirming that smooth HX materials with low surface energy can effectively reducing ice scaling in EFC applications. These findings are supported by extensive research focusing on modifying the surface properties of the HX surfaces to reduce ice scaling (Azimi et al., 2014; Benz, 2020; Fitzner et al., 2015; Förster et al., 1999; Kazi et al., 2015; Lupi et al., 2014; Memon et al., 2020; Schilling et al., 2022; Zettler et al., 2005; Zou et al., 2011). Thus, smooth HX materials with low surface energy materials could potentially reduce the ice scaling in the EFC of brines from coal-impacted waters. It should, however, be noted that employing scale resistant HX materials in EFC processes alone will not eliminate ice scaling. This is because crystallization on a solid interface is also a function of solution chemistry.

Understanding how solute type and concentration influence the ice scaling behavior on smooth HX materials with low surface energy, such as PP-GR, is crucial. This is relevant for industrial brines, which have wide variations in solute types and concentrations. Leyland et al. (2019) and Vaessen et al. (2002) have established that increasing the solute concentration can delay the formation of ice scaling, although only to a certain extent.

Leyland et al. (2019) studied the influence of concentration on ice scaling only up to concentrations of 30 g/L total dissolved solids (TDS), which is very dilute compared to some of the industrial brines produced from South African coal mines, where concentrations can reach TDS of 240 g/L. This suggests that increasing concentration up to TDS these levels can potentially delay the formation of ice scaling further, possibly achieving ice-scale free operations. However, few studies have investigated the influence of concentrated brines on ice scaling tendency in EFC, particularly using a continuous set-up without scrapers. Furthermore, their multicomponent system contained only two different solutes, whereas industrial brines may contain more than 5 different solutes. Therefore, the aim of this study was to investigate the influence

of solute concentration and type on ice scaling formation on the HX surface PP-GR for EFC treatment of local industrial brines with wider range of concentrations and solute type in a non-scraped system.

3.6 Hypothesis and Research Questions

3.6.1 Hypothesis I

It is hypothesized that EFC of brines containing solutes with higher ionic charge density will result in less amount of ice forming on the HX surface during crystallization. This is because solutes with higher charge density bond strongly to the water molecules, limiting the layering of water molecules near the HX surface-brine interface. This affects the ordering of water molecules near the brine-HX surface interface and slows the incorporation of water molecules into the water clusters. Thus, delaying the initiation of ice scaling and subsequently reducing the amount of ice scale layer formed from the EFC of $MgSO_4$ brine than from the Na_2SO_4 brine.

3.6.1.1 Key Questions

- How does the solute with a higher charge density affect the amount of ice scale forming on the HX surface during EFC?
- Does the ionic charge density affect the growth of ice in suspension?
- Is induction time the only mechanism that affects ice scaling in this process?
- How does charge density affect the bulk crystallization of ice during EFC process?

3.6.2 Hypothesis II

It is hypothesized that increasing the solute concentration of the brine will reduce the amount of ice scale layers forming on the HX surface during EFC. This is because the increase in concentration increases the surface tension of the brine. This reduces the strength of interfacial interactions between brine and the HX surface, thus delaying the initiation of ice scaling and subsequently reducing the amount of ice scale formed.

3.6.2.1 Key Questions

- How does the solute concentration affect the amount of ice forming in bulk crystallization?
- Does increasing the solute concentration induce delamination of ice scale layers forming on the HX surface of PP-GR during crystallization?
- How does solute concentration affect bulk crystallization?
- Does extending induction time due to concentration affect bulk crystallization?
- How does concentration affect the production rate of ice?

4. Material and Methods

This chapter provides a detailed methodology used to investigate the influence of both solute type and solute concentration on the HX surface of PP-GR in a continuous EFC process. The chapter is divided into five sub-sections**:** Brine analysis**,** Thermodynamic Simulation, Batch Experiment, Solution Preparation and Continuous FC and EFC experiments.

4.1 Brine Analysis

The industrial brine solution with a Total Dissolved Solids (TDS) of 103 g/L was obtained from the Tweeifontein Water Reclamation Plant (TWRP, referred to here as TWRP 1), which recovers potable water from coal mine wastewater. To obtain brines of varying concentrations, the original brine was pre-concentrated using the cascade method, as described by Randall et al. (2011). resulting in two different brines: referred to here as TWRP 2 and TWRP 3. For precise brine analysis, 50ml samples from each brine were filtered using Avacare 20 ml syringes fitted with 0.22 µm FilterBio Nylon syringe filters to remove any colloidal particles. The analysis of cationic and anionic species from the filtered samples were then conducted using Inductively Coupled Plasma Mass Spectrometry (ICP-MS, ensuring high sensitivity and accuracy in detecting trace elements. The selection of ions for analysis was based on their common presence in brines from South African coal mines. This ensured that the results are relevant for understanding the behavior of industrial brines within the context of EFC. The major ions of interest included Mg^{2+}, Ca^{2+}, Na^{+}, SO_4^{2-}, and Cl^{-}, which are typical of coal mine brines. The concentrations of these ions in the studied industrial brines are summarized in Table 4.1.

Table 4.1: The concentrations of cations and anions of the selected brine solutions for this study.

Species	TWRP 1	TWRP 2	TWRP 3
	Concentrations (mg/l)	Concentrations (mg/l)	Concentrations (mg/l)
Na^{+}	7 354	9 768	10 553
Mg^{2+}	15 853	17 661	20 105
Ca^{2+}	964	984	598
K^{+}	798	1 004	491
Cl^{-}	2290	3 315	4 994
SO_4^{2-}	76 795	89 312	96 781
TDS (mg/L)	103 696	122 044	133 522

The received TWRP brine is mostly composed of cations (Mg^{2+} and Na^{+}) and anions (SO_4^{2-}), as shown in Table 4.1. In addition, the concentrations of the Mg^{2+} and Na^{+} ions are higher than the industrial brines used in studies by Randall et al. (2011) and Dondo et al. (2022), showing that this brine is slightly concentrated. Due to this brine being dominated by SO_4^{2-} ions than Cl^{-} ions, it was assumed that all the Mg^{2+} ions come from the $MgSO_4$, majority of the Na^{+} ions come from Na_2SO_4, and some from NaCl, and all the Ca^{2+} ions come from $CaSO_4$. The brine compositions were estimated the approach detailed in Appendix A.1, and the results are represented in Table 4.2.

Table 4.2: The estimated composition of the species presents in the TWRP brines.

Species	TWRP 1	TWRP 2	TWRP 3
	Concentration (wt.%)	Concentration (wt.%)	Concentration (wt.%)
H_2O	90.5	89.1	88.2
$MgSO_4$	7.1	7.8	8.8
$CaSO_4$	0.3	0.3	0.2
NaCl	0.3	0.5	0.7
Na_2SO_4	1.6	2.1	2.0

The concentration of Na_2SO_4 was less than 3 wt.%, in all three industrial brines, which is lower than the eutectic concentration (3.8 wt.%; (Spencer et al., 2022) of a binary Na_2SO_4 system. The same applies for the $MgSO_4$, which has a eutectic concentration, 15-16 wt.%; (Dondo et al., 2022; Himawan et al., 2006b), of a binary $MgSO_4$ system. These compositions indicate that ice crystallization was expected to occur before any salt crystallization because of the dilute nature of the brine relative to eutectic concentration of identified species in these brines. The estimated compositions of these brines were now used in the thermodynamic modelling in the section below (4.2) to estimate the freezing points of the ice and the identified species in these brine solutions as the temperature is decreased.

4.2 Thermodynamic estimations of ice and salt crystallization temperatures and yields

The OLI Stream Analyzer (V11.5), a thermodynamic modeling software using the electrolyte (MSE) model to calculate the standard thermodynamic properties of aqueous species, was employed to determine the eutectic point of the industrial brines. The predicted freezing temperatures of ice, and the potential salts and their yields on a basis of 1000 g of the TWRP1 brine solution over temperature range of 10 ˚C to -10 ˚C are detailed in section 5. A similar approach was used for these brine solutions; TWRP 2 and TWRP 3 brine, and their results are in Appendix A.2. The results showed that ice would form first due to the dilute nature

of these brines. Thus, this allowed the study to investigate the ice formation exclusively, whether on the HX surface or in suspension, in the absence of salt crystallization.

4.3 Batch Experiments

The batch experiments were conducted to identify the actual freezing point of the sourced industrial brines. These batch experiments were conducted in a 3.5 L glass, jacketed crystallizer, similar to that used by Spencer et al. (2022). The simulation results in section 5.1 were used as the starting point for the freezing points of the investigated brines. More information, such as the temperature profile, during these batch experiments can be found in Appendix A.5.

The temperatures obtained from the batch experiments were used to select appropriate operating conditions, such as the seeding temperature, feed temperature to the crystallizer, during continuous FC and EFC experiments, which is explained into detail in section 4.5. Since this study was also looking into the ice scale formation from binary solutions, synthetic solutions were prepared, and the procedure is detailed in the following section.

4.4 Binary Solutions Preparation

Analytical reagent grade salts, sodium sulphate decahydrate ($Na_2SO_4.10H_2O$) and magnesium sulphate heptahydrate ($MgSO_4.7H_2O$) were obtained from Merck South Africa (Pty) Ltd, and used without any further purification, as their high purity (> 99%) was deemed sufficient for the experimental requirements. All aqueous solutions were prepared using deionized water (conductivity: ≥ 14 MΩ/cm @ 25 ˚C), ensuring minimal contamination from other solutes.

To investigate the effect of solute type and individual solute concentration on ice scale formation on PP-GR, binary synthetic solutions were prepared. Due to low eutectic concentration of Na_2SO_4 system (4 wt.% or 0.613 mol/kg), only the $MgSO_4$ system, with wider concentration (0 wt.% to its eutectic point at 15-16 wt.%, or 1.47 mol/kg), was used for the investigation of solute concentration on ice scale formation. Thus, the effect of solute concentration using binary solutions on ice scaling was investigated using synthetic $MgSO_4$ solutions of 7wt.% (0.613 mol/kg), 12 wt.% (1.13 mol/kg) and 15wt.% (1.47 mol/kg).

The calculations for determining amounts of salts needed to prepare a certain amount of solution are shown in Appendix A.6, and calculations for estimating the concentrations of these solutions in g/L is in Appendix A.4. The resulting aqueous solutions are shown in Table 4.3. Furthermore, the freezing temperatures of these binary solutions were predicted using a similar thermodynamic simulation approach described in section 4.2, and the results are in Appendix A.3 and Appendix A.4.1.

Table 4.3: Composition and the predicted freezing points of the investigated binary synthetic solutions.

Solution	Concentration (wt.%)	Concentration (g/L)	Concentration (mol/kg)	Solution Freezing Point (˚C)
Na_2SO_4	4.00	41.67	0.613	-1.20
	7.00	75	0.613	-1.20
$MgSO_4$	12.9	148	1.130	-2.30
	15.0	176	1.47	-3.20

Although the Na_2SO_4 solution had a eutectic composition comparable to that reported by (Motsepe et al., 2022); Spencer et al. (2022), no salt was formed during the batch experiments. Nonetheless, ice formed, suggesting that freeze crystallization can be used to study ice formation exclusively, whether on the HX surface or in suspension, in the absence of salt crystallization.

4.5 Continuous FC Experiments

4.5.1 Experimental Matrix

In this section, the ice scale formation on the HX surface of PP-GR during EFC of brine with varying chemistry was investigated. This investigation was carried out in two parts: (1) Continuous EFC using industrial brines to investigate the influence of solute concentration on the formation of ice scale on HX surface during freeze crystallization. Using the industrial brines was mimicking real-world conditions more accurately. (2) Continuous EFC uses binary synthetic solutions ($MgSO_4$ and Na_2SO_4) to investigate the influence of solute concentration and solute type on the formation of ice scale on HX surface during freeze crystallization. The use of binary synthetic solutions in the second part was to investigate the influence of specific solutes at equivalent ionic molality. Furthermore, Na_2SO_4 and $MgSO_4$ were selected for this study because they are one of the major constituents in effluents from mining operations specifically in Sub–Saharan Africa. To study the investigations, the experimental matrix shown in Table 4.4 was formulated. This shows detailed information on the aims, controlled variables, which consists of the concentrations of each brine, and the measured variables consisting of the amount of ice scale formed on the HX surface of PP-GR and in suspension.

Table 4.4: Experimental matrix for testing the technical feasibility of using PP-GR in the EFC of local industrial brines.

Aim	Control Variables	Measured Variables
1. Investigate the influence of solute type on ice scaling behaviour on the HX surface of PP-GR	• 0.613 mol Na_2SO_4/kg • 0.613 mol $MgSO_4$/kg	• Mass of ice scale layer. • Mass of ice from suspension
2. Investigate the influence of concentration (TDS) of Industrial brine on the ice scaling behaviour on the HX surface of PP-GR	• 103 g/L • 122 g/L • 133 g/L	
3. Investigate the influence of solute-$MgSO_4$ concentration(mol/kg) on the ice scaling behavior on the HX surface of PP-GR	• 0.613 mol/kg • 1.13 mol/kg • 1.47 mol/kg	

.

4.5.2 Experimental Setup

Figure 4.1 shows the experimental setup that was used throughout this study. The setup comprised a holding tank (V-2), a recycle pump (P-4), a precooler vessel (V-1), an impeller (4), a crystallizer feed pump (P-1), a column crystallizer (C-1), crystallizer recirculation pump (P-2), a precooler chiller (E-1), and a crystallizer chiller (E-2). The experimental set-up shown in Figure 4.1 was in a temperature-controlled room, which was maintained at a temperature equivalent to the freezing point of the brine solution being studied. The brine solution was pre-cooled to target column crystallizer fed temperature using a 3L glass jacketed vessel (V-1) that was connected to a Lauda RE-1050-G thermostatic unit (E-1). This thermostatic unit circulated polydimethyl-phenylsiloxane (Kyro-51) coolant through the jacketed side of the pre-cooler. To efficiently mix the brine solution and transfer heat from the HX surface, an overhead stirrer (Heidolph RZR 2020) set at 300 rpm was used in conjunction with using a Rushton turbine impeller in the pre-cooler vessel.

A Lauda RP245 E thermostatic unit (E-2) unit circulated Kyro-51 coolant inside the tube of the crystallizer from the top to the top section to cool the brine solution following in the annulus of this column. Because of the vertical position of the column, the cooling in this column occurred in a co-current flow.

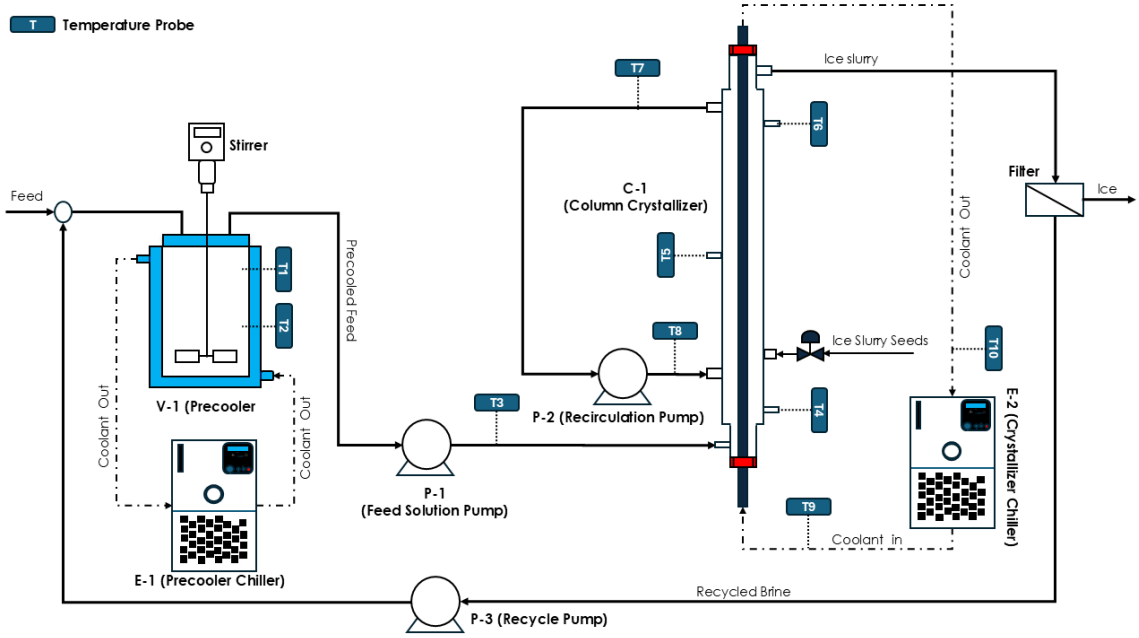

Figure 4.1: Schematic representation of the experimental set-up used to investigate the influence of solute concentration and solute type on ice scaling.

An AC bridge (CTS5000, ASL UK) and a 16-multichanel CTR5000 switchbox, connected to Pt100 thermometers (Tempcontrol, Netherlands) recorded the temperature of the brine solution and the coolant. The data was then captured on a computer running ASL ULog software^{TM} (V 6.1). The temperature was measured in the precooler vessel (T1-T2), feed solution to the crystallizer (T3), crystallizer temperature (T4-T6), inlet, and outlet of recirculation flow (T7-T8), inlet and outlet coolant flow from the crystallizer (T9-T10), and room temperature (T11). Ice scaling and suspension crystallization were investigated in a 3.5 L column crystallizer, designed like a double-pipe heat exchanger same as by a study by Lewis et al. (2023). This column had a port for ice seeding, recirculation points, feed port, overflow port where the ice slurry came out, and temperature probes ports. The brine solution flowed in the annulus, whereas the coolant flowed inside the heat exchanger tube, PP-GR (Technoform. Germany). The Watson Maslow peristaltic were used to pump the feed solution from V-1 to C-1 (P1), recirculation pump for the crystallizer (P2), and recycle brine solution from V-2 to V-1 (P3).

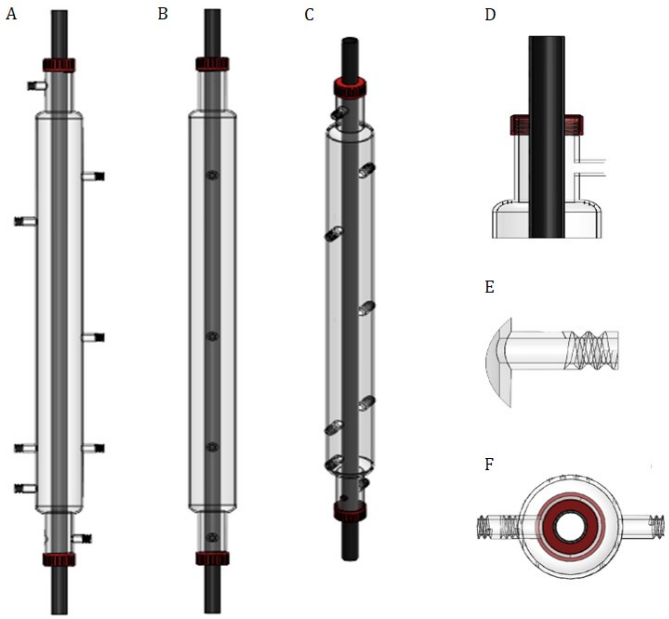

Figure 4.2: A detailed drawing of the column crystallizer used to conduct continuous FC experiments in this study (Lewis et al., 2023).

The 3L column crystallizer (C-1) facilitated ice suspension crystallization and observing ice scale formation on the PP-GR heat exchanger (HX) surface. The mother liquor was removed from the ice production using a filtration system that included a plastic Buchner filtering funnel, a 5L borosilicate glass flask and piston vacuum pump. The ice filtered product was weighed with a grade balance (ML 4002E/ 01), Mettler Toledo, Switzerland).

Brine entered the annulus through the bottom port and exited at the top, directed to a holding tank equipped with a funnel and sieved tray to capture ice crystals from the overflow suspension. Heat exchange in the column crystallizer occurred in co-current flow. This crystallizer also had a port for seeding, which was located at the bottom section to allow the seeds to spend some time in the bulk solution before reporting to the overflow port. Then there were also recirculation flow ports for the inlet and outlet recirculation flow located at the bottom section and the top section, respectively. This allowed mixing of the colder solution from the top section with the warmer solution at the bottom section of the crystallizer. The design of this crystallizer also allowed visual observation of suspension crystallization, and ice scale layer formation on the HX surface of PP-GR tube.

The experimental setup also included a filtration system which consisted of a plastic Buchner funnel (F-1) connected to a 1L borosilicate glass flask (F-2) and vacuum pump (F-3), as shown in Figure 4.3.

Figure 4.3: Filtration System.

4.5.3 Experimental Procedure

Firstly, the storage tank was filled with 10 liters of fresh brine solution. Subsequently, the recycle pump (P3) was switched on and set to 110 rpm, pumping the solution from the storage tank to the precooler vessel (**V-1**). Once the precooler vessel is filled, the feed pump (P-1) to the crystallizer is switched on and pumped the solution from the precooler vessel to the crystallizer (C-1). The crystallizer was allowed to be filled until the overflow occurred, directing the excess brine solution back into the storage tank. Following this, the recirculation pump (P-2) was switched on and set to a speed of 100 rpm, facilitating the circulation of the solution from the top to the bottom part of the crystallizer.

Simultaneously, the precooler stirrer was switched and set to 250 rpm to ensure uniform temperature and concentration throughout the vessel. The ULog software on the lab PC was then configured to capture temperature readings at the points (T1-T10). The precooler chiller (E-1) was switched on and adjusted to the temperatures specified in Table 4.5 ensuring the solution in the precooler remained 0.5 to 0.9 ˚C warmer than the brine saturation temperature, ultimately preventing crystallization in the precooler vessel.

Table 4.5 shows the saturation points of the investigated solutions and set point of the temperature of the room where the experiments were conducted. The crystallizer chiller was switched on and set to required temperatures, as shown in Table 4.5 to achieve an average temperature difference of 3.7 ˚C using Equation 2.10. When the solution temperature in the crystallizer was approximately 0.5 ˚C above the saturation point, ice seeds were prepared by crushing the ice cubes into fine crystal using an ice shaving machine. While this approach is practical for seeding, it is important to note that this may introduce variability in seed size and distribution, potentially affecting nucleation and crystallization process, potentially leading to slight differences in the ice crystallization behavior across the experiments. More controlled seeding methods, such as using standardized seed sizes, could help reduce this variability and provide more consistent results in future studies.

Subsequently, an average of 20 grams of this crushed ice was combined with 30 ml of cooled brine solution from the top part of the crystallizer to make an ice seeds slurry. It should, however, be noted that the average amounts of ice seeds for each brine were 20.18 g for the 4 wt.% Na_2SO_4 solution, 20.19 g for the 7 wt.% $MgSO_4$ solution, 20.26 g for the 12 wt.% $MgSO_4$ solution, and 20.18 g for the 15 wt.% $MgSO_4$ solution. The standard deviation errors in the ice seed amounts are small, with the largest error being 0.0689 for the 12 wt.% $MgSO_4$ brine. These small errors are unlikely to have a significant effect on the crystallization process since the variation in seed amounts is minimal. However, the larger error in the 12 wt.% $MgSO_4$ brine might cause slight differences in nucleation and ice scaling, which could affect the crystallization rates. Overall, the errors are small, but more accurate seeding in future experiments could help reduce any small variation.

Once the solution in the crystallizer reached 0.5 ˚C below the freezing point indicated in Table 4.5, the prepared ice-seeds slurry was injected into the crystallizer through a valve located at point B as shown in the Figure 4.2. This introduction of the ice-seeds initiated ice crystallization process through secondary nucleation. The presence of the seeds provided sites for new ice crystals to form, reducing the energy barrier for nucleation and facilitating growth of ice crystals in supersaturated solutions. This also prevented spontaneous and uncontrolled nucleation, ensuring that ice crystallization occurred in a controlled manner.

Table 4.5: Operating conditions- Ice freezing temperatures, and temperature of the ice lab for different brine solutions.

Brine	**Concentration (mol/kg), [g/L]**	**Ice Freezing Temp (˚C)**	**Lab Room Temp (˚C)**
Na_2SO_4	(0.613)	-1.20	-2.00
$MgSO_4$	(0.613)	-1.20	-2.00
	(1.130)	-2.30	-2.50
	(1.47)	-3.20	-3.50
Industrial Brine	[103]	-1.20	-2.00
	[122]	-2.01	-2.50
	[133]	-2.80	-3.00

The operation time after seeding was limited to 1 hour due to the preliminary experiments that showed that the ice scale layer formed early (0-20 minutes after seeding) from the most dilute brines (0.613 mol Na_2SO_4/kg) resulting in severe ice scaling formation on the PP-GR surface, ultimately blocking the

crystallizer feed port and the overflow port. The product rate of ice was measured by manually collecting ice slurry exiting the crystallize every 20 minutes. The ice slurry was captured using a sieve tray to separate the ice crystals from the mother liquor. The ice product slurry was collected from the ice slurry port of the crystallizer every 20 minutes for a period of 1 hour after seeding. After sieving, the collected ice product slurry was then transferred to the filtration section where it was filtered with a plastic Buchner funnel connected to a 1L borosilicate glass flask and vacuum pump shown in Figure 4.3. The mass of filtered products was then measured using a Mettler Toledo grade balance. Then the total mass of ice collected each 20-minute interval was summed to determine the production rate of ice. The total number of times ice was collected in each interval differed. This was due to ice slurry sometimes filling up the sieve tray faster or slower. Sometimes there were losses of ice during the collection of the slurry, transferring the ice product from the sieve to the filtration system. The period of filtration also differed by the amount of ice collected. This could have introduced variability in the measurements.

The pictures of the ice scale layer on the bottom part of the HX surface of PP-GR were also taken every 20 minutes to gain insight on the growth rate and mechanisms of ice scale formation.

Immediately 1 hour after seeding, both chillers were switched off to stop cooling of the solution. Subsequently, the pumps were switched off, and the solution remaining in the crystallizer was drained into a bucket. The crystallizer chiller was then switched on and set to a temperature of 10 ˚C to melt any ice scale layers that may have formed on the HX surface of PP-GR during the 1 hour of crystallization process. The volume of the melted ice scale layer was measured and recorded, followed by the collection of samples of the residual brine solution, ice product and melted ice scale layer. These samples were filtered using 20 ml-syringes equipped with nylon filters with a pore size of 0.22 μm to remove any colloidal particles before sent for further analysis.

An additional investigation studied the interfacial interactions between the PP-GR surface and various brine solutions by measuring contact angle and estimating surface tensions. These measurements help assess the affinity of brine solutions for the material, where brines with lower contact angle and surface tension are expected to show high affinity for the PP-GR surface, potentially making them prone to ice scaling. In contrast, higher contact angles show lower affinity and adhesion strength, which may help delay the onset of ice scaling.

4.6 Surface Tension and Contact Angle Measurements

To conduct these measurements, surface tensions were estimated using OLI software (V11.5), while contact angles were measured on a flat PP-GR plate using a manual method. Brine droplets (5 μl) were manually deposited on the surface using a syringe to control droplet volume and ensure consistency. Room

evaporation effects at the room temperature (25.0 ˚C) were considered minimal, assuming they did not significantly alter the brine droplet volumes on the test surface. At least 4 photos of each brine droplet were taken using an HD camera and analyzed using ImageJ software with drop-analyses feature to estimate the contact angle, and the average of four contact angles was reported. Due to equipment limitations, all tests were conducted at room temperature (25.0 ˚C), even though lower temperatures (< -1.00 ˚C) would better replicate the operating conditions of FC of industrial brines. This study acknowledges that measuring at such lower temperatures would provide more accurate insights into interfacial interactions under FC conditions.

5. Results and Discussion

This chapter presents the results of the thermodynamic simulation, and laboratory investigations conducted on the feasibility of using polypropylene-graphite (PP-GR) heat exchanger tube in continuous EFC, focusing on the ice production rate and ice scaling. The first sub-section presents freezing temperature of ice and salt and their yields that were predicted using OLI simulation tool. The second sub-section presents the results of the investigations conducted in EFC of industrial brines, and the third sub-section focuses on the synthetic binary solutions.

5.1 Thermodynamic estimations of ice and salt crystallization temperatures

Figure 5.1 shows the predicted influence of temperature on the yield and freezing temperature of both ice and salt for the TWRP 1 over at a temperature range of 6.0 to -10.0 ˚C.

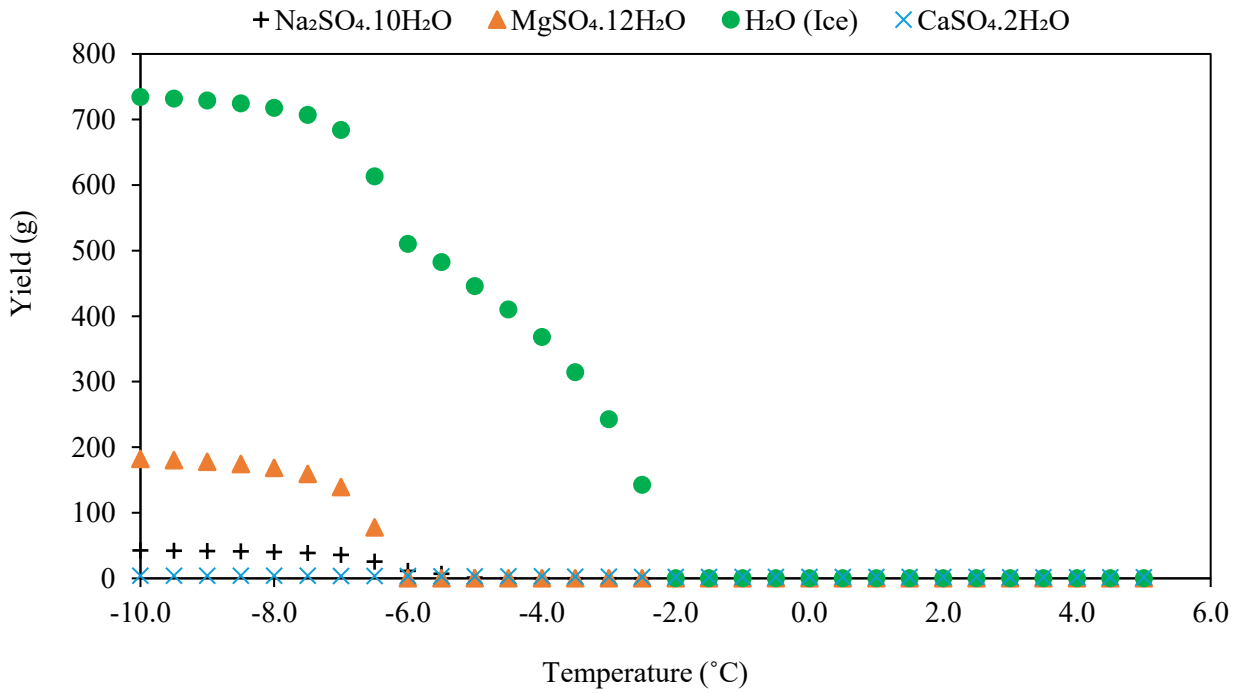

Figure 5.1. The predicted influence of temperature on the yield and nucleation temperature of both ice and salt for the TWRP brine with a TDS of 103 g/L.

Figure 5.1 shows that $CaSO_4.2H_2O$ was predicted to crystallize at relatively warmer temperatures around 10 ˚C, however in smaller quantities. Subsequently, ice crystallization was expected to occur at a temperature of -2.1 ˚C, followed by the formation of $Na_2SO_4.10H_2O$ at -3.4 ˚C. Finally, $MgSO_2.12H_2O$ was predicted to crystallize out at a lower temperature of -6.5 ˚C. The thermodynamic simulations for the other

two brines, TWRP 2 and TWRP 3, also showed that ice was expected to crystallize first but at slightly lower temperatures. These findings show that freeze crystallization can be used to study ice formation exclusively, whether on the HX surface or in suspension, in the absence of salt crystallization.

The freezing temperatures of ice from these brines that were determined through batch experiments are summarized in Table 5.1.

Table 5.1: Freezing temperatures of the industrial brines obtained from batch experiments.

TDS (g/L)	Ice Freezing Temperature (˚C)
103	-1.60
122	-2.01
133	-2.74

The freezing points of ice obtained from the batch experiments as shown in Table 5.1 are significantly different from the ones obtained from the thermodynamic simulations as shown in Figure 5.1. The ones obtained experimentally were slightly higher than those predicted by OLI. The differences may be due to several factors. Firstly, not all the components in the industrial brines were considered when OLI was used. Only major components or those that are generally found in the industrial brines were considered. These brines contain elements like manganese, cobalt, iron, zinc, Nickel, or antiscalants which were not accounted for in the simulation. These impurities can significantly affect the freezing point by either depressing it further or causing localized freezing.

The OLI Systems simulation tool has some limitations because it relies on the quality of the experimental data it uses. For example, Aspeling et al. (2020) reported that the eutectic composition of the $MgSO_4$-Na_2SO_4-H_2O system was found to be 2.74 wt.% Na_2SO_4 and 16.55 wt.% $MgSO_4$ in OLI Systems Stream Analyzer version 9.5, but in version 9.6, it was 3.06 wt.% Na_2SO_4 and 15.6 wt.% $MgSO_4$. This difference is due to better experimental data being added to the newer version for temperatures above 0 °C, which also affects how the tool predicts solubility at lower temperatures. These changes show that the tool's predictions can vary as the data improves. In my study, this might have affected the accuracy of my simulation results, especially for conditions close to the eutectic point. This highlights the need to carefully evaluate simulation results and be aware of the tool's limitations.

5.2 Effect of total solute concentration on ice from suspension and HX surface during continuous EFC of Industrial brines

Figure 5.2 shows the total amounts of ice obtained from the wall and suspension from three different industrial brines 1 hour after seeding.

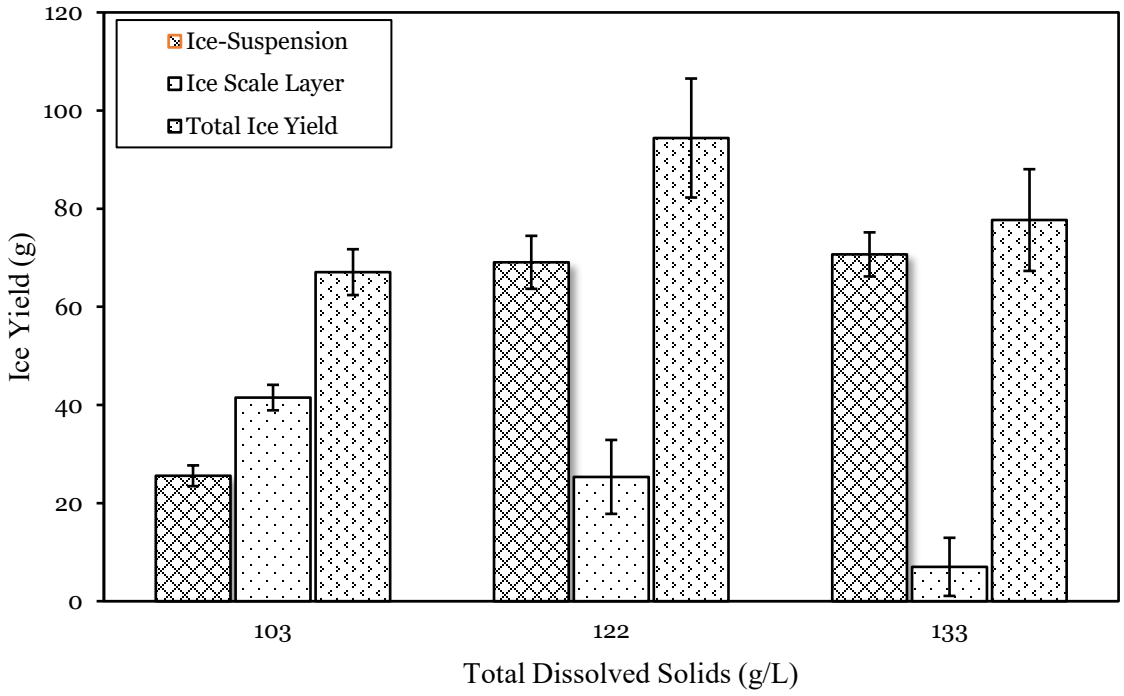

Figure 5.2: Amount of ice-scaling, ice-suspension, and overall ice yield from brines with TDS of 103, 122 and 133 g/L.

The increase in the total solute concentration of the brine resulted in a decrease in the amount of ice scale layer formed on the wall of the crystallizer, and an increase in the amount of ice produced from the suspension. The brine with a TDS of 103 g/L showed a larger amount of ice scale compared to the other brines (122 g/L and 133 g/L). This brine also had less ice from suspension as compared to other brines. The total production of ice from brines with TDS of 122 g/L and 133 g/L were comparable. However, the brine with TDS of 122 g/L showed a slightly higher ice scaling than that of 133 g/L. Ice scale layer from the brine with TDS of 103g/L contributed 62% to the total ice yield, but it accounted for only 18% and 9% in the brines with TDS of 122 g/L and 133 g/L, respectively. The error bars for ice scale layer between the most dilute brine (103 g/L), and concentrated brine (133 g/L) do not overlap, suggesting a statistically significant decrease in the amount of ice scale layer as the concentration of the brine increased.

Figure 5.3 shows the production rate of ice over time during the FC of three industrial brines for a period of 1 hour.

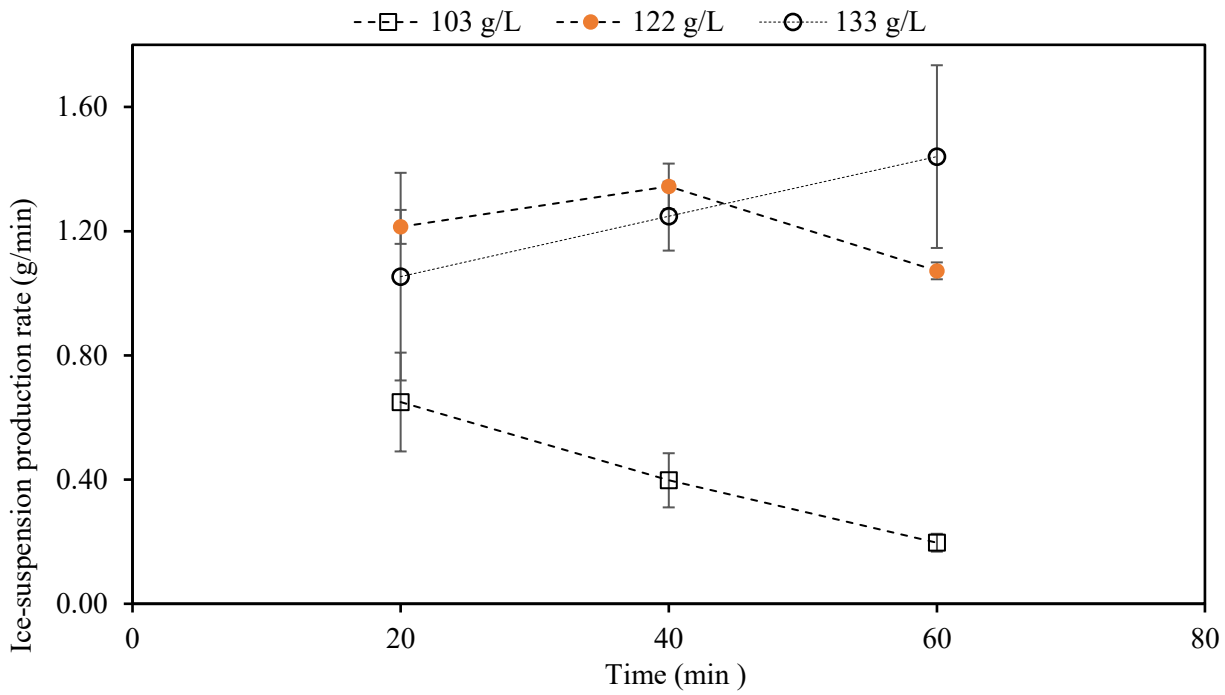

Figure 5.3. Ice production rate from three different TWRP brines with TDS of 103, 122 and 133 g/L.

Fig 5.2 shows that for the brine with TDS of 103 g/L, the production rate consistently decreases over time, starting at 0.65 g/min at 20 minutes, and decreasing to 0.19 g/min at 60 minutes. This steady decrease suggests a reduction in ice production efficiency over time. In contrast, for higher concentrations (122 g/L and 133 g/L), the production rates fluctuate rather than declining steadily. For instance, for the 122 g/L brine, the production rate peaks at 40 minutes (1.34 g/min), while for 133 g/L, it peaks at 60 minutes (1.4 g/min).

Although overall, the production rate of ice for 133 g/L brine seems to be increasing over time, the standard errors are higher, especially at 20 minutes (0.33 g/min) and 60 minutes (0.29 g/min), showing greater variability. This comes from the challenges in collecting the ice slurry from the crystallizer using a sieve tray, then transferring this ice product to the filtration system, and accurately measuring ice at concentrations.

In addition, the experimental limitations due to crystallizer design have also affected the measurement accuracy of production rates. The relatively small diameter of the outlet port for the ice slurry led to blockages, as ice crystals regularly blocked the opening, resulting in pipe bursts. This issue was amplified by the delamination of ice scale layers from the HX surface, where larger pieces of ice scale layers sometimes became entrapped near the top of the column adjacent to the port. These delaminated ice scale

layers adhered to the HX surface at the top section, creating additional ice scaling over time and further obstructing the outlet port. Consequently, these blockages limited consistent ice removal, impacting the accuracy of production rate measurements, especially at higher concentrations where delamination and blockages were more frequent. To improve measurement reliability and maintain consistent ice removal, future experimental set-up would benefit from a modified column design with a larger outlet port and smoother flow paths for the ice slurry. Therefore, the trends observed at these concentrations should be interpreted cautiously, as they may reflect both the actual changes and measurement inconsistencies.

Comparing across brine concentrations, the production rate of ice increases with concentration at the 20th minute, with 103 g/L producing the least ice and 122 g/L producing the most, as shown in Figure 5.2. However, the large standard errors at 133 g/L may suggest that the difference in production rates between 122 g/L and 133 g/L may not be statistically significant, as the error bars overlap. At the 60th minute, 133 g/L brine showed the highest production rate, 1.4 g/min, but the significant standard error of 0.29 introduces uncertainty. This greater variability at this concentration reduces confidence that this production rate truly represents a peak in ice formation. Overall, this data suggests that both time and brine concentration impacted ice production rates. Lower concentrations (103 g/L and 122 g/L) provide more consistent results with smaller error bars, indicating more reliable trends. Higher concentrations, 133 g/L, introduce more variability, as seen in the larger standard errors, which may hide the true trends.

Ice scaling caused a decrease in the production rate of ice for the brine with TDS of 103 g/L after 20 minutes of seeding. This possibly reduced the heat transfer rate between the coolant and bulk solution. As a result, the available supersaturation within the solution decreased, hence the production rate of ice decreased. The same applies for the brine with TDS of 122 g/L, where ice scaling formed within 40 minutes after seeding, affecting the production rate of ice. Interestingly, although ice scaling formed about 50 minutes after seeding for the brine with TDS of 133 g/L, the production rate of ice did not decrease. This may suggest that at this TDS level, the induction time increased, delaying the formation of ice scale layer, and thus possibly reducing its effect on heat transfer within the timeframe of this experiment. This is substantiated by the amount of ice scale layer obtained for this brine, which was 72% and 82% lower than the brine with TDS of 122 g/L and 103 g/L, respectively.

It was hypothesized that increasing the TDS will delay the formation of ice scale layer and subsequently reduce the amount of ice scale formed and allow ice production in suspension. From visual observations, the ice scale layer formed within 20 minutes for the most dilute brine (103 g/L TDS), within 30-40 minutes for the moderately concentrated brine (122 g/L TDS), and within 40-60 minutes for the concentrated brine (133 g/L TDS). This increased in scaling induction time with brine concentration aligns with findings by Leyland et al. (2019), who attributed it to the increased mass transfer resistance from solutes. Interestingly,

in this study, it was also observed that in the dilute brine, not only did the ice scaling formed early but grew faster. In contrast, in the concentrated brines, the formation of ice scaling was delayed, and slower, resulting in overall low amount of ice scale layer forming on the HX surface.

The increase in induction time with increasing TDS was attributed to reduced interfacial strength between the brine and the surface of PP-GR. It was found that as the TDS of this brine increased from 103 g/L to 133g/L, the surface tension increased from 79 to 81 mN/m. The increase in surface tension has been linked to the increase in contact angle between the liquid phase and the HX surface by various studies (Al-Zaidi & Fan, 2018; Si et al., 2022). The increase in contact angle is believed to result in weaker attraction between the liquid and HX surface (Benz, 2020; Liu et al., 2017; Schilling et al., 2022). In this study, it is thought that the increase in concentration reduced the strength of interfacial interactions between water molecules and the HX surface, possibly increasing the contact angle between the brine and the HX surface. As it was shown in Table 2.2, and described by Equation 2.6, an increase in contact angle results in an increase in the surface reduction factor term for overall energy for nucleation, thus increasing the overall energy needed for ice heterogenous nucleation on the HX surface. As a result, the formation of ice scaling was delayed.

While surface tension was expected to play a role in the observed differences in ice scaling with increasing solute concentration, it was not fully investigated in this study. This is because other factors, such as low ice seed loading and low mixing intensity, could have overshadowed the influence of surface tension. The increase in surface tension with solute concentration, though observed, was not significant enough to dominate the ice scaling process. The presence of ice seeds in the bulk brine provides surface area for the consumption of supersaturation, promoting bulk crystallization (Aspeling et al., 2020; Spencer et al., 2022). Since in this study bulk crystallization was initiated through the introduction of ice seeds, it is assumed that the energy barrier for nucleation and growth is lower, favoring crystallization in the bulk solution. In contrast, the energy barrier for surface crystallization, which in this study is ice scaling, is higher because the brine makes it more difficult for nucleation to occur. However, supersaturation near the HX surface is higher because this is the coldest region in the crystallizer, which favors nucleation on the surface. Therefore, there is a competition between bulk nucleation and surface nucleation, with the outcome depending on how evenly supersaturation is distributed in the solution.

To favor bulk nucleation, the supersaturation needs to be evenly distributed throughout the solution so that it can be consumed by the ice crystals in the suspension (Hasan et al., 2017; Spencer et al., 2022). In this study, low mixing intensity (around a Reynolds number of 700) likely limited the distribution of supersaturation, leading to regions of high supersaturation near the heat exchanger surface, favoring surface nucleation. This could have overshadowed the impact of surface tension on ice scaling. Additionally, the ice seed loading in this study was around 0.5 wt.%, which is closest to the lowest ice seed loading (0.1

wt.%) studied by Spencer et al. (2022). Their research showed that low ice seed loading results in more severe ice scaling, which further complicates isolating the effect of surface tension.

Therefore, to fully investigate the role of brine surface tension on ice scaling, future studies should increase mixing intensity to eliminate heat and mass transfer limitations near the surface thus ensuring even distribution of supersaturation in the crystallizer volume. Increasing the ice seed loading to about 10 wt.% would also help isolate the effect of surface tension by providing sufficient surface area for growth or promoting bulk secondary nucleation. Only then could the influence of brine surface tension on ice scaling on PP-GR be investigated without interference from these other variables.

It was, however, found that that the differences in the amount of ice scale layer could not solely be attributed to induction time but also to the growth rate and delamination of ice scale layer when the concentration was varied. It was observed for concentrated brines that even after the ice scale layer had formed, its growth rate was slower compared to the most dilute brine (103 g/L TDS). This was observed with the brine of 103 g/L TDS, in which the ice scale layer seemed to be growing faster, covering most of the bottom section of the PP-GR tube, while with the brine of TDS of 133 g/L, a small ice scale layer formed which grew slowly. This aligns with findings by Zhang et al. (2021) and Matsumoto et al. (2012), who observed a reduced growth of the ice scale layer at higher concentrations of solutes. During the growth of ice, solute molecules must diffuse away from the interface of ice for it to grow. These solutes are generally rejected to the ice-solution interface. As a result, these ions aggregate around this interface increases the interfacial resistance to the transport of water molecules from the bulk solution to this interface (Kapembwa et al., 2014). Consequently, this limits the attachment of water molecules into the ice crystal lattice, hence the growth of ice scale layer in concentrated brines seemed to be slower, resulting in less amount of ice scale layer accumulating on the HX surface.

It was also observed that the ice scale layer on the surface of PP-GR from the dilute brine was difficult to remove, yet the ice scale layer delaminated from the HX surface of PP-GR easily in moderately and highly concentrated brines (TDS of 122 g/L and 133 g/L). Although studying the adhesion strength of ice was not part of this work, it is believed that the delamination of ice scale layers from the HX surface was due to the reduced adhesion strength of ice induced by increased solute concentration. The phenomenon was observed in a study by Matsumoto et al. (2010), in which it was shown that the required scraping force decreased with the increase in concentration of the EG solution. Y. Zhang et al. (2022) also observed a similar trend where the sliding probability of ice on a solid surface started to increase after a range of concentration.

There are several mechanisms in which the adhesion strength of ice could be affected when the solute concentration increases. Y. Zhang et al. (2022) attributed the reduction of adhesion strength to the

interactions between ions and the surface of ice, which induce the formation of a liquid-like layer the ice interface. Similarly, Deshmukh et al. (2013) have demonstrated that the presence of ions around ice disrupts the orientation of water molecules, causing the ordered interfacial structures into bulk-like water structures. This results in the formation of a liquid layer between the heat exchanger (HX) surface and the ice scale layer, reducing the interfacial interaction strength between the two. As a result, the effective contact area between the ice scale layer and the HX surface is reduced, promoting delamination. Interestingly, Vrbka and Jungwirth (2005) observed that at low concentrations, more ordered water layers form at the ice interface compared to normal bulk water. This could suggest that for the dilute brine, there are more ordered layers that had around the ice surface, making it more stable, and able to adhere strongly to the HX surface. However, at higher concentrations, the water layers on the surface of the ice possibly become disordered. This suggests that highly concentrated brines (TDS of 122 g/L and 133 g/L) may have induced disordered water layers on the surface of ice scale layers, weakening its adhesion strength. Consequently, ice scale layers formed from highly concentrated brines possibly had low adhesion strength and were more prone to delamination.

The contact angle between the brine and the HX surface could also be one of the factors that resulted in the variations in the delamination of the ice scale. Liu et al. (2017) has shown that lower contact angle promotes ice growth along the surface, while higher contact angle promotes off-surface growth. The ice scale layer grown off-surface may be prone to delamination due to less contact area with the HX surface. The differences in surface tension of the tested industrial brines likely caused variations in the contact angle. The dilute brine (103 g/L) probably had a lower contact angle, promoting stronger interfacial interactions, which facilitated ice growth along the surface. Consequently, the ice scale layer formed from this brine adhered strongly to the HX surface, leading to the accumulation of a thicker scale layer. In contrast for concentrated brines (122 g/L and 133 g/L), the contact angle was possibly higher, reducing the effective contact area between the ice scale layer and HX surface. This reduced interaction possibly made the growing ice scale layer more prone to delamination. However, the exact mechanisms behind the increased delamination of the ice scale layer with higher brine concentrations remain unclear and may involve additional factors.

Overall, higher TDS levels in brines led to less ice scaling and more ice in suspension, delayed and slower ice scale formation, and possibly reduced adhesion strength of ice. These findings indicate that managing solute concentrations in industrial brines can efficiently control ice formation, improving the productivity of the freeze crystallization processes. Furthermore, it is worth noting that the observed decrease in the overall amount of ice scale layer as solute concentration increased throughout the treatment of this multi-component industrial brine, could not be clearly attributed to any individual solutes. This is due to the

combined effect of higher concentrations of various solutes such as Mg^{2+}, Cl^-, Na^+, and so on., each of which might have different impacts on ice scaling. Thus, further experiments were conducted to study the influence of individual solutes and their concentrations in a binary system. This was done to gain a better understanding of the effect of individual solutes on the formation of ice scaling.

5.3 Effect of solute type on ice from suspension and HX surface during EFC of binary solutions

Figure 5.4 shows the total amount of ice product from suspension and wall collected 1 hour after seeding for four different binary solutions.

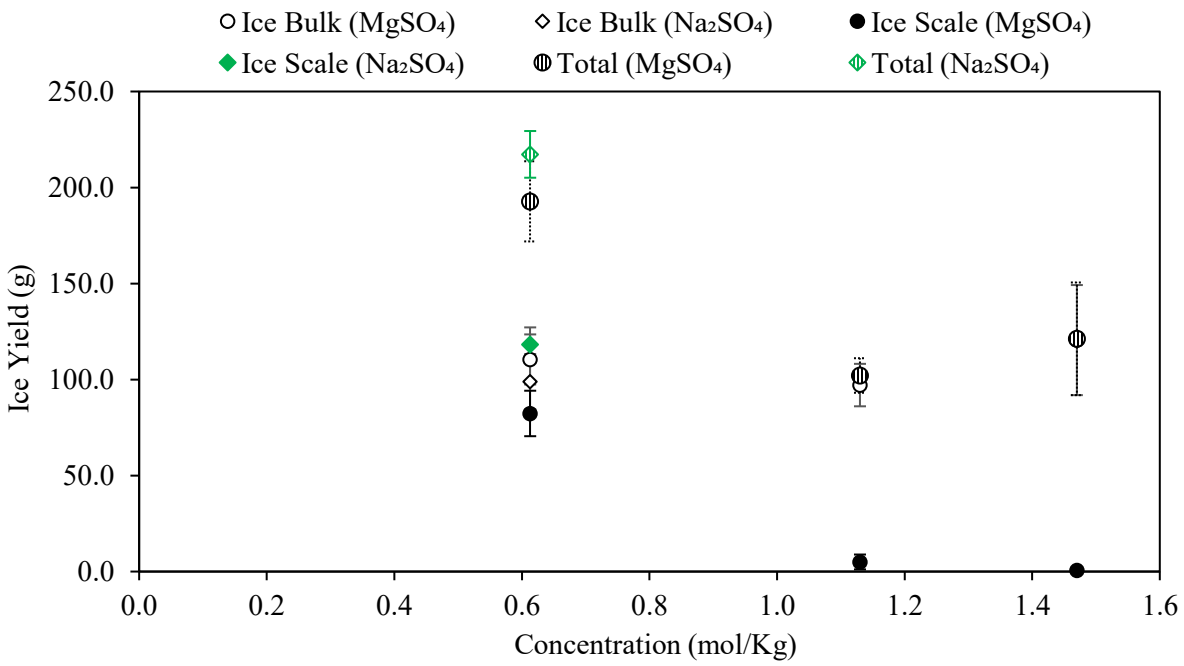

Figure 5.4. The total production of ice from ice scaling and suspension for different brine solutions.

Figure 5.4 shows the total amount of ice product from suspension and wall collected one hour after ice seeding for two different brine solutions. Overall, the 0.613 mol Na_2SO_4/kg system produced more ice than the 0.613 mol $MgSO_4$ mol/kg, resulting in a larger total amount of ice. However, due to faster formation of the ice scale layer, this brine also recorded the maximum amount of ice scale, with 0.613 mol Na_2SO_4/kg brine having 1.7 times more ice scale layer than that the 0.613 mol $MgSO_4$/kg brine. The total amount of ice scale layer relative to the amount of ice from suspension was also higher for the 0.613 mol Na_2SO_4/kg brine than for the 0.613 mol $MgSO_4$/kg. Particularly, the ice scale layer from the 0.613 mol Na_2SO_4/kg brine contributed 54 % to the total ice yield, compared to 45% for the brines with 0.613 mol $MgSO_4$/kg brine.

Figure 5.5 shows the ice scale layer on the HX surface of PP-GR near the feed port of the CC after 60 minutes, marking the end of the experiment. These images capture the formation of ice scaling during the treatment of (A) Na_2SO_4 and (B) $MgSO_4$ brines. The other images showing the progression of the ice scale layers are in the appendix. When all the images were combined, they were not appearing clearer as shown in Figure A.11, hence only the ones showing the ice scale layer at the 60th minute were used

Image A of the 0.613 mol Na_2SO_4/kg, as seen in Figure 5.5 shows that significant HX surface area at the bottom was covered by the ice scale layer after 60 minutes, more than that of $MgSO_4$. This substantial ice coverage likely caused a significant reduction in heat transfer rate between the coolant and the suspension.

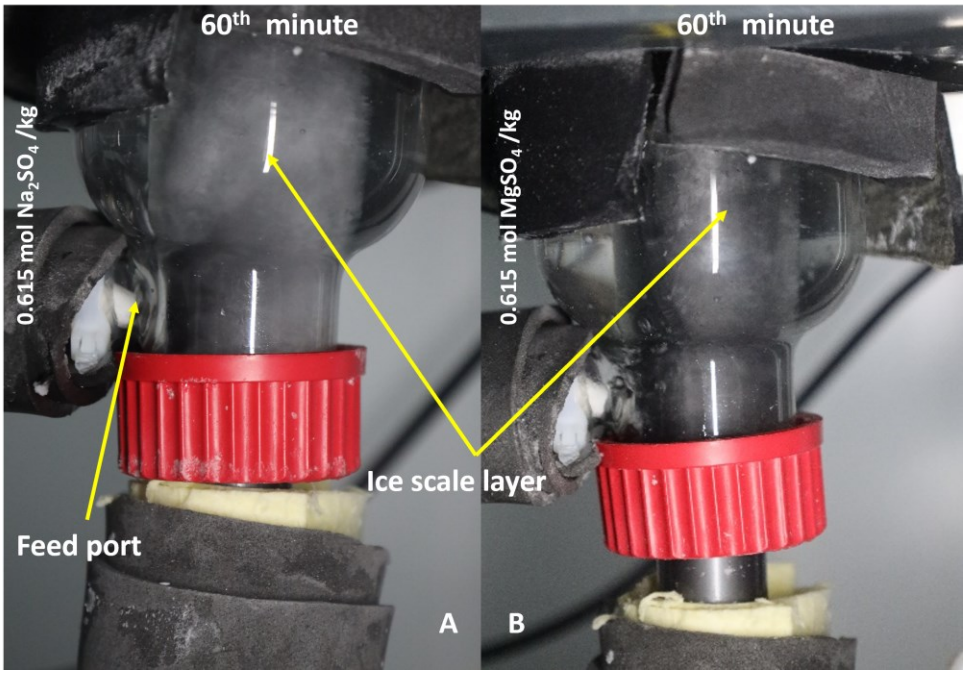

Figure 5.5. Images of the ice scaling formation on the bottom section of HX surface of PP-GR from a 0.613 mol Na_2SO_4/kg and 0.613 mol $MgSO_4$ /kg brine solutions after 60 minutes.

Observations from the experiments using 0.613 mol Na_2SO_4/kg brine showed significant ice scale layer coverage on the heat exchanger (HX) surface. Within 20 minutes, a substantial portion of the HX surface was covered by an ice scale layer, much more than in the $MgSO_4$ brine. This extensive scaling possibly caused a significant reduction in the heat transfer rate between the coolant and the suspension. By 40 minutes, the ice scale layer appeared to have grown thicker and stronger, covering most of the HX surface and demonstrating that Na_2SO_4 led to faster and thicker ice scaling.

Between the 40th and 60th minute after ice seeding, it was also observed that bulk ice crystallization had significantly decreased in both solutions. However, in the $MgSO_4$ brine, a fraction of the ice continued to

report to the overflow port. This was attributed to the detachment of ice scaling layers from both the heat exchanger (HX) surface and the main ice scaling layer. When these layers detached and reentered the bulk suspension, they provided new surfaces for water molecules in the supersaturated solution to deposit and grow, thus promoting further bulk crystallization. This mechanism is consistent with secondary nucleation, where fragments of existing ice crystals act as new nucleation sites as described as Benz (2020). In contrast, no delamination of ice scale layers was observed in the Na_2SO_4 solution. Instead, substantial ice coverage formed on the HX surface, which is believed to have significantly reduced the heat transfer rate between the coolant and the suspension.

Although the heat transfer rate was not directly measure in this study, other studies, as those by Hasan et al. (2017) and Spencer et al. (2022), reported that ice scaling reduced the heat transfer coefficient by a factor of 10-20 and heat transfer between the heat transfer surface and the bulk solution by 68%, respectively. However, these studies did not specify the thickness of the ice layer under which these reductions were observed, and since the thicker ice layer results in higher thermal resistance, this makes it difficult for heat to transfer. Despite this lack of specific details, their results clearly demonstrated that ice scaling can significantly reduce the heat transfer coefficient. In this study, the effect of ice scaling on the crystallization process was evident in the measured production rate of ice over time.

Figure 5.6 shows the production rates of ice for two different binary solutions. Specifically, there was a significant decrease in the production rate of ice for Na_2SO_4 between 40^{th} minute and 60^{th} minute, as seen in Figure 5.6. The faster formation of ice scaling for Na_2SO_4 brine resulted in an overall decrease in the production rate of ice by 65% (from 2.6 to 0.9 g/min), while for 0.613 mol $MgSO_4$/kg brine the rate decreased by 22% (2.0 to 1.6 g/min). This suggests that Na_2SO_4 brine may initially have faster production rate of ice but experience a greater decline over time compared to $MgSO_4$. Although the production rates of ice for $MgSO_4$ seem to show a slight decrease from 20 to 40 minutes (2.0 to 1.9 g/min), and a further decrease at the 60^{th} minute (1.6 g/min), the changes were smaller compared to the size of error bars. The errors bars for this brine overlap significantly from the 20^{th} minute to the 60^{th} minute in Figure 5.6, showing that the observed differences in production rates of ice are within the margin of error.

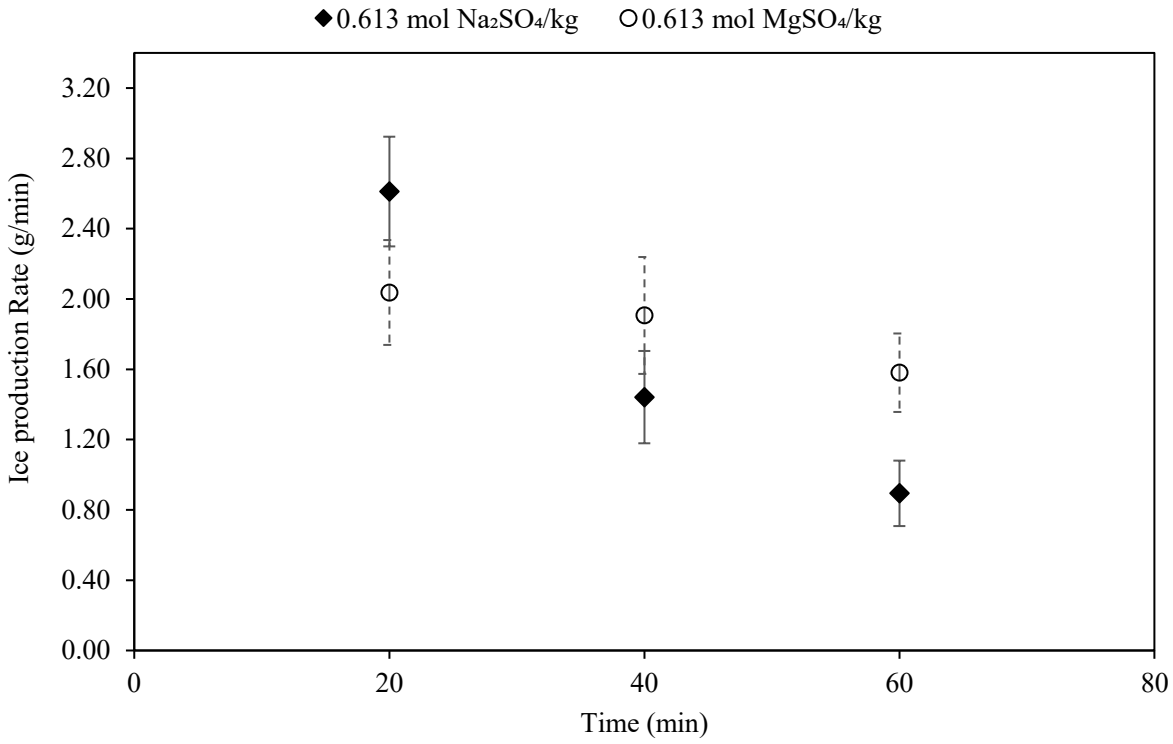

Figure 5.6. Ice production rate over from suspension during FC of Na_2SO_4 and $MgSO_4$ binary solutions at a constant total ionic molality of 0.613 mol/kg.

Therefore, it is difficult to conclude that the production rate of ice truly changes over time. However, for Na_2SO_4, the error bars between the 20th minute and 60th minute do not overlap, suggesting a statistically significant decrease in production rate of ice over time. It should also be noted that the large error bars relative to the observed trend could be to several factors that introduced variability in the measurement of ice production rate. This includes the manual collection of ice slurry from the crystallizer, introducing inconsistencies in the amount of ice collected and measured. The interval at which ice was collected may also be short to obtain a stable production rate of ice. Therefore, measuring the production rate at least every 5 minutes instead of every 20 minutes is recommended to determine the exact time when the production rate starts to decrease, especially for dilute brines which form ice scaling very early.

Differences in amounts of ice between $MgSO_4$ and Na_2SO_4 brine solutions were initially attributed to the variations in ice scale layer induction times. The Mg^{2+} ions were predicted to delay the formation of ice scale layer due to their high charge density, which would possibly disrupt the prenucleation local ordering of water layers near the HX surface. The ice scale layer for both solutions seem to have formed early and fast, therefore, due to the limitations of the experimental set-up, the exact time when ice scaling occurred for both solutions could not be determined. It was, however, observed that the progression of ice scale layer

differed, resulting in different amounts of ice formed from suspension and on the HX surface. These differences were due to other ice scaling mechanisms like growth and delamination.

The growth rate of ice scale layer in the $MgSO_4$ brine was observed to be slower than that of Na_2SO_4. The differences could be attributed to factors like charge density and diffusion coefficients. Mg^{2+} has a higher charge density than Na^+, causing it to be more strongly attracted to hydrogen-bonded networks between water molecules and the surface of ice scale layer. This strong attraction results in some Mg^{2+} ions aggregating on the ice surface. This then creates a diffusive boundary layer around the interface of ice scale layer. This layer delays the addition of water molecules to the growing ice-scale layer front and consequently slowing its growth (Kapembwa et al., 2014).

In contrast to this study, Zhang et al. (2021) observed that F^- ions, which had lower charge density than Cl^- and Br^-, aggregated more on the ice interface. Similarly, the NH_4^+ ions also aggregated more on the interface of ice compared to Na^+, K^+, and Cs^+ ions, which also slowed the incorporation of water molecules into the lattice structure of ice. Zhang et al. (2021) attributed these differences to increase of potential energy of bulk ice when was F^- was incorporated in ice, whereas Sei et al. (2002) attributed the variations in growth rates of ice from trehalose and sucrose solutions, to trehalose attaching to water molecules more than sucrose. These studies collectively highlight that solutes are generally excluded from the ice crystal lattice during freeze crystallization due to their size and charge, meaning that different solutes, like in this case, Na^+ and Mg^{2+} can have varying impact on the growth of ice scale layer.

Furthermore, due the difference in diffusion coefficients between Na^+ ions (1.334 nm^2/s) and Mg^{2+} (0.706 nm^2/s) (Samson et al., 2003) in water, this may have also contributed to the slower rejection rate of Mg^{2+} ions away from the interface of ice scale layer. This possibly increased the resistance to both mass transfer of water molecules and their integration into the ice lattice and subsequently limiting the growth rate of the ice scale layer.

It is believed the slower growth rate of ice scale layer from the $MgSO_4$ brine was due to enhanced resistance to mass transfer of water molecules and their integration into the ice scale layer. However, the contribution of either charge density or diffusion coefficient to the mass transfer resistance could not be distinguished. Nonetheless, these findings imply that the nature of the solute can have varying effects on ice growth. Further investigations should be conducted to observe the development and growth of the ice scale layer in the presence of various solutes using DIC technique used by Motsepe et al. (2022).

Instances of delamination of the ice scale layers from the HX surface were observed in the $MgSO_4$ brine. This phenomenon may be attributed to the reduced adhesion strength of ice or weaker bonds between the ice scale layer and the HX surface in the presence of Mg^{2+}. Due to their higher charger density, Mg^{2+} ions

can disrupt the hydrogen-bonded networks within the liquid-like layer on the ice surface. This disruption likely disordered the stable structure of water molecules on the surface of ice, reducing the adhesion strength of ice. This led to increased delamination of ice scale layers in the presence of Mg^{2+} ions. Additionally, the screening of surface charges on the ice may have contributed to this effect. Since electrostatic potential is proportional to ionic charge as described by Petrenko and Whitworth (2002) , the divalent Mg^{2+} ions exert a stronger electrostatic interaction than the monovalent Na^{+} ions. This makes Mg^{2+} more effective in neutralizing or screening the negative surface charges on ice, further reducing adhesion strength.

However, it should be noted that the exact mechanism responsible for the delamination remains inconclusive. Both the disruption of hydrogen-bonded networks and the electrostatic screening of surface charges likely played a role in the observed delamination of ice scale layers from the HX surface.

Nonetheless, the study indicates that while 0.613 mol Na_2SO_4/kg brine initially produces more ice, the faster formation of ice scaling significantly hinders long-term ice production due to reduced heat transfer efficiency. In contrast, 0.613 mol $MgSO_4$/kg brine, despite a slower initial ice production, maintains a steadier rate over time due to less impactful ice scaling and frequent delamination of ice scale layers. According to these findings, ions with large charge density, such as $Mg^{2+,}$ may have the potential to reduce ice scaling, and allow longer periods of freeze crystallization. However, to gain a more comprehensive understanding of these interactions on ice scale layer formation in freeze crystallization, it would be beneficial to investigate at least three different types of ions or to examine the same two solutes under varying operating conditions, such as different temperature driving forces or mixing intensities.

5.4 Influence of total solute concentration of $MgSO_4$ on ice scaling formation on the HX surface during EFC

The amount of ice scale layer decreased significantly with higher $MgSO_4$ concentration as shown in Figure 5.4 occasionally showing ice-scale free operations in the 1.47 mol brine. These results are like those obtained during the FC of industrial brines showing less ice scaling tendency with increasing concentration. At 0.613 mol/kg $MgSO_4$, the ice scale layer formed in 20 minutes, while at 1.13 mol/kg and 1.47 mol/kg, ice layer formed with 40-60 minutes after ice seeding, reducing accumulation on the HX surface, and enabling ice crystallization in suspension. The findings on the delay in ice scale formation with increasing solute concentration are similar to those obtained by Leyland et al. (2019), and Vaessen et al. (2002).

Figure 5.7 shows the production rates of ice for different concentrations of $MgSO_4$ brines. Although the ice scaling formed at the latest in 1.47 mol $MgSO_4$/kg brines, it was observed that the production rate of ice decreased by 15% between the 20^{th} and 40^{th} minute. However, between the 40^{th} and 60^{th} minute, the production rate of ice remained steady. However, the increasing standard errors at 40 and 60 minutes

indicate greater uncertainty in the measurements as time progresses. This suggests that while the production rate changes, there is a noticeable decrease in consistency and reliability of the measurements over time, making it difficult to confidently conclude that there was a true increase in ice production.

Furthermore, it was surprising that the most concentrated brine (1.47 mol/kg) had a higher production rate of ice than the dilute brine, particularly at the 20th minute. The dilute brine was expected to produce more ice in the 20th minute due to having more water molecules than the concentrated brine. However, it was the other way around. Early and faster formation of ice scale layer in the 0.613 mol $MgSO_4$/kg brine, possibly reduced the heat transfer rate between the suspension and the HX surface significantly within this period. As a result, the available supersaturation decreased over time, hence the production rate of ice in suspension also decreased. This can be supported by the production rate of ice value at the 20th minute being lower than that of 1.47 mol $MgSO_4$/kg brine. Interestingly, the production rate of ice from the 1.13 mol brine was close to that of 0.613 mol, across all intervals, despite forming less amount of ice scale layer. Clearly, ice scaling was not a factor in this decrease. It is believed that the heat gained from the room possibly reduced the heat transfer rate during this period.

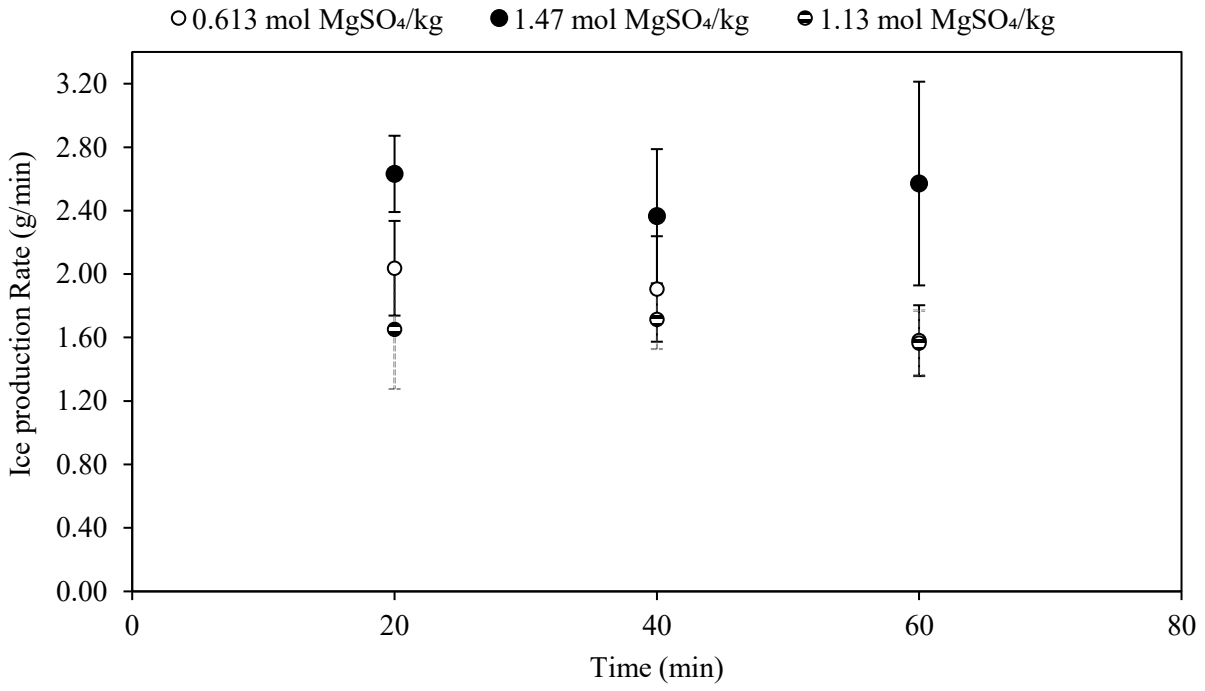

Figure 5.7. Ice production rate over from suspension during FC of $MgSO_4$ binary solutions at total ionic molality of 0.613, 1.13 and 1.47 mol/kg.

It was hypothesized that increasing the solute concentration of $MgSO_4$ will delay the formation of ice scale layer and subsequently reduce the amount of ice scale formed. As was shown in Figure 5.4 higher solute

concentration delayed the formation of ice scaling and resulted in lower amount of ice scale. These experimental results are similar to the findings of previous studies by Vaessen et al. (2002), which investigated the influence of solute concentrations on ice scaling and found low ice scaling tendency as the concentration increased. These authors attributed the increase in ice scaling induction time with an increase in solute concentration to enhanced mass transfer resistance to water molecules moving from the bulk to the water-clusters forming on the HX surface. This is believed to have delayed the formation of the ice scale layer.

In this study, the delay in the formation of ice scale layer with increasing $MgSO_4$ concentration was attributed to reduced interfacial strength between the brine and the surface of PP-GR. As the concentration increased, so did the surface tension of the brines, as shown in Table 5.2.

Table 5.2: Influence of concentration of $MgSO_4$ aqueous solution on surface tension and contact angle.

Inorganic Salt	Concentration (mol/kg)	Surface Tension (mN/m)	Contact Angle (˚)
$MgSO_4$	0.613	77.4	75.9 ±2.1
	1.130	78.0	81.4± 2.3
	1.47	79.4	99.7 ± 3.8

The increase in surface tension and contact angle is believed to have decreased the contact area between the brine and the surface of PP-GR. This possibly decreased brine-HX surface interfacial interactions, causing the ice scale layer to take longer to form. Studies, such as by Al-Zaidi and Fan (2018), also shown that increased salt concentration in higher contact angles between the liquid phase and solid surface. Higher surface tension and contact angles suggest weaker bonds between water molecules and the PP-GR surface. This weakens the adherence of water molecules or clusters to the HX surface. This, in turn, delays the formation of ice hetero nuclei. Thus, it is assumed that as the solute concentration increased, the contact angle also increased, possibly increasing the energy barrier for the ice heterogeneous nucleation, hence the ice scaling was delayed.

While the contact angles in this study were measured at a temperature of 25˚C, it is believed that they still provide insight into the strength of interfacial interactions between the brine, water molecules, and the HX material during crystallization. However, it should be noted that these contact angles were measured at warmer temperatures, which are significantly higher than the subzero temperatures where freeze crystallization usually occurs, and where ice scaling formation is most relevant. Ice scaling is influenced by the interfacial properties between the heat exchanger surface, brine, and ice as described by Gribanova et al. (2016), which may vary significantly under colder conditions. Future work should focus on measuring contact angles of these brines at subzero temperatures and under the specific supersaturation conditions

where ice crystallization from the brines typically takes place. This would give a clearer understanding of how interfacial properties influence ice scaling and help develop strategies to reduce it.

It was, however, found that that the differences in the amount of ice scale layer as shown in Figure 5.4, could not solely be attributed to induction time but also to the growth rate and delamination of ice scale layer when the concentration was varied. In the case of growth, it was observed that in the dilute $MgSO_4$ brine, the ice scale layer grew faster, whereas in the concentration brines, it grew slow. During ice growth, foreign ions are rejected to the ice-solution interface (Hasan & Louhi-Kultanen, 2015). It is believed that as concentration increases, more ions are rejected from the ice-solution interface. This possibly increased the resistance to both mass transfer of water molecules and their integration into the ice lattice, consequently limiting the growth of ice scale layer. Matsumoto et al. (2012) found that the growth rate of ice scale layer was slower as the concentration of trehalose increased. Zhang et al. (2021) also observed a slower growth of ice crystals when the concentration of different ions increased.

Instances of delamination were observed more frequently at higher $MgSO_4$ concentrations. This was attributed to decreased adhesion strength between ice scale layers and the surface of PP-GR, possibly removing the ice scale layer, and thus increasing the availability of the HX surface of PP-GR. This demonstrates a decrease in the adhesion strength of ice with increasing water salinity and aligns with the previous study by Matsumoto et al. (2010), which showed that the required scraping force decreased with the increase in concentration of the EG solution. This is further supported by findings from a study by Y. Zhang et al. (2022).

The study demonstrates that higher concentrations of $MgSO_4$ brine delay the formation of ice scale layers, reduce their growth rate, and possibly decreased their adhesion strength. These factors collectively result in less ice scaling and promote crystallization suspension. The findings suggest that increasing the concentration of $MgSO_4$ can enhance ice production efficiency by minimizing ice scaling, which is critical for optimizing industrial ice production processes.

6. Conclusion

The formation of an ice scale layer on the HX surface within the EFC process hinders its industrial implementation. Ice scaling resistant HX materials like PP-GR have been shown to have low scaling tendency, having the potential to reduce the ice scaling in the EFC of industrial brine from coal mine impacted waters. However, relying solely on such HX materials may not entirely reduce the scaling challenges. The concentration and type of solutes within the brine should also play a role in ice scaling on HX surfaces. Given the variability of solute type and concentration in industrial brines, an investigation was undertaken to investigate on how both factors influence the ice scale layer formation on the HX surface of PP-GR, thereby evaluating its applicability for treating industrial brines through EFC.

The study involved a continuous EFC process with a 3L column crystallizer equipped with a PP-GR heat exchanger tube, designed to observe the formation of ice scale layers and bulk crystallization. The production of ice was measured every 20 minutes for 1 hour. The amount of ice scale layer was measured after the experiment.

The initial phase investigated the influence of total dissolved solids in industrial brine on the amount of ice scale layer formation during continuous EFC operation. These brines were obtained from reclamation plant and had different TDS levels (103 g/L, 122 g/L, 133 g/L). The results indicated that higher TDS levels significantly reduced the formation of the ice scale layers on the HX surface of PP-GR. Furthermore, at higher TDS levels, a greater proportion of ice formed in suspension rather than on the HX surface, suggesting a more favorable ice suspension process. Notably, some instances of ice scale-free operations were observed at higher TDS levels. This is important in the industrial implementation of EFC as it can reduce the downtimes due to ice scaling on the HX surface and potentially achieving longer production times and sustained ice production under these conditions. However, it is important to note that the decrease in the amount of ice scale layer with increasing TDS level could not be attributed to specific solutes alone but rather to combination of factors influenced by the increased concentrations of various solutes, such as Mg^{2+}, Na^{2+}, K^{+}, Cl^{-}, and so on. Therefore, this study also investigated the influence of specific solutes on the formation of ice scaling.

The second phase focused on understanding the influence of individual solute types, specifically $MgSO_4$ and Na_2SO_4, both at equivalent ionic molality of 0.613 mol/kg, on the ice scale layer formation. The results showed that the amount of ice scale layer was 30% less in the 0.613 mol $MgSO_4$/kg brine compared to that of 0.613 mol Na_2SO_4/kg brine. However, the total yields of ice from brines were comparable with ice crystallization from the 0.613 mol Na_2SO_4/kg brine predominately occurring on the surface of PP-GR rather in suspension. The lower amount of ice scale layer in the 0.613 mol $MgSO_4$/kg brine was attributed to Mg^{2+}

ion having a higher charge density, bonding strongly to the water molecules, thereby slowing their incorporation into the surface of ice scale layer. Thus, ionic solute with higher ionic charge density may potentially reduce the amount of ice forming on the HX surface of PP-GR as it was hypothesized. However, for solute type, it could not be precisely determined which factor, whether differences in ionic charge or mass transfer coefficient were responsible for the variations in induction times and growth rates between the two solutes.

Additionally, increasing the concentration of $MgSO_4$ (from 0.613 mol/kg to 1.47 mol/kg), in a binary system significantly decreased the ice scale formation by 99% (from 82 g to 0.7 g), respectively. This was attributed to the delay in formation, slower growth and instances of delamination of ice scale layer with increasing solute concentration of $MgSO_4$. At lower concentrations, the ice scale layer formed early and faster. Therefore, the results suggest that increasing concentration can potentially limit the formation of ice scaling significantly in EFC. Therefore, it is important to select the best solute concentrations to achieve low ice scaling tendency.

Overall, the findings of this study show that while PP-GR materials showed low scaling tendencies in the previous study, understanding the influence of solute concentration and solute type on ice scale formation on this material could further help in reducing the ice scale formation in EFC. The current study has shown that selecting highly concentrated binary and industrial brines along with PP-GR would be beneficial in delaying the formation of ice scaling, reducing the growth rates of ice scale layers, and increasing the frequency of delamination of ice scale layers. Furthermore, the type of solute presents in a brine affects the formation of ice scaling as there are solutes that can reduce ice scaling by inhibiting the heterogenous nucleation of ice, whereas some can have negligible impact. Thus, managing solute concentration and type can prolong ice production times and enhance operational efficiency in EFC of industrial brines.

7. Limitations and Recommendations

One main limitation of this study was the difficulty in accurately measuring induction time, particularly due to challenges in observing ice scaling on the heat exchanger (HX) surface of PP-GR. The cylindrical column crystallizer, which is about 1.5 m long, made it difficult to observe all sides. Additionally, the crystallizer was insulated to minimize heat gain from the environment, limiting visibility to only a few sections. The ice slurry outlet port had a relatively small diameter, which led to ice crystals blocking the opening and causing pipe bursts. Furthermore, ice scale layers occasionally delaminated from the bottom surface of PP-GR, and larger pieces got stuck near the top area, adhering to the HX surface and contributing to scaling. Over time, this ice would grow and block the outlet port. To improve measurement accuracy, the column design should be modified.

The ice production rate was manually measured by collecting ice slurry exiting the crystallizer every 20 minutes. The ice slurry was separated using a sieve tray, then filtered with a vacuum pump and measured on a balance. Variability in ice collection times, losses during collection, and filtration periods introduced some measurement uncertainty. Measuring the ice production rate less often than every 20 minutes likely increased variability and made the error bars larger. Longer intervals would allow more ice to build up before collection, which can lead to uneven ice collection, blockages, and ice loss during handling. This makes the data less reliable and reduces the ability to see small changes in the ice production rate over time.

On the other hand, measuring ice production more often, such as every 5 or 10 minutes, can reduce the error bars by capturing more data and balancing out any small differences between measurements. More frequent measurements also make it easier to spot changes in ice production and reduce the chance of ice loss, since smaller amounts of ice are handled each time. This provides more detailed and accurate data, making it easier to understand how factors like solute concentration and mixing intensity affect ice production.

It was also visually observed that the growth rate of ice scale layers differed with solute concentration and solute type, but accurate determination of these effects was not possible. The induction time could not be measured accurately, and delamination of ice scale layers from the HX surface could not be captured consistently. Further investigations should be conducted to observe the development and growth of the ice scale layer in the presence of various solutes using the Differential Interference Contrast (DIC) technique, as employed by Motsepe et al. (2022). A crystallizer designed to facilitate direct visual observation of the HX surface would be beneficial for studying these phenomena more accurately.

It would also be beneficial to conduct experiments at higher solute concentrations (e.g., 1.47 mol $MgSO_4$/kg) for longer durations (more than 1 hour) to determine whether ice scaling will eventually form

and, if so, how fast the ice scale layer grows. Further experiments should explore the influence of solute types like K_2SO_4 and $CaSO_4$, which are dominant in brines from coal mine-impacted waters after Na_2SO_4 and $MgSO_4$. Solutes with similar charges, such as Ca^{2+} and Mg^{2+}, should also be compared. Additionally, the influence of solute concentration and type on ice growth rate and the probability of delamination should be studied using the DIC method for accurate scaling mechanism observation.

In this study, low mixing intensity likely limited the distribution of supersaturation, causing regions of high supersaturation near the heat exchanger surface, which favored surface nucleation. Increasing mixing intensity would help distribute the supersaturation more evenly, allowing for a clearer investigation of surface tension's role in ice scaling. Moreover, increasing the ice seed loading to about 10 wt.% would help isolate surface tension's impact by reducing the influence of other factors.

While surface tension was expected to influence ice scaling with increasing solute concentration, it was not fully investigated in this study. Other factors, such as low ice seed loading (0.5%) and low mixing intensity (Reynolds number of 700), likely overshadowed the effect of surface tension. The increase in surface tension with solute concentration was observed but not significant enough to dominate the ice scaling process.

The presence of ice seeds in the bulk brine provides surface area for supersaturation consumption, promoting bulk nucleation, where ice crystals form on ice, lowering the energy barrier for nucleation and growth. In contrast, surface nucleation has a higher energy barrier as the brine and the surface are not in direct contact with ice crystals. However, the supersaturation near the surface is higher, suggesting surface nucleation is also favored. This creates competition between bulk and surface nucleation, with the outcome depending on how evenly the supersaturation is distributed in the solution. To favor bulk nucleation, supersaturation needs to be evenly distributed throughout the solution.

Surface tensions were estimated using OLI software (V11.5), and contact angles were measured on a flat PP-GR plate using a manual method. Brine droplets (5 μl) were deposited on the surface using a syringe, with minimal evaporation effects considered at room temperature (25.0 ˚C). The contact angles were analyzed using ImageJ software, and the average of four measurements was reported. While the contact angles in this study were measured at 25˚C, they still provided some valuable insight into the strength of interfacial interactions between the brine, water molecules, and the HX material during crystallization. However, it should be noted that these measurements were conducted at temperatures significantly higher than the subzero conditions under which freeze crystallization and ice scaling typically occur.

Ice scaling is influenced by the interfacial properties between the HX surface, brine, and ice, which may vary significantly under colder conditions. Future work should also focus on measuring contact angles of

these brines at subzero temperatures and under specific supersaturation conditions relevant to ice crystallization. This would provide a clearer understanding of how interfacial properties influence ice scaling and help develop strategies to mitigate it.

8. References

Al-Zaidi, E., & Fan, X. F. (2018). Effect of aqueous electrolyte concentration and valency on contact angle on flat glass surfaces and inside capillary glass tubes. *Colloids and Surfaces a-Physicochemical and Engineering Aspects*, *543*, 1-8. https://doi.org/10.1016/j.colsurfa.2018.01.045

Ali, U., Zhang, H., Abedrabbo, S., & Janajreh, I. (2023). Freeze desalination via thermoacoustic cooling: System analysis and cost overview. *Energy Nexus*, *10*, 100195. https://doi.org/10.1016/j.nexus.2023.100195

Asakawa, H., Sazaki, G., Nagashima, K., Nakatsubo, S., & Furukawa, Y. (2016). Two types of quasi-liquid layers on ice crystals are formed kinetically. *Proceedings of the National Academy of Sciences of the United States of America*, *113*(7), 1749-1753. https://doi.org/10.1073/pnas.1521607113

Aspeling, B. J., Chivavava, J., & Lewis, A. E. (2020). Selective salt crystallization from a seeded ternary eutectic system in Eutectic Freeze crystallization. *Separation and Purification Technology*, *248*. https://doi.org/10.1016/j.seppur.2020.117019

Astilleros, J. M., Pina, C. M., Fernández-Díaz, L., & Putnis, A. (2003). Nanoscale growth of solids crystallising from multicomponent aqueous solutions. *Surface Science*, *545*(1-2), L767-L773. https://doi.org/10.1016/j.susc.2003.08.031

Azimi, G., Cui, Y. H., Sabanska, A., & Varanasi, K. K. (2014). Scale-resistant surfaces: Fundamental studies of the effect of surface energy on reducing scale formation. *Applied Surface Science*, *313*, 591-599. https://doi.org/10.1016/j.apsusc.2014.06.028

Benz, K. W. (2020). Handbook of Industrial Crystallization. 3rd ed. *Journal of Applied Crystallography*, *53*, 861-862. https://doi.org/10.1107/S160057672000148x

Boinovich, L. B., Emelyanenko, K. A., & Emelyanenko, A. M. (2022). Superhydrophobic versus SLIPS: Temperature dependence and the stability of ice adhesion strength. *Journal of Colloid and Interface Science*, *606*, 556-566. https://doi.org/10.1016/j.jcis.2021.08.030

Cevallos, J. G., Bergles, A. E., Bar-Cohen, A., Rodgers, P., & Gupta, S. K. (2012). Polymer Heat Exchangers-History, Opportunities, and Challenges. *Heat Transfer Engineering*, *33*(13), 1075-1093. https://doi.org/10.1080/01457632.2012.663654

Chatterjee, R., Thanjukutty, R. U., Carducci, C., Neogi, A., Chakraborty, S., Bapu, V. P. B. R., Banik, S., Sankaranarayanan, S. K. R. S., & Anand, S. (2023). Adhesion of impure ice on surfaces. *Materials Horizons*. https://doi.org/10.1039/d3mh01440a

Chernyy, S., Järn, M., Shimizu, K., Swerin, A., Pedersen, S. U., Daasbjerg, K., Makkonen, L., Claesson, P., & Iruthayaraj, J. (2014). Superhydrophilic Polyelectrolyte Brush Layers with Imparted Anti-Icing

Properties: Effect of Counter ions. *Acs Applied Materials & Interfaces*, *6*(9), 6487-6496. https://doi.org/10.1021/am500046d

Chivavava, J., Rodriguez-Pascual, M., & Lewis, A. E. (2014). Effect of Operating Conditions on Ice Characteristics in Continuous Eutectic Freeze Crystallization. *Chemical Engineering & Technology*, *37*(8), 1314-1320. https://doi.org/10.1002/ceat.201400094

Chu, F., Li, S., Zhao, C., Feng, Y., Lin, Y., Wu, X., Yan, X., & Miljkovic, N. (2024). Interfacial ice sprouting during salty water droplet freezing. *Nature Communications*, *15*(1), 2249. https://doi.org/10.1038/s41467-024-46518-y

De Goede, R., & De Jong, E. J. (1993). Heat transfer properties of a scraped-surface heat exchanger in the turbulent flow regime. *Chemical Engineering Science*, *48*(8), 1393-1404. https://doi.org/10.1016/0009-2509(93)80046-S

Deshmukh, S., Kamath, G., Ramanathan, S., & Sankaranarayanan, S. K. R. S. (2013). Chloride ions induce order-disorder transition at water-oxide interfaces. *Physical Review E*, *88*(6). https://doi.org/10.1103/PhysRevE.88.062119

Dondo, A., Motsepe, L. A., Li, Q., Mgabhi, S., Chivavava, J., & Lewis, A. E. (2022). *Project-8.4.6-Unlocking-Obstacles-to-Commercialisation-of-Eutectic-Freeze-Crystallization*. https://coaltech.co.za/wp-content/uploads/2022/10/Project-8.4.6-Unlocking-Obstacles-to-Commercialisation-of-Eutectic-Freeze-Crystallization-August-2022.pdf

Faust, J. A., & House, J. E. (2018). *Physical Chemistry of Gas-Liquid Interfaces*. Elsevier. https://app.knovel.com/hotlink/toc/id:kpPCGLI002/physical-chemistry-gas/physical-chemistry-gas

Fitzner, M., Sosso, G. C., Cox, S. J., & Michaelides, A. (2015). The Many Faces of Heterogeneous Ice Nucleation: Interplay Between Surface Morphology and Hydrophobicity. *Journal of the American Chemical Society*, *137*(42), 13658-13669. https://doi.org/10.1021/jacs.5b08748

Förster, M., Augustin, W., & Bohnet, M. (1999). Influence of the adhesion force crystal/heat exchanger surface on fouling mitigation. *Chemical Engineering and Processing-Process Intensification*, *38*(4-6), 449-461. https://doi.org/10.1016/S0255-2701(99)00042-2

Gribanova, E. V., Kuchek, A. E., & Larionov, M. (2016). Factors influencing the contact angle value. The contact angle, as a characteristic of the properties of solid surfaces. *Russian Chemical Bulletin*, *65*(1), 1-13. https://doi.org/10.1007/s11172-016-1259-5

Hasan, M., Filimonov, R., Chivavava, J., Sorvari, J., Louhi-Kultanen, M., & Lewis, A. E. (2017). Ice growth on the cooling surface in a jacketed and stirred eutectic freeze crystallizer of aqueous Na_2SO_4 solutions. *Separation and Purification Technology*, *175*, 512-526. https://doi.org/10.1016/j.seppur.2016.10.014

Hasan, M., & Louhi-Kultanen, M. (2015). Ice growth kinetics modeling of air-cooled layer crystallization from sodium sulfate solutions. *Chemical Engineering Science*, *133*, 44-53. https://doi.org/10.1016/j.ces.2015.01.050

He, Y. B., Tilocca, A., Dulub, O., Selloni, A., & Diebold, U. (2009). Local ordering and electronic signatures of submonolayer water on anatase TiO

(101). *Nature Materials*, *8*(7), 585-589. https://doi.org/10.1038/Nmat2466

He, Z., Xie, W. J., Liu, Z., Liu, G., Wang, Z., Gao, Y. Q., & Wang, J. (2016). Tuning ice nucleation with counterions on polyelectrolyte brush surfaces. *Science Advances*, *2*(6), e1600345. https://doi.org/10.1126/sciadv.1600345

He, Z. Y., Xie, W. J., Liu, Z. Q., Liu, G. M., Wang, Z. W., Gao, Y. Q., & Wang, J. J. (2016). Tuning ice nucleation with counterions on polyelectrolyte brush surfaces. *Science Advances*, *2*(6). https://doi.org/10.1126/sciadv.1600345

Himawan, C., Kramer, H. J. M., & Witkamp, G. J. (2006a). Study on the recovery of purified $MgSO_4.7H_2O$ crystals from industrial solution by eutectic freezing. *Separation and Purification Technology*, *50*(2), 240-248. https://doi.org/10.1016/j.seppur.2005.11.031

Himawan, C., Kramer, H. J. M., & Witkamp, G. J. (2006b). Study on the recovery of purified $MgSO_4 \bullet 7H_2O$ crystals from industrial solution by eutectic freezing. *Separation and Purification Technology*, *50*(2), 240-248. https://doi.org/10.1016/j.seppur.2005.11.031

Jha, K. C., Anim-Danso, E., Bekele, S., Eason, G., & Tsige, M. (2016). On Modulating Interfacial Structure towards Improved Anti-Icing Performance. *Coatings*, *6*(1). https://doi.org/10.3390/coatings6010003

Kapembwa, M., Rodríguez-Pascual, M., & Lewis, A. E. (2014). Heat and Mass Transfer Effects on Ice Growth Mechanisms in Pure Water and Aqueous Solutions. *Crystal Growth & Design*, *14*(1), 389-395. https://doi.org/10.1021/cg401428v

Kazi, S. N., Teng, K. H., Zakaria, M. S., Sadeghinezhad, E., & Bakar, M. A. (2015). Study of mineral fouling mitigation on heat exchanger surface. *Desalination*, *367*, 248-254. https://doi.org/10.1016/j.desal.2015.04.011

Kolasinski, K. W. (2020). *Surface Science - Foundations of Catalysis and Nanoscience* John Wiley & Sons. https://app.knovel.com/hotlink/toc/id:kpSSFCNE01/surface-science-foundations/surface-science-foundations

Kowacz, M., & Putnis, A. (2008). The effect of specific background electrolytes on water structure and solute hydration: Consequences for crystal dissolution and growth. *Geochimica Et Cosmochimica Acta*, *72*(18), 4476-4487. https://doi.org/10.1016/j.gca.2008.07.005

Lewis, A., Seckler, M., Kramer, H., & van Rosmalen, G. (2015). *Industrial Crystallization: Fundamentals and Applications*. Cambridge University Press. https://doi.org/DOI: 10.1017/CBO9781107280427

Lewis, A. E., Chivavava, J., Motsepe, L. A., Nxiwa, B., Netshiomvani, K., & Zimu, N. (2023). Novel materials and crystallizer design for freeze concentration. *Scientific African*, *20*. https://doi.org/10.1016/j.sciaf.2023.e01675

Lewis, A. E., Nathoo, J., Reddy, T. R., Randall, D. G., Zibi, L. M., & Jivanji, R. B. (2010). Novel Technology for recovery of water and solid salts from hypersaline brines: Eutectic Freeze Crystallization.

Leyland, D., Chivavava, J., & Lewis, A. E. (2019). Investigations into ice scaling during eutectic freeze crystallization of brine streams at low scraper speeds and high supersaturation. *Separation and Purification Technology*, *220*, 33-41. https://doi.org/10.1016/j.seppur.2019.03.025

Liu, J., Yang, T., Yuan, J. W., Chen, X. J., & Wang, L. (2020). Study on Eliminating the Water Blocking Effect in Coal Seams Using Gas-Wetting Reversal Technology. *Acs Omega*, *5*(47), 30687-30695. https://doi.org/10.1021/acsomega.0c04858

Liu, J., Zhu, C. Q., Liu, K., Jiang, Y., Song, Y. L., Francisco, J. S., Zeng, X. C., & Wang, J. J. (2017). Distinct ice patterns on solid surfaces with various wettabilities. *Proceedings of the National Academy of Sciences of the United States of America*, *114*(43), 11285-11290. https://doi.org/10.1073/pnas.1712829114

Lupi, L., Hudait, A., & Molinero, V. (2014). Heterogeneous nucleation of ice on carbon surfaces. *Journal of the American Chemical Society*, *136*(8), 3156-3164. https://doi.org/10.1021/ja411507a

Ma, Y. Q., Svärd, M., Xiao, X., Sahadevan, S. A., Gardner, J., Olsson, R. T., & Forsberg, K. (2022). Eutectic freeze crystallization for recovery of $NiSO_4$ and $CoSO_4$ hydrates from sulfate solutions. *Separation and Purification Technology*, *286*. https://doi.org/10.1016/j.seppur.2021.120308

Macias-Bu, L., Guerra-Valle, M., Petzold, G., & Orellana-Palma, P. (2023). Technical and Environmental Opportunities for Freeze Desalination. *Separation & Purification Reviews*, *52*(4), 326-335. https://doi.org/10.1080/15422119.2022.2098504

Marcus, Y. (2009). Effect of Ions on the Structure of Water: Structure Making and Breaking. *Chemical Reviews*, *109*(3), 1346-1370. https://doi.org/10.1021/cr8003828

Marcus, Y. (2016). Specific ion effects on the surface tension and surface potential of aqueous electrolytes. *Current Opinion in Colloid & Interface Science*, *23*, 94-99. https://doi.org/10.1016/j.cocis.2016.06.016

Matsumoto, K., Akimoto, T., & Teraoka, Y. (2010). Study of scraping force of ice growing on cooling solid surface. *International Journal of Refrigeration*, *33*(2), 419-427. https://doi.org/10.1016/j.ijrefrig.2009.10.011

Matsumoto, K., Inuzuka, M., Teraoka, Y., Hayashi, K., & Murahashi, K. (2012). Fundamental study on freezing characteristics of trehalose solution (investigation based on scraping characteristics). *International Journal of Refrigeration-Revue Internationale Du Froid*, *35*(4), 897-906. https://doi.org/10.1016/j.ijrefrig.2011.12.005

Meewisse, J. W., & Ferreira, C. A. I. (2003). Validation of the use of heat transfer models in liquid/solid fluidized beds for ice slurry generation. *International Journal of Heat and Mass Transfer*, *46*(19), 3683-3695. https://doi.org/10.1016/S0017-9310(03)00171-6

Memon, H., Liu, J. P., De Focatiis, D. S. A., Choi, K. S., & Hou, X. H. (2020). Intrinsic dependence of ice adhesion strength on surface roughness. *Surface & Coatings Technology*, *385*. https://doi.org/10.1016/j.surfcoat.2020.125382

Metya, A. K., & Singh, J. K. (2018). Nucleation of Aqueous Salt Solutions on Solid Surfaces. *Journal of Physical Chemistry C*, *122*(15), 8277-8287. https://doi.org/10.1021/acs.jpcc.7b12495

[Record #55 is using a reference type undefined in this output style.]

Mittal, K. L., & Choi, C. H. (2020b). *Ice Adhesion- Mechanism, Measurement and Mitigation*. John Wiley & Sons. https://app.knovel.com/hotlink/toc/id:kpIAMMM002/ice-adhesion-mechanism/ice-adhesion-mechanism

Motsepe, L. A., Chivavava, J., & Lewis, A. E. (2022). A novel, in-situ observation of the initial ice scale layer development on different heat exchanger surfaces during EFC. *Desalination*, *522*. https://doi.org/10.1016/j.desal.2021.115404

Mullin, J. W. (2001). *Crystallization*. Elsevier.

Murase, H., & Nanishi, K. (1985). On the Relationship of Thermodynamic and Physical-Properties of Polymers with Ice Adhesion. *Annals of Glaciology*, *6*, 146-149. https://doi.org/10.3189/1985AoG6-1-146-149

Nathoo, J., Jivanji, R., & Lewis, A. (2009). Freezing your brines off: Eutectic Freeze Crystallization for brine treatment. *International Mine Water Conference, Pretoria, South Africa*.

Panagopoulos, A., Haralambous, K.-J., & Loizidou, M. (2019). Desalination brine disposal methods and treatment technologies - A review. *Science of The Total Environment*, *693*, 133545. https://doi.org/10.1016/j.scitotenv.2019.07.351

Panagopoulos, A., & Haralambous, K. J. (2020). Minimal Liquid Discharge (MLD) and Zero Liquid Discharge (ZLD) strategies for wastewater management and resource recovery - Analysis, challenges and prospects. *Journal of Environmental Chemical Engineering*, *8*(5). https://doi.org/10.1016/j.jece.2020.104418

Pegram, L. M., & Record, M. T. (2007). Hofmeister salt effects on surface tension arise from partitioning of anions and cations between bulk water and the air-water interface. *Journal of Physical Chemistry B*, *111*(19), 5411-5417. https://doi.org/10.1021/jp070245z

Petrenko, V. F., & Whitworth, R. W. (2002). *Physics of Ice*. Oxford University Press. https://doi.org/10.1093/acprof:oso/9780198518945.001.0001

Pronk, P., Ferreira, C. A. I., & Witkamp, G. J. (2006). Influence of solute type and concentration on ice scaling in fluidized bed ice crystallizers. *Chemical Engineering Science*, *61*(13), 4354-4362. https://doi.org/10.1016/j.ces.2006.02.019

Randall, D. G., Nathoo, J., & Lewis, A. E. (2011). A case study for treating a reverse osmosis brine using Eutectic Freeze Crystallization-Approaching a zero waste process. *Desalination*, *266*(1-3), 256-262. https://doi.org/10.1016/j.desal.2010.08.034

Ryzhkin, I. A., & Petrenko, V. F. (1997). Physical mechanisms responsible for ice adhesion. *Journal of Physical Chemistry B*, *101*(32), 6267-6270. https://doi.org/10.1021/jp9632145

Samson, E., Marchand, J., & Snyder, K. A. (2003). Calculation of ionic diffusion coefficients on the basis of migration test results. *Materials and Structures*, *36*(257), 156-165. https://doi.org/10.1007/Bf02479554

Schilling, S., Glade, H., & Orth, T. (2022). Investigation of Crystallization Fouling on Novel Polymer Composite Heat Exchanger Tubes. *Heat Transfer Engineering*, *43*(15-16), 1326-1336. https://doi.org/10.1080/01457632.2021.1963533

Sei, T., Gonda, T., & Arima, Y. (2002). Growth rate and morphology of ice crystals growing in a solution of trehalose and water. *Journal of Crystal Growth*, *240*(1-2), 218-229. https://doi.org/10.1016/S0022-0248(02)00875-8

Shi, R., Cooper, A. J., & Tanaka, H. (2023). Impact of hierarchical water dipole orderings on the dynamics of aqueous salt solutions. *Nature Communications*, *14*(1). https://doi.org/10.1038/s41467-023-40278-x

Si, L. L., Xi, Y. J., Wei, J. P., Wang, H. Y., Zhang, H. T., Xu, G. X., & Liu, Y. (2022). The influence of inorganic salt on coal-water wetting angle and its mechanism on eliminating water blocking effect. *Journal of Natural Gas Science and Engineering*, *103*. https://doi.org/10.1016/j.jngse.2022.104618

Spencer, A., Chivavava, J., & Lewis, A. E. (2022). Effect of Heat Transfer Driving Force and Ice Seed Loading on the Production of Ice and Salt from a Dilute Brine Treated Using Eutectic Freeze Crystallization. *Minerals*, *12*(9). https://doi.org/10.3390/min12091094

Stamatiou, E., Meewisse, J. W., & Kawaji, M. (2005). Ice slurry generation involving moving parts. *International Journal of Refrigeration*, *28*(1), 60-72. https://doi.org/10.1016/j.ijrefrig.2004.07.016

Stepakoff, G. L., Siegelma.D, Johnson, R., & Gibson, W. (1974). Development of a Eutectic Freezing Process for Brine Disposal. *Desalination*, *15*(1), 25-38. https://doi.org/10.1016/S0011-9164(00)82061-5

Stocking, J. H., & King, C. J. (1976). Secondary Nucleation of Ice in Sugar Solutions and Fruit Juices. *Aiche Journal*, *22*(1), 131-140. https://doi.org/10.1002/aic.690220116

Ting, W. H. T., Tan, I. A. W., Salleh, S. F., Abdul Wahab, N., Atan, M. F., Abdul Raman, A. A., Kong, S. L., & Lam, L. S. (2024). Sustainable saline wastewater treatment using eutectic freeze crystallization: Recent advances, challenges and future prospects. *Journal of Environmental Chemical Engineering*, *12*(3), 112919. https://doi.org/10.1016/j.jece.2024.112919

Vaessen, R. J. C., Himawan, C., & Witkamp, G. J. (2002). Scale formation of ice from electrolyte solutions on a scraped surface heat exchanger plate. *Journal of Crystal Growth*, *237*, 2172-2177. https://doi.org/10.1016/S0022-0248(01)02263-1

Vaessen, R. J. C., Seckler, M. M., & Witkamp, G. J. (2004). Heat transfer in scraped eutectic crystallizers. *International Journal of Heat and Mass Transfer*, *47*(4), 717-728. https://doi.org/10.1016/j.ijheatmasstransfer.2003.07.028

van der Ham, F., Witkamp, G. J., de Graauw, J., & van Rosmalen, G. M. (1998). Eutectic freeze crystallization: Application to process streams and waste water purification. *Chemical Engineering and Processing-Process Intensification*, *37*(2), 207-213. https://doi.org/10.1016/S0255-2701(97)00055-X

Vrbka, L., & Jungwirth, P. (2005). Brine rejection from freezing salt solutions: A molecular dynamics study. *Physical Review Letters*, *95*(14). https://doi.org/10.1103/PhysRevLett.95.148501

Wan, X. S., Liu, E. L., & Qiu, E. X. (2021). Study on ice nucleation temperature and water freezing in saline soils. *Permafrost and Periglacial Processes*, *32*(1), 119-138. https://doi.org/10.1002/ppp.2081

Yazdanpanah, N., & Nagy, Z. K. (2020). *Handbook of Continuous Crystallization*. Royal Society of Chemistry (RSC). https://app.knovel.com/hotlink/toc/id:kpHCC00021/handbook-continuous-crystallization/handbook-continuous-crystallization

Zettler, H. U., Weiss, M., Zhao, Q., & Müller-Steinhagen, H. (2005). Influence of surface properties and characteristics on fouling in plate heat exchangers. *Heat Transfer Engineering*, *26*(2), 3-17. https://doi.org/10.1080/01457630590897024

Zhang, S. Z., Zhang, C. B., Wu, S. W., Zhou, X., He, Z. Y., & Wang, J. J. (2021). Ion-Specific Effects on the Growth of Single Ice Crystals. *Journal of Physical Chemistry Letters*, *12*(36), 8726-8731. https://doi.org/10.1021/acs.jpclett.1c02601

Zhang, Y., Zhang, Y., Luo, G., & Cui, B. (2022). Effects of Freezing Temperature and Salinity on the Adhesion Shear Strength of Amphibious Aircraft Tires under Static Icing. *Aerospace*, *9*(3), 170. https://doi.org/10.3390/aerospace9030170

Zhang, Y. J., Zhang, Y. H., Luo, G. S., & Cui, B. (2022). Effects of Freezing Temperature and Salinity on the Adhesion Shear Strength of Amphibious Aircraft Tires under Static Icing. *Aerospace*, *9*(3). https://doi.org/10.3390/aerospace9030170

Zou, M., Beckford, S., Wei, R., Ellis, C., Hatton, G., & Miller, M. A. (2011). Effects of surface roughness and energy on ice adhesion strength. *Applied Surface Science*, *257*(8), 3786-3792. https://doi.org/10.1016/j.apsusc.2010.11.149

Appendices

Appendix A Composition of the brine and Thermodynamic Modelling

This section gives the calculations for estimating the composition of the salts present in the brine, and the results from the thermodynamic simulation of the investigated brine solutions. The software OLI Stream Analyzer was used to estimate the freezing temperatures of these solutions, TWRP brine (TDS= 103 g/L, 122 g/L and 133 g/L), $MgSO_4$ (7 wt.%, 12 wt.%, and 15 wt.%), and 4 wt.% Na_2SO_4.

Appendix A.1 Estimating the composition of the salts present in the solution:

The solution was analyzed to measure the concentrations of the following cations. TWRP 1 was used example.

Table 8.1: The measured concentrations of the cations present in the solution.

	Concentration (g/L)	**Molar Mass (g/mol)**	**Concentration (mol/L)**
Na^+	7.354	22.98	0.320
Ca^{2+}	0.964	40.00	0.024
Mg^{2+}	15.85	24.31	0.652

Assumptions Made:

- The only anions present in the solution were SO^{2-}_4 and Cl^-.
- The salt initially present in the solution was determined based on the measured concentrations of the cations and the assumed anions.

The following salts were assumed to be present:

$$Na_2SO_4 \longrightarrow 2Na^+ + {SO_4}^{2-}$$

$$CaSO_4 \longrightarrow Ca^{2+} + {SO_4}^{2-}$$

$$NaCl \longrightarrow Na^+ + Cl^-$$

$$MgSO_4 \longrightarrow Mg^{2+} + {SO_4}^{2-}$$

Calculating the total moles of salts in solution:

To estimate the number of moles of each salt, the following approach was used:

For $MgSO_4$:

- All the moles of Mg^{2+} (0.652 mol/L) were assumed to come from $MgSO_4$.
- Therefore, [$MgSO_4$] = 0.652 mol/L, and this implies that [SO_4] = 0.652 mol/L.

For $CaSO_4$:

- All of moles of Ca^{2+} (0.024 mol/L) were assumed to come from $CaSO_4$,
- Therefore, [$CaSO_4$] = 0.024 mol/L, and the total moles of SO_4 contributed by $CaSO_4$ is 0.024 mol/L.
- New total [SO^{2-}_4] =0.652+ 0.024= 0.676 mol/L.

For Na_2SO_4:

- The total number moles of Na+ in the solution were 0.320 mol/L.
- It was assumed that 90% of Na^+ moles come from Na_2SO_4, while the remaining 10% come from NaCl.
- Moles of Na_2SO_4: 0.9 x 0.320= 0.288 mol/L.
- Since each of molecule of Na_2SO_4 produces 2 moles of Na^+:
- Moles of Na_2SO_4: 0.288/2= 0.144 mol/L
- SO_4^{2-} contributed by Na_2SO_4: 0.144 mol/L
- Updated total number of moles of SO^{2-}_4 = 0.144+ 0.676= 0.804 mol/L

For NaCl:

- The remaining 10% of Na+ moles come from NaCl:
- Moles of NaCl = 0.1 x 0.320 = 0.032 mol/L.

Final Salt Concentrations and Composition:

Table 8.2: The calculated concentrations and compositions of the salts in the solutions.

	Concentration (mol/L)	**(g/L)**	**Composition (wt.%)**
Na_2SO_4	0.13	18.14	1.6
$CaSO_4$	0.02	3.27	0.3
NaCl	0.06	3.78	0.3
$MgSO_4$	0.65	78.51	7.1
H_2O	55.56	1 000	90.6
Total	-	1104	100

Appendix A.2 Industrial Brine solutions

Figure A.1 shows the influence of temperature on the yield and freezing temperature of both ice and salt for the TWRP brine with a TDS of 122 g/L over at a temperature range of 10 to -10 ˚C.

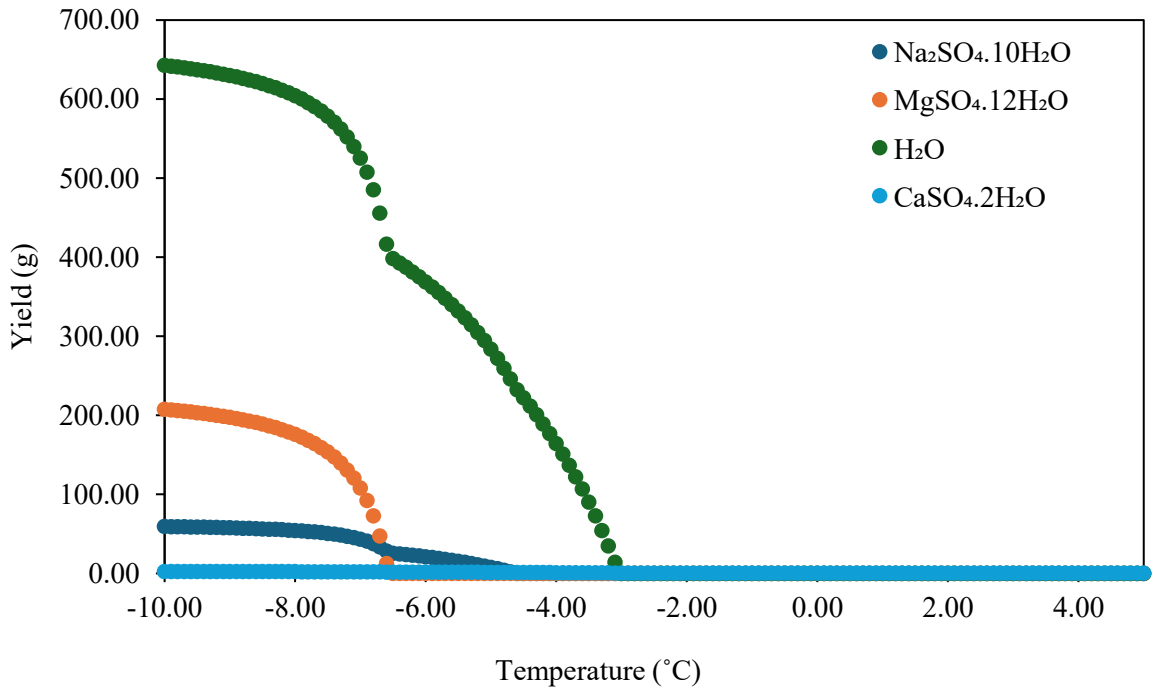

Figure A.1: The influence of temperature on the yield and freezing temperature of both ice and salt for the TWRP brine with a TDS of 122 g/L over at a temperature range of 4 to -10 ºC.

The results show that $CaSO_4.2H_2O$ forms at relatively warmer temperatures around 5 ˚C, however in smaller quantities(<0.5g/L). Subsequently, ice crystallization occurs at a temperature of -3.1 ˚C, followed by the formation of $Na_2SO_4.10H_2O$ at -4.7 ˚C. Finally, $MgSO_4.12H_2O$ crystallizes out at a lower temperature of -6.6 ˚C. These findings showed that freeze crystallization can be used to study ice formation exclusively, whether on the HX surface or in suspension, in the absence of salt crystallization.

Figure A.2 shows the influence of temperature on the yield and freezing temperature of both ice and salt for the TWRP brine with a TDS of 133 g/L over at a temperature range of 4 to -10 ˚C.

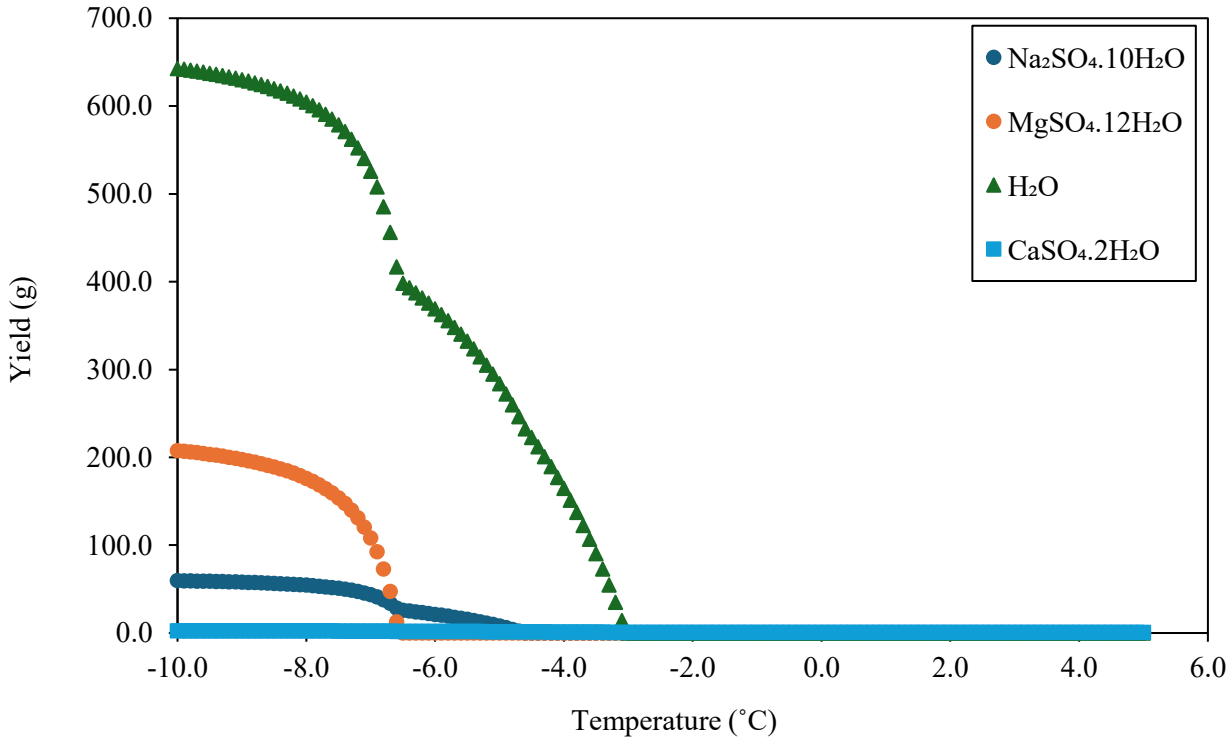

Figure A.2: The influence of temperature on the yield and freezing temperature of both ice and salt for the TWRP brine with a TDS of 133 g/L over at a temperature range of 4 to -10˚C

The results show that $CaSO_4.2H_2O$ forms at relatively warmer temperatures around 10˚C, however in smaller quantities. Subsequently, ice crystallization occurs at a temperature of -2.7˚C, followed by the formation of $Na_2SO_4.10H_2O$ at -4.9˚C. Finally, $MgSO_4.12H_2O$ crystallizes out at a lower temperature of -6.5˚C. These findings showed that freeze crystallization can be used to study ice formation exclusively, whether on the HX surface or in suspension, in the absence of salt crystallization

˚

Appendix A.3 Freezing point of ice in Binary Solutions

The OLI Stream Analyze software was used to predict the freezing point of ice in both Na_2SO_4 and $MgSO_4$ solutions from a concentrations of 0 wt.% up until to the eutectic point of both solutions, and the results are shown in Figure A.3.

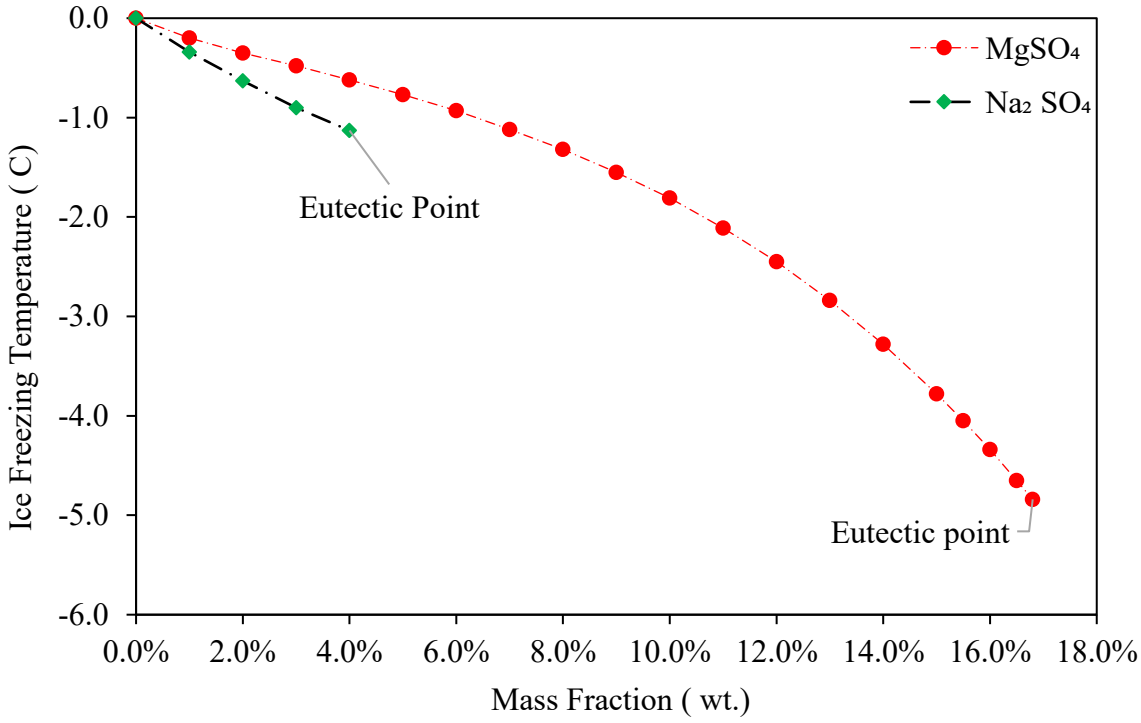

Figure A.3: The influence of concentration in $MgSO_4$ and Na_2SO_4 solutions on freezing temperature of water over at a temperature range of 0 to -6 ˚C.

Figure A.3 shows that the freezing point of water decreases as the mass fraction increases for both solutions. It also shows that the solubility line of $MgSO_4$ has a wider range, allowing to study ice formation exclusively over wide range of concentrations as opposed to Na_2SO_4 solution, whose solubility ends at a concentration of 4 wt.%. For the study of solute concentration, 7 wt.%, 12 wt.%, and 15 wt.% $MgSO_4$ were selected to study the impact of dilute and concentrated solutions on ice scaling formation. For the study of solute type on ice scaling formation, freezing point of the solution was kept the equal as at that point, the total ionic molality is also equal. For this study, the ice freezing point of -1.12 ˚C was chosen as the concentrations of Na_2SO_4. This translates to the equivalent total ionic molality of the solution (0.613 mol/kg),

Appendix A.4 Concentration (g/L) of binary solutions

Using a 4wt.% Na_2SO in a 1000 g of an aqueous solution as an example:

To calculate the concentration of Na_2SO_4 in grams per liter (g/L), these steps were followed:

1. **Determining the mass of Na_2SO_4**:

   There are 40 grams of Na_2SO_4

2. **Calculating the volume of the solution**:

   There are 960 grams of water, which corresponds to 960 mL or 0.96 liters (assuming the density of water is approximately 1 g/mL).

3. **Calculating the concentration in g/L**:

$$[\mathrm{Na_2SO_4}] = \frac{\text{Mass of}\mathrm{Na_2SO_4}}{\text{Volume of solution}} = \frac{40\ \mathrm{g}}{0.96\ \mathrm{L}} = 41.67\ \mathrm{g}/L$$

Appendix A.4.1 Temperature vs yield

Although the freezing temperature of ice and eutectic points for binary solutions were determined in the previous section, their expected yields per 1000 grams of solution were estimated, hence further thermodynamic simulations were conducted, as shown in Figure A. 5, Figure A. 4, Figure A. 7, and Figure A. 6.

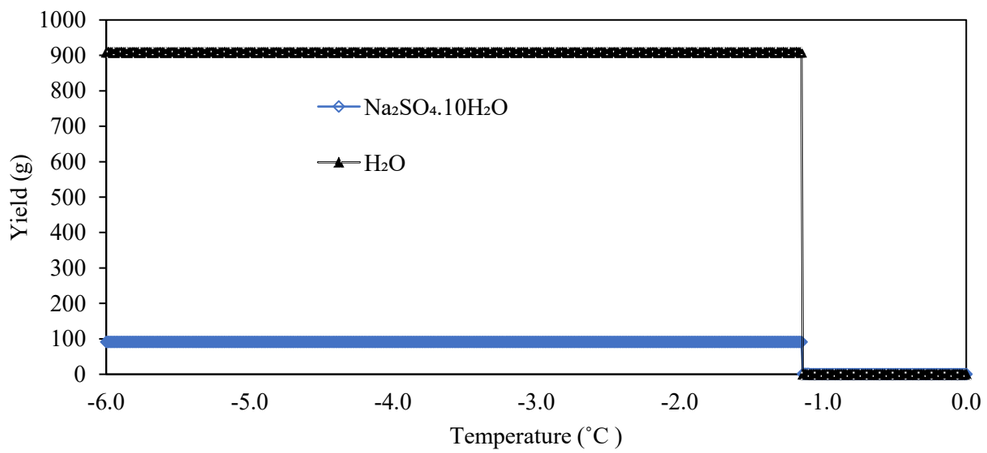

Figure A. 5 :The influence of temperature on the yield and freezing temperature of both ice and salt for the 0.613 mol Na_2SO_4/kg brine over at a temperature range of 0 to – 6 ˚C.

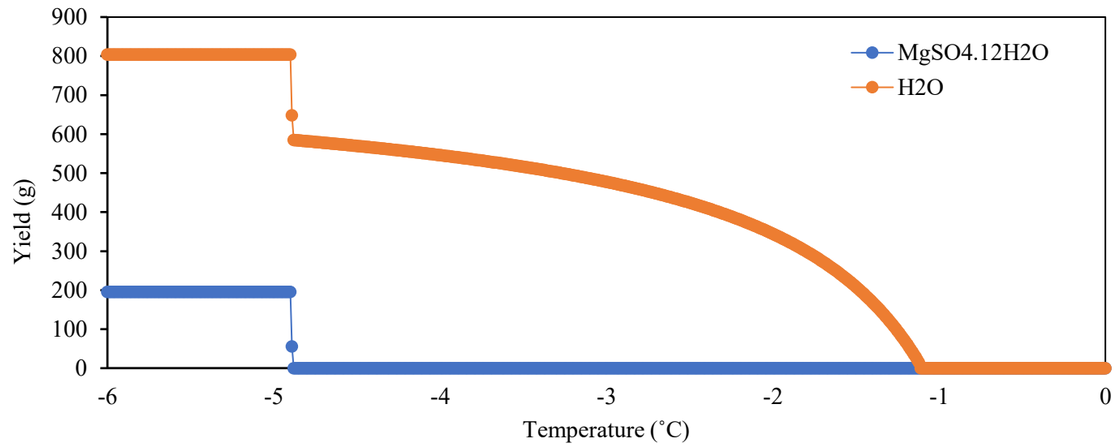

Figure A. 4 :The influence of temperature on the yield and freezing temperature of both ice and salt for the 0.613 mol $MgSO_4$/kg brine over at a temperature range of 0 to – 6 ˚C.

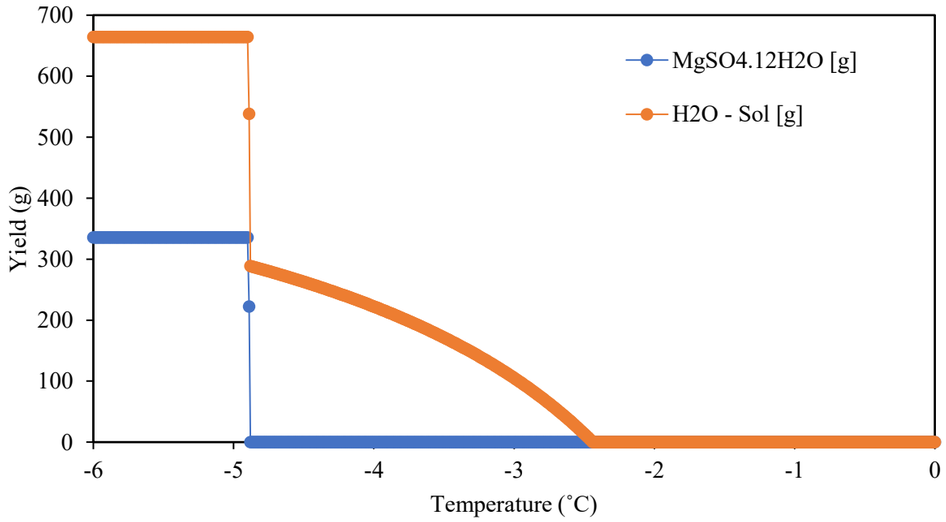

Figure A. 7 :The influence of temperature on the yield and freezing temperature of both ice and salt for the 1.13 mol $MgSO_4$/kg brine over at a temperature range of 0 to – 6 ˚C.

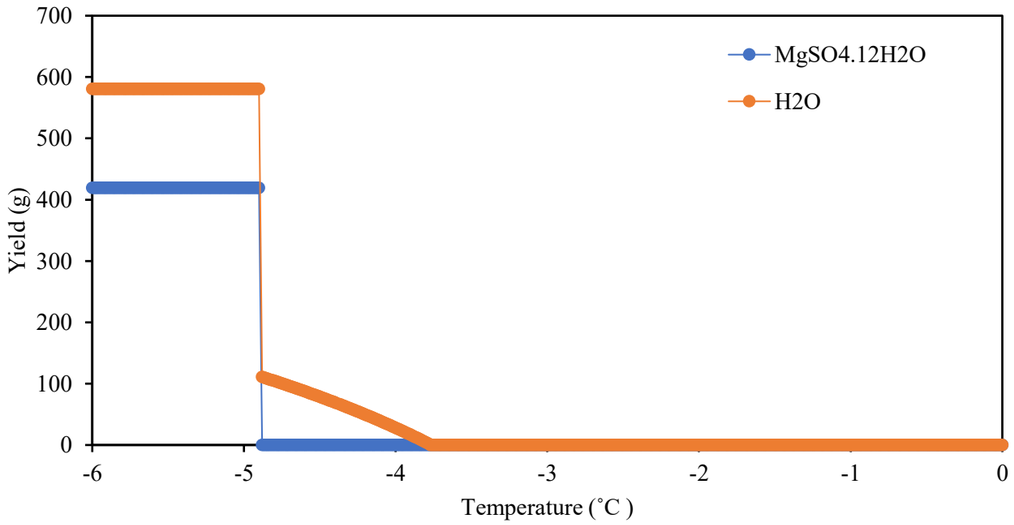

Figure A. 6: The influence of temperature on the yield and freezing temperature of both ice and salt for the 1.8 mol $MgSO_4$/kg brine over at a temperature range of 0 to – 6 ˚C.

Appendix A.5 Temperature Profile for batch experiments of industrial brines

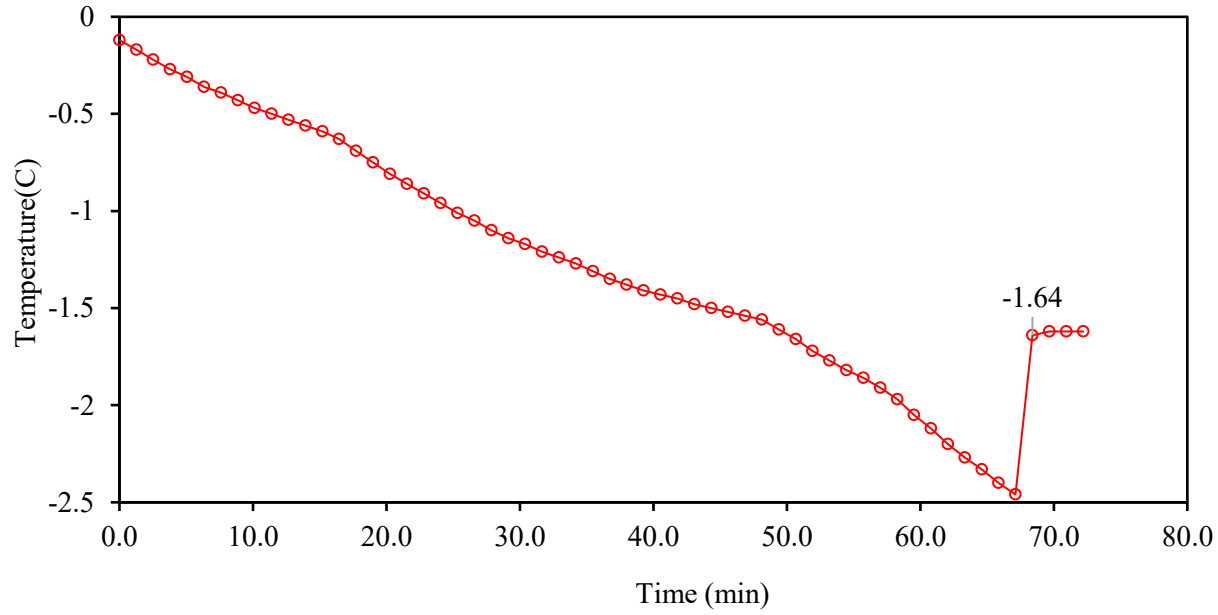

Figure A.8: The temperature profile inside the crystallizer during a batch crystallization of the industrial Brine 1(TWRP 1).

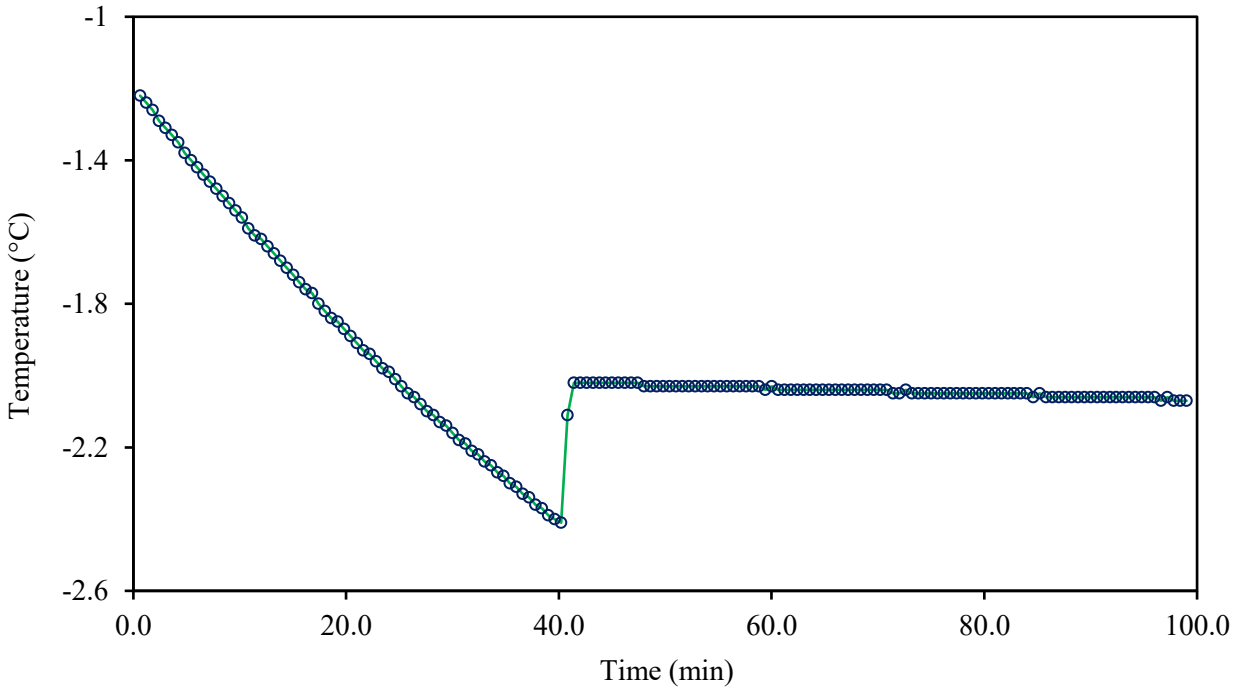

Figure A.9: The temperature profile inside the crystallizer during a batch crystallization of the industrial Brine 2 (TWRP2).

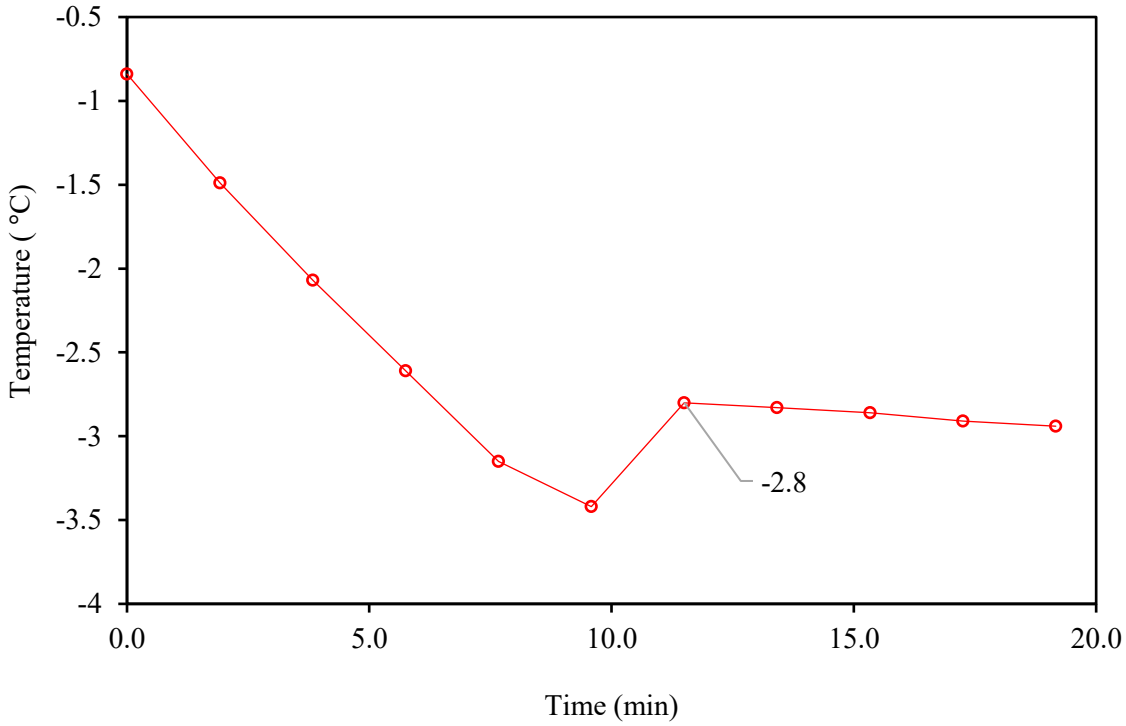

Figure A.10: The temperature profile inside the crystallizer during a batch crystallization of the industrial Brine 3 (TWRP3).

Appendix A.6 Brine Solution Preparation

Using a 4 wt.% Na_2SO_4 as an example

Table 8.3: Properties of the components used to make a 4wt.% Na_2SO_4 solution.

Component	Molar Mass (g/mol)	Density (kg/m^3)
H_2O	18.02	977 (OLI)
Na_2SO_4	142	

Density of the solution (from OLI): 1200 kg/m^3

Volume of the solution: 1 L

Desired composition: H_2O (96 wt.%) and Na_2SO_4 (4 wt.%)

Step 1: Calculate the mass of the solution:

$$\mathrm{m} = \mathrm{V} * \mathrm{L} = 1\ \mathrm{L} * \frac{1\ \mathrm{m}^3}{1000\ \mathrm{L}} \frac{1032\ \mathrm{kg}}{\mathrm{m}^3} = 1.032\ \mathrm{kg}$$

Step 2: Mass of water needed:

$$\mathrm{m}_{\mathrm{H_2O}} = \text{mass fraction} * \text{mass of the solution}$$

$$\mathrm{m}_{\mathrm{H_2O}} = 0.96 * \ 1.032\ \mathrm{kg} = 0.99\ \mathrm{kg}$$

Step 3: Mass of Na_2SO_4 needed:

$$\mathrm{m}_{\mathrm{Na_2SO_4}} = \mathrm{m}_{\mathrm{solution}} - \ \mathrm{m}_{\mathrm{H_2O}} = 1.032 - 0.99 = 0.041\ \mathrm{k}g$$

To prepare this solution, $Na_2SO_4.10H_2O$ salt was used, which comes with a certain amount of H_2O. To find the actual amount of $Na_2SO_4.10H_2O$ required to make a solution containing 4 wt.% Na_2SO_4, the following equation was used.

$$\mathrm{Na_2SO_4.10H_2O} \longrightarrow \mathrm{Na_2SO_4} + 10\mathrm{H_2O}$$

It was assumed that 1 mol of $Na_2SO_4.10H_2O$ dissociates into 1 mol of Na_2SO_4 and 10 mol of H_2O.

Finding number of moles of Na_2SO_4 in a 1 L of solution containing 4wt.% Na_2SO_4:

$$\mathrm{n}_{\mathrm{Na_2SO_4}} = \frac{\mathrm{M}_{\mathrm{Na_2SO_4}}}{\mathrm{m}_{\mathrm{Na_2SO_4}}} = \frac{0.041\frac{\mathrm{kg}}{\mathrm{L}}}{\frac{142\ \mathrm{kg}}{\mathrm{kmol}}} = 0.00029\frac{\mathrm{kmol}}{\mathrm{L}}$$

Since the mole ratio of Na_2SO_4 is 1:1 to $Na_2SO_4.10H_2O$, then amount of moles needed from $Na_2SO_4.10H_2O$ is 0.00029 kmol/L of solution.

Step 4: Mass of the $Na_2SO_4.10H_2O$ salt needed for 1 L of 4wt.% Na_2SO_4 solution:

$$m_{Na_2SO_4.10H_2O} = n_{Na_2SO_4.10H_2O} * M_{Na_2SO_4.10H_2O} = 0.00029\ \text{kmol} * 322\frac{\text{kg}}{\text{kmol}} = 0.09\ \text{kg}$$

Mass of water that will come from $Na_2SO_4.10H_2O$:

$$n_{H_2O} = 10 * n_{Na_2SO_4.10H_2O} = 10 * 0.00029\ \text{kmol} = 0.0029\ \text{kmol}$$

Step 5: Mass of water that needs to be added:

(Total mass of water in 1L of solution with 4wt.% Na_2SO_4) - (Water coming from $Na_2SO_4.10H_2O$)

$$m_{H_2O,\text{to bee added}} = 0.96 * 1.032\ \text{kg} - \left(0.0029\text{kmol} * \frac{18.02\text{kg}}{\text{kmol}}\right) = 0.938\ \text{kg}$$

Step 6: Volume of water needed to be added:

$$V_{H_2O} = \frac{m_{H_2O}}{\rho_{H_2O}} = \frac{0.938\ \text{kg}}{\frac{997\ \text{kg}}{\text{m}^3}} * \frac{1000\ \text{L}}{1\text{m}^3} = 0.941\ \text{L} = 941\ \text{ml of water}$$

Therefore, to make a 1 L solution with 4wt.% Na_2SO_4, 941 ml of pure water and 0.09 kg of $Na_2SO_4.10H_2O$ salt were mixed. The same method was followed for 0.613, 1.13 and 1.47 mol $MgSO_4$/kg solutions.

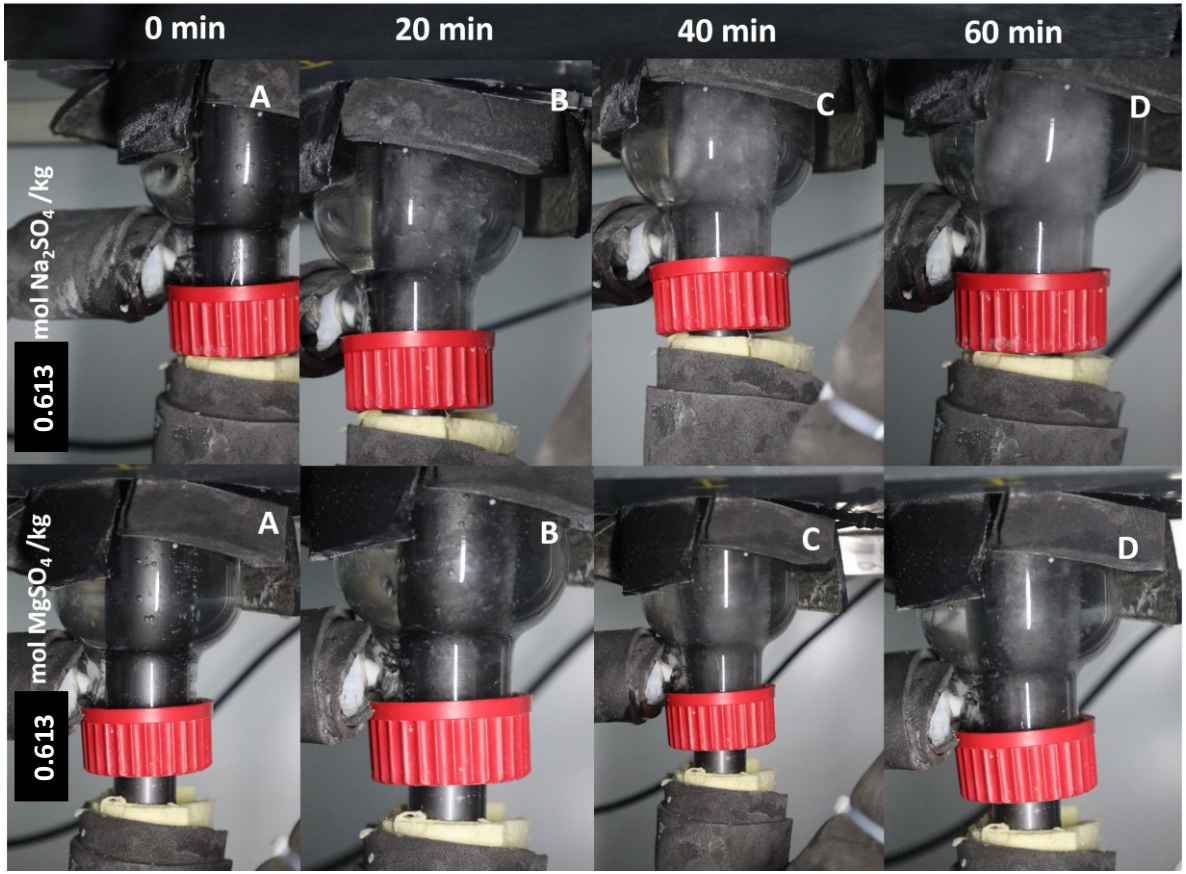

Figure A. 11. Images of the ice scaling formation on the bottom section of HX surface of PP-GR from a 0.613 mol Na_2SO_4/kg and 0.613 mol $MgSO_4$ /kg brine solutions. These images were taken for times 0 min to 60 min at 20 minute-intervals.

M